The physical processes influencing morphodynamics in braided rivers

A case study on the Ayeyarwady River

D. Ligthart

Master thesis

July 6, 2017

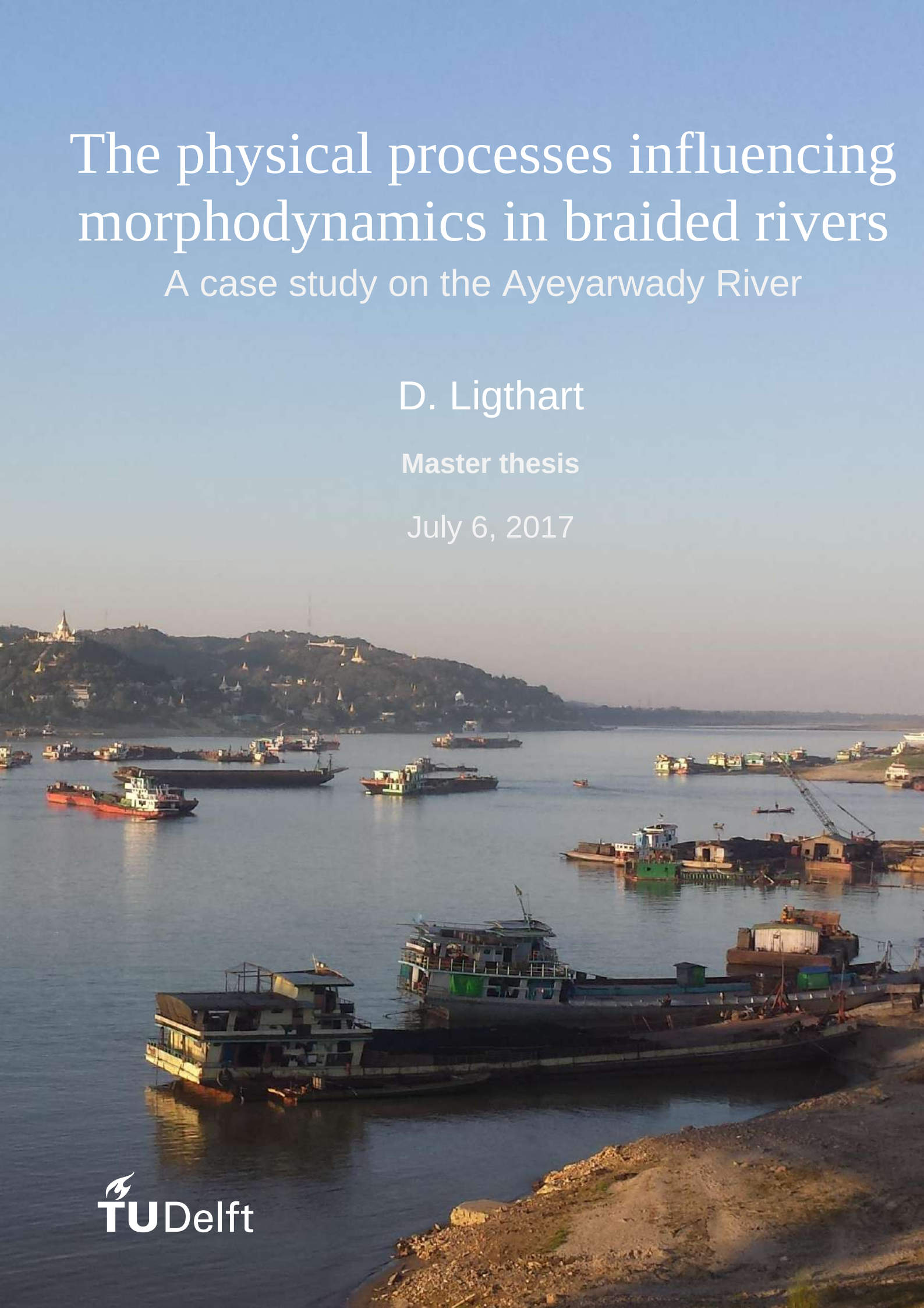

TU Delft

The physical processes influencing morphodynamics in braided rivers

A case study on the Ayeyarwady River

By

D. Ligthart

in partial fulfilment of the requirements for the degree of

Master of Science
in Applied Physics

at the Delft University of Technology,
to be defended publicly on Thursday July 6, 2017 at 15:30 PM.

Supervisor:	Prof. dr. ir. W. S. J. Uijttewaal	
Thesis committee:	Dr. ir. C. J. Sloff,	TU Delft & Deltares
	Dr. ir. M. M. Rutten,	TU Delft

TU Delft

Summary

Large hydrological variations and an abundance of fine non-cohesive sediment cause the dynamic behaviour of the Ayeyarwady River, with fast moving channels and passing bars. The dynamic behaviour of this braided river, together with the large hydrological variations, is the source of a frequently flooding river with a moderate navigability. In order to find suitable and sustainable solutions, increasing the understanding of the morphodynamics in braided rivers is required. In this research the physical processes forcing the morphodynamics in these rivers are investigated using the 2D depth-averaged morphodynamic model Delft3D and satellite imagery. This is done for a river reach of thirty kilometres of the Ayeyarwady River, located next to Mandalay. This reach contains multiple channels around three large islands and has two floodplains. The braid plain is restricted by on one side a mountain ridge and on the other side the city Mandalay.

The most dominant physical processes in braided rivers were found from literature and can be divided into system forcing processes and internal flow and sediment transport processes. The system forcing processes are the hydrological variations, input of sediment, the availability of erodible sediment, the bed roughness and vegetation. The internal flow and sediment transport processes are sediment transport by primary flow, deflection of sediment transport by spiral flow and bed-slope effects, turbulence and bank erosion. The system forcing processes are imposed by the system and have a forcing influence on the internal flow and sediment transport processes. All these processes are interrelated with each other in different ways, all having different influence on each other and on the morphology. Because the morphology also affects these processes, positive feedback exists where change in one processes enhances change in all the other processes. Since the morphology also affects the different processes, a positive feedback exists. This positive feedback between all processes makes the change in morphology, or the morphodynamics, hard to predict.

The morphodynamics in the research area were studied from satellite imagery. These showed that the most significant morphodynamics are during the wet seasons, when the complete river area is submerged (all bars, islands and floodplains). The effects of the morphodynamics propagated in downstream direction and were restricted by poorly or non-erodible reaches. These restrictions caused morphodynamics of a different character for the different regions in the research area and were influenced by the morphodynamics in the reach upstream. Most important features for the four reaches, from upstream to downstream, are:

- the incoming bars, resulting in the shift of channels
- the change of the trifurcation, causing redistribution of flow and sediment over the downstream channels
- the narrowing, widening and shift of the left and morphological most active channel due to the passing side and mid-channel bars
- the development of the confluence in downstream direction

In a sensitivity analysis performed with the Delft3D 2D morphodynamic model, the effects of several physical processes are estimated. These processes are hydrological variation, input of sediment, sediment transport by primary flow and deflection of sediment transport by spiral flow and bed-slope effects. The processes were tested quantitatively for the width, depth and the yearly change in width of the channels. Qualitatively, the effects of the processes on the shapes of the bars and channels were tested. It was found that the sediment transport by primary flow, spiral flow and bed-slope effect had the most significant effect on the widths and depths of the channel. The sediment transport by primary flow was tested by varying the power above the velocity in the sediment transport formula. A lower power above the velocity resulted in wider and shallower channels. The spiral flow causes deepening and narrowing of the channels. By enhancing curvature, it also enlarged the probability at channel incision (meander cutoff). Large bed-slope effects resulted in wide and shallow channels and flat bars. Hydrological variations also had a significant effect on the morphology. During rising and falling stage deepening of existing channels and incision of new channels can be found, where during high water all bars and islands move. The subtle interaction between the morphodynamics in the different stages causes complex shapes of bars and channels.

The change in channel width in the sensitivity analysis was used as measure for the dynamics of the system. The channel width change rate turned out to be significantly lower for the model simulations than on the satellite images. The comparison with satellite imagery showed that the movement of bars, or pulses in sediment, is the main process causing dynamics of the river. Larger dynamics were indeed found in the model with larger pulses in sediment at the upstream boundary. The comparison of the satellite imagery with the model also showed that vegetation causes decrease of the mobility of the islands and is of main importance for a correct simulation of the morphodynamics. Finally, it was observed that the absence of bank erosion by failure in the model was the cause for the absence of the development of mid-channel bars.

The input of sediment pulses is the main driving factor of the dynamics of the system, but a large uncertainty exists in the forecast of this process. Together with the absence in the model of vegetation and bank erosion by failure, it is impossible to predict the exact morphodynamics with the model. However, the model was able to simulate many local morphodynamics as the incision of new channels, the accretion and erosion of the island heads and the dynamic channel pattern at the inflow boundary. The model can therefore be used to increase the understanding on possible morphodynamics and to asses areas of risk (for erosion or deposition). For engineering purposes the model can be used for the assessment of possible effects of river training works, the locations for dredging and the amounts of sediment to be dredged. To obtain more accurate results with the model, data about sediment transport is needed. Further research on the implementation of sediment pulses at the upstream boundary will be necessary to obtain more realistic dynamics of the system.

Preface

This master thesis is the final product of my master Hydraulic engineering at the Technical University Delft. In this research an analysis is performed on the physical processes influencing the morphodynamics in braided rivers. The analysis is done for a case study on the Ayeyarwady River in Myanmar. I have carried out the thesis in cooperation with Deltares, an institute for applied research in the field of water and subsurface.

After doing an additional thesis at Deltares on modelling of the bedrock channels of the Mekong, I was enthused by the complicated dynamics in rivers and the way in which we can learn about those dynamics with numerical modelling. To enhance my knowledge in the field of river dynamics, I chose to perform my master thesis in this field of research as well. Kees Sloff, Martine Rutten and Alwin Commandeur provided me the subject of investigating the Ayeyarwady River with satellite imagery and the Delft3D numerical model.

Doing research on the Ayeyarwaddy is part of a collaboration between Myanmar and the Netherlands in the field of water management. The focus of this collaboration is to share knowledge on the protection against water, but also the knowledge on how to benefit from the water resources. With this thesis I hope to attribute in this and to bring the country Myanmar a small step closer to their fights against floods and solutions to improve navigability. Therefore, I am grateful to have had the opportunity to go Myanmar and share the learnings in my research on the Ayeyarwaddy. It was a great experience, made possible by the Lamminga fund, to share this knowledge at the Myanmar Maritime University and the Mandalay Technological University, where I found a greatly enthusiastic audience of other potential engineers.

I would like to thank my academic supervisors for their guidance through the process of this research. Kees Sloff shared his extensive knowledge on river hydro- and morphodynamics in rivers, but also how this is implemented in the Delft3D model. I especially enjoyed the discussions we had to show our results when we worked on the analysis parallel, you for the project and me for my research. To escape from the details of the processes and models, I could always go for council to Martine Rutten. She helped me in finding the ways to analyse the results. As head of the committee, Wim Uijttewaal was there to steer the process in the right direction.

I am also grateful to the Deltares employees who helped me. Gennadii Donchyts, as experts in the Google Earth Engine, was a pleasure to work with. I enjoyed your enthusiasm on the opportunities there are with the Google Earth Engine. This really helped me to make the analysis I performed. Frank Platzek, many thanks to you for working on the Delft3D model with moving bank lines. Unfortunately, it was not possible to make the model workable before the end of my research, but I really appreciate the work you did. Others who were always there to answer my additional questions were Sanjay Giri, Amgad Omer and Willem Ottevanger. Thank you all for your help.

Dook Ligthart
Delft, July 6, 2017

Contents

Nomenclature

Abbreviations

DEM	Digital elevation map
DMH	Department of meteorology and hydrology
DWIR	Directorate of water resources and improvement of river systems
GEE	Google Earth Engine
MBCCDL	Mandalay business capital city development ltd.
MNDWI	Modified normalised difference water index
NDVI	Normalised difference vegetation index
NDWI	Normalised difference water index
NIR	Near infrared
RGB	Red, green and blue
RVO	Rijksdienst voor ondernemend Nederland
SNG	Short wave infrared, near infrared and green
SRTM	Shuttle radar topography mission
SWIR	Short wave infrared
TIR	Thermal infrared
TM	Termal mapper
TOA	Top of atmosphere
USGS	United States geological survey

Symbols

α	-	Calibration parameter sediment transport formula
ϵ	m/s	Erosion rate
κ	-	Von Karman constant
λ_p	-	Bed porosity
$\triangle$	-	Relative density
ϕ_τ	$^\circ$	Bedload transport direction
ϕ_s	$^\circ$	Final direction bedload transport
ρ	kg/m^3	Density water
ρ_{green}	-	Intensity green radiation
ρ_{nir}	-	Intensity near infrared radiation
ρ_s	kg/m3	Density soil
ρ_{swir}	-	Intensity short wave infrared 1 intensity
θ_{cr}	-	Critical mobility parameter
τ	N/m^2	Shear stress
τ_c	N/m^2	Critical shear stress

θ	-	Shields mobility parameter
A_{shield}	-	Calibration parameter bed-slope effect
B_{shield}	-	Calibration parameter bed-slope effect
C	$m^{1/2}/s$	Chézy roughness coefficient
C_{shield}	-	Calibration parameter bed-slope effect
D	m	Particle diameter
D_{shield}	-	Calibration parameter bed-slope effect
D_{50}	m	Median particle diameter
D_i	m	Particle diameter of fraction i
E_{spir}	-	Calibration parameter spiral flow
F_x	-	External forcing in x-direction
F_y	-	External forcing in y-direction
g	m/s^2	Gravitational acceleration
h	m	Water depth
i	-	Bed slope
i_w	-	Free surface water level slope
I_s	m/s	spiral flow intensity
k_d	m^2s/kg	Erodibility coefficient
k_s	m	Nikuradse roughness height
q	$m^3/s/m$	Specific discharge
q_s	$kg/s/m$	Specific sediment discharge
Q	m^3/s	Discharge
S	kg/s	Sediment discharge
s	$kg/s/m$	Specific sediment discharge
u	m/s	Flow velocity (in x-direction)
U	m/s	Depth averaged flow velocity
v	m/s	Flow velocity in y-direction
V	m^2/s	Horizontal eddy viscosity
x	m	x-coordinate
y	m	y-coordinate
z_b	m	Bed level
z_w	m	Free surface water level

Chapter 1

Introduction

1.1 Context

1.1.1 The Ayeyarwady River

Myanmar, a developing country in South East Asia, is a place where the large navigable network plays an important economic role. Since ancient times, the many rivers and creeks are used for most of the transport (Nam and Win, 2014), leading to densely populated areas along the waterways. The longest river in Myanmar, the Ayeyarwady River, is flowing from the North to the South of the country and connects important cities such as Yangon and Mandalay, as displayed in Figure 1.1. The river offers the possibility of relatively low cost transport between the cities, but is also a connection with the countryside and China.

Besides that the river is of large economic value, the Ayeyarwady River is also of great risk for the country and its population. The heavy monsoon rain provokes severe river floods. Between wet and dry season, discharges can vary a factor ten, causing water level differences up to twelve metres (Commandeur, 2014). Yearly, numerous villages are flooded and destroyed. According to Floodlist (2016a), 1.5 million people were affected by the floods in 2015. During the period of June till half August 2016, also almost half a million Myanmar citizens were affected by floods (Floodlist, 2016b). In Figure 1.2, it is clearly visible that most of these fatalities are around the Ayeyarwady River. The river floods are due to the large hydrological variations. These variations, together with an abundance of relatively small and non-cohesive sediment, induce the dynamic braided behaviour of the river, characterised by fast moving bars and channels. The fast moving channels are of large danger for many villages (Ko, 2016).

In addition to the problems with big floods and erosion, the navigability of the Ayeyarwady River is not as desired (RVO, 2015). With the on-going growth of the total transport in the country, the improvement of inland water infrastructure has a high potential (Nam and Win, 2014). The problems around navigability are threefold, all caused by the discharge difference during the wet and dry season (van der Velden, 2015). With low water, during the dry season, the navigable depth is too low at several locations. Therefore, passing lanes are blocked. In the wet season, with high water, the flow velocities can be very high, leading to very dangerous situations. Also the braided behaviour (the behaviour of shifting channels around alluvial islands) of the river causes problems for the navigability. After every wet season, the exact location of the main navigable channel is hard to predict.

To improve the situation around the Ayeyarwady, it is expected that several projects will be

Figure 1.1: Map of Myanmar showing the Ayeyarwady and main cities

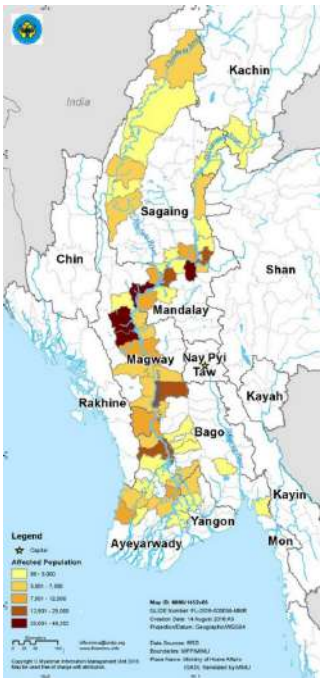

Figure 1.2: Map of Myanmar showing affected population in the different areas hit by floods in 2016 (Floodlist, 2016b)

released in the period of 2017-2020 by the World Bank (World Bank, 2016). Also the European Union and the Dutch government are investing in the river system of Myanmar, which all emphasizes the importance of some structural change. Due to the investment done by the Dutch government, in particular the Netherlands Enterprise Agency (Rijksdienst voor Ondernemend Nederland, RVO), many Dutch companies are also involved in the improvement projects of the river (RVO, 2016). Examples of these companies are Deltares, Arcadis and Royal HaskoningDHV. Two examples of projects in the Mandalay region (see Figure 1.1) are the Amarapura urbain floodplain development project and the World Bank navigational project. With the first, a floodplain will be urbanized. Therefore, the floodplain has to be protected against river floods. The latter has as goal to ensure a certain minimum navigable depth around Mandalay. In order to find suitable and sustainable solutions with these type of projects, it is important to understand the complex dynamics of braided rivers. An example of a river training measure where the river dynamics were insufficiently understood is displayed in Figure 1.3. This picture is made near Mandalay and shows how a shift of one of the channels in a braided reach of the Ayeyarwady found a way around a barrier, completely undermining the functioning of the barrier. With a better understanding of the morphodynamics and underlying processes, interventions in the river can be made in a more effective manner to avoid these type of situations.

For this thesis it is important to clarify the use of several terms. With morphology is meant the bed topography at a certain moment in time. The change or the development of the morphology is referred to as morphodynamics. Further is also spoken about the dynamics of the river (or the system), which is used for the extent in which the river changes.

Figure 1.3: Bypassed barrier after a shift of a channel in the braided river the Ayeyarwady (January, 2017)

1.1.2 Research on braided rivers

Braided rivers are studied all over the world, concerning subjects as flood risk, navigability and ecology. The understanding has developed the past decades using flume experiments (Ashmore, 1982; Ferguson, 1993), field observations (Ferguson et al., 1992; Mosselman, 2009; Baki and Gan, 2012) and to a lesser extent numerical modelling (Schuurman et al., 2013; Nicholas, 2013; Yang et al., 2014; Williams et al., 2016). Flume experiments proved to be very useful to explore singular processes, such as vegetation (Gran and Paola, 2001), bar movement (Ferguson, 1993) and the importance of bedload fluxes for the morphodynamics (Ashmore, 1987). However, limitations are there on spatial and temporal scale, based on the space and time required to perform the experiments. Scaling is of course an option, but this comes with simplification and abstraction from reality (Peakall et al., 1996). For field measurements limitations on spatial and temporal scale also exist. Because large variations are found in the extensive braided rivers, large amounts of samples are needed in space and time to create a reliable dataset (Ferguson et al., 1992). With the development of technologies such as multibeam echo-soundings and airborne and terrestrial LiDAR, more accurate data could be obtained, but with these costly measurement methods it is hard to cover the change in time. The low availability of data forms one of the the main problems in the study of braided rivers (Surian, 2015).

To cover the development of braided rivers in time, historical maps, aerial photographs and satellite data are a valuable source. Baki and Gan (2012), Wang et al. (2014), Pahlowan and Hossain (2015) and Bhunia et al. (2016) are examples where satellite data is used to determine bank migration rates. They found that vegetation, island size, bank material and human interventions are the main influencing factors of these rates. Donchyts et al. (2016a) did not investigate river morphology in specific, but used the Google Earth Engine (GEE, a processing platform for satellite data) to determine land-water surface change for the whole world. This is very useful for the study on braided rivers. Using the GEE and the method of Donchyts et al. (2016a) gives the opportunity to calculate cloud free images, automatically detect the water surface, calculate bank migration rates, determine the quality of vegetation, etc. The limitation of satellite data is that it only contains information of the earth surface and not the bathymetry below the surface. Combining satellite data with other sources of information (a model for example) could be very valuable. Ziliani and Surian (2012) used a numerical cellular model (CAESAR) to provide extra information on his observation of the land surface. He only used aerial photographs instead of satellite data. By combining the time development observed from the aerial photographs and the results from the model, they where able to estimate bedload transports of the river. The model was also very useful to increase the understanding on the development in between two aerial photographs. It did not only fill the gap of data in between the aerial photographs, but it also returned extra information about depth development of the channels. Van der Velden (2015) also performed a combined analysis (the numerical model Delft3D as support for observations from satellite imagery) for research on navigability of the Ayeyarwady. However, the model had limited additional value, since no bathymetric data was available. The focus was more on the

interaction between changes in the planform (as observed from satellite imagery).

According to summarizing studies of Surian (2015) and Williams et al. (2016), numerical modelling shows high potential by creating new data and having less limitations on spatial and temporal scale. Schuurman et al. (2013) and Yang et al. (2014) are examples where datasets were created for further analysis, using physics-based numerical models of straight river reaches. However, with the Delft3D-software, used by Schuurman et al. (2013), dry banks cannot be eroded, and also vegetation is not included. The model in Yang et al. (2014) misses a formulation for spiral flow. Even though not all important processes are represented in these models, application on braided rivers showed to be a valuable method to obtain information about river development. In Schuurman et al. (2016a) for example, the numerical model is used to look at the effects of river training measures on the development of the planform. More complete models are used by Jang and Shimizu (2005) and Nicholas (2013), which also include bank erosion and vegetation processes. What is still lagging, is that the calibration, validation and sensitivity analysis on 'real' rivers with all these models has been limited (Surian, 2015; Williams et al., 2016). Surian (2015) adds to this that improvements have to be found to create later mobility of the channels and islands in the models. He also mentions that the connection between models and the other approaches (flume experiments, field measurements, satellite data) is still lacking. He also states that attention is needed for a correct implementation of the processes in the models. Another problem with the simulation of braided rivers, is that they are relatively wide. To keep the computational time workable (within a week), the river length that can be simulated is limited. This limitation is also there in the use of 3D simulations.

1.2 Problem definition

The Ayeyarwady River is a river with large hydrological variations and an abundance of relatively small non-cohesive sediment, causing the dynamic behaviour of the river with fast shifting channels. This dynamic behaviour, together with large hydrological variations, is the source of a frequently flooding river with a moderate navigability. In order to reduce flood risk and to improve navigability, river training measures and sediment management are needed. For an effective and sustainable implementation of measures, one has to be able to predict the effects of these measures. For braided rivers, of which their behaviour is regarded as complex and hard to predict, this still remains challenging. It requires a good understanding of all the processes playing a role in the morphodynamics of the river.

To gain more knowledge on how these physical processes play a role in the morphodynamics of braided rivers, the use of physics-based numerical models shows high potential. They are very useful in the investigation of processes on reach scale. Processes can be adjusted, which gives the opportunity to investigate them. However, calibration and validation on 'real' rivers has barely been done in the past. This means that the actual performance of the model still has to be tested. In addition, not all processes important for braided river dynamics are included in the available model software Delft3D. Bank erosion of dry banks and vegetation are not included. The limited amount of data available on sediment transport is another problem in the simulation of the behaviour of the Ayeyarwady River. This brings uncertainty in the results of the model, which also has to be explored.

1.3 Goal

The understanding of the physical processes in braided rivers causing the morphodynamics remains limited. Because this understanding is needed to find suitable and sustainable solutions to reduce flood risk and improve navigability, this study focusses on a better understanding of these physical processes. The goal of this study exists of two parts, both with focus on the research area as given in Figure 1.4. The first part is to explore the most relevant physical processes and their effects on the morphodynamics and the second part is to investigate the ability of a 2D morphodynamic model to simulate the morphodynamics to make reasonable predictions. The following sub questions should be answered to reach the goal:

- Which are the most important physical processes in the morphodynamics of braided rivers?
- What morphodynamics can be observed in the research area from satellite imagery?
- What physical processes have the largest influence on the dynamics of the Ayeyarwady River?
- What physical processes have the largest influence on the morphology of the Ayeyarwady River?
- What is the predictive value of a 2D morphodynamic model for the simulation of morphodynamics in the Ayeyarwady River and which physical processes play a role in this?

Figure 1.4: Map showing the research area of this study

1.4 Thesis outline

The analysis is performed in four steps. The first step, presented in chapter 2, is a literature review on the main processes playing a role in the morphological development of a braided river. In this chapter is explained how these processes work, what the consequences of these processes are on braided rivers and, where necessary, with what kind of formulations these are implemented in the 2D depth-averaged Delft3D model. This chapter is followed by an analysis of the system in chapter 3. This contains a global review on the complete river system, including climate and flooding and navigability problems of the Ayeyarwady River. The research area will be analysed in more detail. Different available data is discussed here and also observations from satellite imagery are described. The study on the morphological changes forms a basis for the interpretation of the model results. In chapter 4, a sensitivity analysis with the Delft3D model is performed to explore the effects the different physical processes have on the morphodynamics. Not all processes discussed in chapter 2 can be implemented in the Delft3D model, which is why these processes are tested in a different way in chapter 5. With a combined analysis of satellite images and the model these processes are evaluated. The report concludes with a discussion and conclusion and recommendations.

Chapter 2

Physical processes in morphodynamics of braided rivers

Morphodynamics are a function of many different physical processes. To understand the dynamics of the system, it is essential that these processes are understood. In this chapter, the most important of these physical processes in braided rivers are explained from literature. A distinction is made between system forcing processes and internal flow and sediment transport influencing processes. The system forcing processes are imposed by the system, so by the climate, soil structure, vegetation, etc. How these processes occur in the research area is investigated in chapter 3. The internal flow and sediment transport processes are a consequence of the system forcing processes and cause the actual change in morphology. The different processes are summarized in table 2.1.

Table 2.1: Main morphodynamics influencing physical processes in braided rivers, divided into system forcing processes and internal flow and sediment transport processes.

	Process		
System forcing processes	Hydrological variations		
	Sediment input in the system		
	Availability erodible sediment		
	Bed roughness		
	Vegetation		
Internal flow and sediment transport influencing processes	Transport by primary flow	Total load	Bedload
			Suspended load
		Wash load	
	Transport by spiral flow		
	Turbulent flow	Effects of dunes	
		Confluence scour	
		Eddies	
	Bed-slope effect		
	Bank erosion	Fluvial erosion	
		Geotechnical instability	

2.1 System forcing processes

The hydrological variations, the input of sediment in the system, the availability of erodible sediment, the bed roughness and vegetation belong to the system forcing processes. All available data of how these processes occur in the research area is discussed in chapter 3. In this section is explained why and how these processes have an effect on the morphodynamics in braided rivers.

2.1.1 Hydrological variations

As well in laboratory experiments (Ashmore, 1982; Jang and Shimizu, 2005) as with numerical models (Schuurman et al., 2013), braided river patterns were established with a constant discharge on a flat bed. This demonstrated that a variation in discharge is not a prerequisite for braiding. This does, however, not mean that the variations in discharge is of no importance for the development of the braided planform. Richard and Julien (2003) explained for example, that a change in both the water and sediment regime could lead a large change in planform. With the implementation of a dam, a part of the Rio Grande (New Mexico) changed from a braided river into a single-thread straight and meandering river. This dam reduced only the largest peaks in discharge, which was already enough to change the whole system. Large peaks in discharge could for instance cause the removal of vegetation (Gurnell et al., 2001), which increases the movability of the system. Large peaks could also lead to the flooding of usually not submerged areas, leading to erosion of islands and bars or incision of new channels.

Not only large peaks are important considering the morphological change. The four different stages in the hydrograph, the falling stage, low water period, rising stage and the high water period, all show different flow distributions and so have a different effect on sediment transport. With model studies van der Velden (2015) and Yang et al. (2014) found that new channels were especially created during the falling stage. Coleman (1969) also observed this in the field. He explained that large amounts of bedload and suspended load are deposited during the falling stage due to the rapid decrease in flow velocity during the falling stage. This has as consequence that bars can be created. By blocking existing channels or deviating the flow direction, the bars enhance the incision of new channels. During falling stages the probability at instability and collapse of the banks is also largest (S. Giri, personal communication). During high water the soil in the banks saturates. When the water level decreases faster than the water can flow out of the bank, shear strength in relatively low (due to the pore water pressure) and the bank relatively heavy, which gives a higher probability of collapse. During low flow stage, solely erosion and sedimentation takes place within the channels. The main channels in braided rivers are commonly slightly curved, moving from one bank to the other. When only these channels are submerged, the river seeks for a path with little curvature. This leads to straightening of the thalweg. During rising stage, the increase in discharge has to be accommodated in the river. This has widening and deepening of the channels as consequence. With the channel approaching the banks in a slight angle, undercutting of the banks could also be found (Coleman, 1969).

2.1.2 Sediment input into the system

Sediment transport rates in braided rivers vary largely in space and time. Coleman (1969) and Chein et al. (1961) already mentioned the importance of fluxes in sediment transport as an important factor for braiding of rivers. Schuurman et al. (2013) created a braided planform without fluxes in sediment transport at the upstream end of the system, but the mobility of this system decreased significantly after the the braided planform was established. Ashmore (1987) showed in his laboratory study that the fluxes in sediment transport indeed are important for the dynamics in braided rivers. A sediment wave enhances local aggradation, leading to the creation of bars and new channels in the surrounding. After passing of the sediment pulse,

erosion can be found again. The eroded material is deposited again in other aggradation sites, where also bars will be created. In this way the sediment pulses propagate through the system.

Similar to the observations of Richard and Julien (2003) as discussed in the previous section, many other dams also reduced the braiding activity in rivers in the Alps. Marti and Bezzola (2009) investigated this in flume experiments, where a reduction in fluxes and quantity of bedload transport lead to the creation of a single channel system from a braided planform. They also noted that the transport in a single incised channel is larger than for the multiple small channels together. With the sediment transport depending on the cross-sectional area of existing channels, this means that fluxes in sediment transport are created by growth, closure and incision of channels as well. Where in an active braided river channels grow, close and incise continuously, it amplifies its own activity again. Marti (2002) adds to this that large fluxes also arise whit the failure of banks.

2.1.3 Availability of erodible sediment

For the dynamics in a braided river it is essential to have a wide non-restricted channel bed with an abundance of erodible sediment (Coleman, 1969; Chein et al., 1961). Logically, a low availability of erodible sediment reduces the mobility of the system. Availability of sediment could be decreased with non-erodible layers close to or at the bed, but also due to hiding and exposure or armouring phenomena. Erodibility is another property that determines whether erosion occurs. For this, a first distinction can be made between cohesive and non-cohesive soil. The most cohesive soil type, e.g. rock, is hardly erodible and does in this case already mean an unavailability of the sediment. Less cohesive soil types are mud, clay or silt, but also mixtures of sand and clay or silt can be very cohesive. Van Ledden (2003) describes that already small amounts (from 3%) can cause a critical erosion stress of 2 - 5 times higher. Solely larger particles as sand or gravel are more easily erodible. For the dynamics in braided rivers, an abundance of these sediment types is needed.

2.1.4 Bed roughness

The bed roughness is determined by the composition of the bed. Different sizes or types of sediment have a different influence on the bed roughness. Large gravel particles for example induce more bed resistance than for example fine clay. This resistance causes a shear stress on the bed, which largely influences the flow distribution and the sediment transport. Whether an increase in bed shear stress has an increasing or decreasing effect is location specific. A larger bed shear stress causes deceleration of the flow, which reduces sediment transport. On the other hand, larger forces can be found on the particles, which has an increasing effect on the sediment transport. This makes it hard to determine in advance whether sediment transport will increase or decrease with a increase in bed roughness.

When modelling the flow in a river with Delft3D, not only the bed composition is important for the bed roughness. Factors as dunes and vegetation also form a resistance on the flow. Because these factors are mostly subgrid, they are included in the bed roughness. Different bed roughness models can be used within the Delft3D model. It is possible to use a uniform Chézy value. Other options are to use White-Colebrook or Manning, which both are depth dependent. The formulation for Manning reads:

$$C = \frac{h^{1/6}}{n} \tag{2.1}$$

and for White-Colebrook:

$$C = 18log_{10}\left(\frac{12h}{k_s}\right) \tag{2.2}$$

Where C is the Chézy roughness coefficient $[m^{1/2}/s]$, n the Manning coefficient $[-]$, h the water depth and k_s the Nikuradse roughness height $[m]$. Both relations have as result that the bed roughness is larger in shallow areas than in deep areas. According to E. Mosselman (personal communication, 2016), does the use of a different roughness model in large sand-bed braided rivers (as the Ayeyarwady) give better estimations of the sediment transport. A better fit for the bed roughness would be:

$$C = \frac{h^{1/2}}{n} \tag{2.3}$$

However, this cannot be implemented in the Delft3D model. For this reason, this different bed roughness model is incorporated in a different sediment transport formula. This is explained in more detail in section 2.2.1.

2.1.5 Vegetation

Vegetation has a twofold effect on the sediment transport. With roots it keeps the sediment together, inducing a reduction of the availability of sediment. In addition, it also pushes the high-velocity field away from the bed. This leads to a decrease in stress on the bed particles (Thorne and Furbish, 1995). Both the decrease in available sediment and the reduction of shear stress in the particles have a sediment transport decreasing effects. These effects are also mentioned in the previous two sections, but because vegetation influences both, it is mentioned as a separate process. Gran and Paola (2001) investigated the effect of vegetation in a flume experiment. They specifically looked at the stabilizing effect on banks. This stabilization of banks causes a lower lateral mobility of the system. However, vegetation can also be found on the bed. This is for example the case on the islands when these are submerged. The vegetation will than have a stabilizing effect on the islands.

The stabilizing effect of vegetation forms a restriction for the river to change. Where, as mentioned in section 2.1.3, it is essential for the dynamics in a braided river to have a wide non-restricted channel bed, the vegetation has a dynamics reducing effect in braided rivers. Pahlowan and Hossain (2015) also found this in the braided Jamuna River, where vegetated banks shifted slower than unvegetated banks. Vegetated banks can shift due to failure of the bank or by removal of the vegetation under large flow velocities.

2.2 Internal flow and sediment transport processes

Internal flow and sediment transport processes are a result of the system forcing processes. Belonging to these processes are: sediment transport by primary flow, sediment transport by spiral flow, sediment transport due to turbulence, effect of bed slopes on the sediment transport and the erosion of banks.

2.2.1 Sediment transport by primary flow

Sediment transport by primary flow can be divided in three types of load, namely bedload, suspended load and wash load. Wash load is the suspension of very small particles with very large adoption lengths. This material does by definition not interact with the bed and has therefore no influence on the bed development. In contrary, bedload and suspended load do have a large influence on the development of the bed. Together they form the so called total or material load (Delft3D-FLOW manual, 2016).

The primary flow induces sediment transport when a certain bed shear stress is reached. Shields (1936) described a dimensionless parameter to determine the initiation of motion of a non-cohesive particle. The formula to calculate this parameter, θ $[-]$, is derived from a equilibrium

of forces and reads:

$$\theta = \frac{\tau}{(\rho_s - \rho)gD} \tag{2.4}$$

With τ the bed shear stress $[N/m^2]$, ρ_s the density of the sediment $[kg/m^3]$, ρ the density of the water $[kg/m^3]$, g the gravitational acceleration $[m/s^2]$ and D the diameter of the sediment $[m]$. Incipient motion can be found for a critical value for θ. This θ_{cr} can be determined from the Reynolds number. With relation 2.4, the critical shear stress can be determined from θ_{cr}. So for the movement of a particle, a certain shear stress is necessary. These shear stresses are a function of the flow velocity and bed roughness, which are used in many sediment transport estimators for flows. Examples of these estimators for non-cohesive sediment transport in rivers are the Engelund and Hansen formula (Engelund and Hansen, 1967), the Meyer-Peter & Müller formula (Meyer-Peter and Müller, 1948) and van Rijn formula (Van Rijn, 1993). The transport of sand or gravel is based on a capacity of the flow to carry the sediment, with exchange and interaction between the sediment in the bed and in the flow. The capacity is what is calculated with the sediment transport estimators. In section 2.1.4 was explained that a different sediment transport formula is used for this study to incorporate a different roughness model. A basic formulation for sediment transport is:

$$s = m \cdot u^n \tag{2.5}$$

where s is the specific sediment discharge $[m^3/s/m]$, m a coefficient depending on the sediment diameter, bed roughness, relative density and gravitational acceleration, u the flow velocity $[m/s]$ and n the coefficient determining the power above the velocity $[-]$. With $n = 5$ this formulation is the Engelund and Hansen formula. To incorporate the bed roughness model that is more likely for large sand-bed rivers, as given in equation 2.3, n has to be lower than five. A minimum value for n is three. For lower values of n, the sediment would be more movable than water, which is off course impossible. The complete derivation of this sediment transport formula with lower power above the velocity is given in section C.2.4.

Where the sediment transport estimators determine a capacity op the flow to carry the sediment, a too low availability of non-cohesive sediment can be a limiting factor (see section 2.1.3). For transport of cohesive sediment this is different. Here the transport of sediment is not determined by the capacity of the flow to carry this sediment, but by the ability of the flow to erode this sediment from the bed. Subsequently, sediment transport formulations for cohesive sediments are different than for non-cohesive sediments. These transport formulations are based on a capacity for erosion.

The transport of sediment is highly non-linear, which also can be seen in the sediment transport formulas. With significant spatial and temporal differences in flow velocity in braided rivers, even larger fluxes can be found in the sediment transport. The fluxes in sediment transport lead to deposition and erosion, causing changes in the bed. This can be explained with the Exner equation:

$$\frac{\partial z_b}{\partial t} = -\frac{1}{1 - \lambda_p}\frac{\partial s}{\partial x} \tag{2.6}$$

with z_b the bed level $[m]$, λ_p the bed porosity $[-]$ and s the specific sediment discharge $[m^3/s/m]$. This equation shows the bed level change is determined by a flux in the sediment transport. Examples of bed level changes are the creation and movement of bars or the incision of new or deepening of existing channels. These changes are all very typical in braided rivers, which means that sediment transport plays an important role here. How fast and where these changes occur, is dependent on for example the discharge, the availability of erodible sediment or the presence of vegetation.

2.2.2 Sediment transport deflection by spiral or helical flow

Spiral flow is found in curvatures of the flow. It can be described as a circling flow through the bend, as shown in Figure 2.1. Together with the primary flow, it forms a helical flow through the bends. Spiral flow only causes a deflection of the sediment transport by primary flow, because it is much weaker then the primary flow. The deflection of the the sediment transport is towards the inner bend, causing deepening of the channel at the outer bend (1). More sediment deposits in the inner bend, forming point bars (2). In addition of moving the sediment from the outer bend to the inner bend, deepening of the outer part of the channel can also cause of instability of the bank (3). In these ways, the spiral flow contributes to the lateral movement of the channels. In braided rivers spiral flow is found at many locations in the complex system of bifurcating and joining channels. The many bars are also a cause of the curvature of the flow. This curvature of the results in spiral flow, with leads to a deflection of the sediment transport. Schuurman et al. (2013) also emphasizes the importance of spiral flow for the development of bars and channels in braided rivers. Without spiral flow, the development of bars and channels was slower.

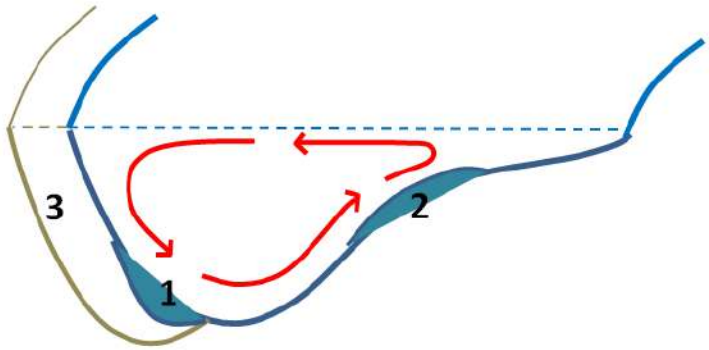

Figure 2.1: The effect of spiral flow on morphology in a bend

In depth-averaged computations in Delft3D the direction of the bedload transport as combination of primary and spiral flow is calculated following:

$$tan(\phi_\tau) = \frac{v - \alpha_I \frac{u}{U} I_s}{u - \alpha_I \frac{v}{U} I_s} \tag{2.7}$$

in which:

$$\alpha_I = \frac{2}{\kappa^2} E_{spir} \left(1 - \frac{1}{2} \frac{\sqrt{g}}{\kappa C}\right) \tag{2.8}$$

where v is the flow velocity in y-direction $[m/s]$, u the flow velocity in x-direction $[m/s]$, U the depth-averaged velocity $[m/s]$, I_s the spiral flow intensity $[m/s]$, C the Chézy coefficient $[m^{1/2}/s]$, g the gravitational acceleration $[m/s^2]$, κ is the Von Kármán constant $[-]$ and E_{spir} the user defined calibration coefficient for the spiral flow $[-]$.

2.2.3 Turbulent flow

Turbulence exists on different scales. The largest scales of turbulence found in braided rivers is the one around the large islands and in confluences. Going smaller, turbulence can be found around the bars, discontinuities at the bank or around structures. Even more in detail, one can find turbulence around dunes, in the mixtures of suspended sediment and for example around the particles in the bed. All these types of turbulence disturb the flow, having an effect on the sediment transport. These effects are expressed in different ways. Turbulence around particles in the bed and dunes cause for example the bed shear stress, turbulence in a suspended sediment mixture plays a role in the advection and diffusion of the mixture, and turbulence on larger

scales gives direct change in the flow patterns with scour or deposition as results. In this way, turbulence on all scales plays a role in the transport of sediment. Scour and deposition due to turbulence can also have large affects on the channel system. Where scour holes can attract the channels, deposition areas can deflect the channel direction.

Turbulence models in Delft3D are all based on the eddy viscosity concept. Decreasing viscosity enables larger differences of flow velocities within the flow, so more sensitivity to small deviations in the channels. However, it remains difficult to capture the effects of turbulence with a depth-averaged model on reach scale, due to the simplification for the determination of the flow field.

2.2.4 Bed-slope effects

With the bed slope-effect is meant: the influence of gravitational force on the movement of sediment particles on a slope. On a flat bed, the gravitational force has no component in a direction in which the sediment particle could move. The gravitation is only a resistance on the movement of the particle (as in Shields formula, equation 2.4). However, on top of a slope, the gravitational force does have a component in a direction in which the particle could move. Both situations (a particle on a flat bed and on a slope) are illustrated in Figure 2.2. In this figure the component in direction of the slope is marked with $F_{z,s}$. With an increase of angle α, the force $F_{z,s}$ also increases. Until the moment the angle reaches a magnitude of the angle of internal friction of the bed material, the particle will not move without external force. However, it does reduce the stress needed for incipient motion. In this way the slope does influence the transport of the sediment. Just like with spiral flow, the bed-slope effect deflects the direction of the sediment transport. For the bed-slope effect, this deflection is in the direction of the downstream slope. The effect of the slope on the sediment transport works in both the direction of the flow and in the transverse direction. In principle, this effect flattens the whole morphology.

Although the physical explanation of this process is straightforward, the implementation of this process in numerical models is not. Several methods can be used to determine this effect, of which the one of Talmon et al. (1995) is used in this study. The set of equations to determine this effect reads:

$$tan(\phi_s) = \frac{sin(\phi_\tau) + \frac{1}{f(\theta)} \frac{\mathrm{d}z_b}{\mathrm{d}y}}{cos(\phi_\tau) + \frac{1}{f(\theta)} \frac{\mathrm{d}z_b}{\mathrm{d}x}} \tag{2.9}$$

in which:

$$f(\theta) = A_{shield} \theta_i^{B_{shield}} \left(\frac{D_i}{H} \right)^{C_{shield}} \left(\frac{D_i}{D_{50}} \right)^{D_{shield}} \tag{2.10}$$

where A_{shield}, B_{shield}, C_{shield} and D_{shield} are user defined variables $[-]$, D_i the median grain size of the fraction $[m]$, D_m the median grain size of the bed $[m]$, θ_i the fraction mobility $[-]$, ϕ_s the direction of sediment transport $[^\circ]$, z_b the bed level $[m]$ and ϕ_τ the direction of the shear stress $[^\circ]$.

How large the effect is on the sediment transport, is hard to determine. The choice of how large this effect has to be in models, remains an arbitrary one (Schuurman and Kleinhans, 2013). Especially in braided rivers, where with the multiple channels and many bars many slopes can be found, this parameters influences the results significantly (Schuurman et al., 2013). It effects the width and depth of channels, the width and height of bars, but is for example also a negative feedback on bar growth.

2.2.5 Bank erosion

Bank erosion is an important process for the lateral movement of the channels. In the Ayeyarwady River bank erosion was found in the field at many locations. Also in other braided rivers, bank

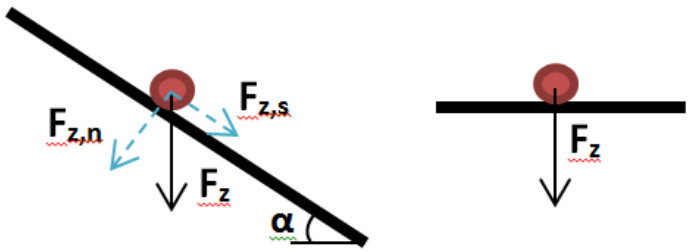

Figure 2.2: The gravitational force on a particle on a slope and on a flat bed

erosion is found in large extent. Examples are the Upper Yellow River (Wang et al., 2008) and the Brahmaputra (Mosselman, 2009; Baki and Gan, 2012). Because bank erosion causes a lateral movement of the channels, it is well observable from satellite imagery (Baki and Gan, 2012; Pahlowan and Hossain, 2015).

Rinaldi and Darby (2007) reflect that bank erosion is a function of three interacting processes, namely weathering and weakening, fluvial erosion and mass failure. Fluvial erosion is the removal of bank erosion by hydraulic forces. A common way to model this erosion is by calculating the erosion rate (Partheniades, 1965):

$$\epsilon = k_d(\tau - \tau_c)^a \tag{2.11}$$

where k_d is an erodibility coefficient $[m^2 s/kg]$, τ $[N/m^2]$ the shear stress on the bank, τ_c the critical shear stress as threshold for erosion $[N/m^2]$ and a an empirically derived parameter (commonly equal or close to 1). Weathering and weakening, together with the soil properties, are included in the parameters k_d, τ_c and a. The critical shear stress is a function of the erodibility factors described in section 2.1.3. With all different existing soil types, compositions of soils and the presence of vegetation, the critical shear stress is a hard to determine parameter. Near bank shear stress is also a complex parameter, with a high variability in space and time. So although the formulation of the bank erosion rate is simple, estimation of bank erosion rates is difficult due to the variability in soil strength and hydraulic forces on the bank.

Mass failure is the failure of large amounts of sediment by gravitational force. Important parameters for mass failure are the soil properties, pore water pressures and the presence of vegetation. Many mechanism for mass failure exist. Coleman (1969) described two main mechanisms in the braided Brahmaputra river, namely shear failures and failures due to liquefaction and flowage of material. Liquefaction and flowage of material is caused by high pore water pressures. This can happen with a rapid decrease of the water level in the channel, or with heavy rainfall. Shear failures occur when fluvial erosion leads to oversteepening or undermining of the bank. Pore water pressures also play an important role here, since they are of large influence on the soil strength. Another factor of influence is vegetation, which is able to keep the soil together. This decreases the probability on as well shear failure, as failure by liquefaction and flowage of material.

In the Delft3D software the process of bank erosion by failure is not described. For braiding it necessary to have lateral movement of banks, which can be both by the failure of banks as by fluvial erosion when islands and bars are submerged. Since the process of fluvial erosion (actually sediment transport by primary flow) is included in the model, lateral movement of the channels can be found in a Delft3D model and the absence of bank erosion by failure does not necessarily have to be a limitation when modelling braided rivers.

2.3 Interconnection of physical processes

In the explanation of physical processes, already many interrelations can be found. Examples are the effect of erodibility and availability of sediment on the sediment transport, but also on bank erosion. Another example is the effect of the input of sediment on the formation of bars, which enhance flow curvature and so spiral flow. The amount of spiral flow could again have an effect on the erosion of banks. In Figure 2.3, the interrelations of the physical processes in the morphodynamics in braided rivers are schematized. The scheme is split in two parts to keep it readable. In the left scheme the interrelations between all physical processes are given, except the ones for the process bank erosion by failure. In the right scheme all additional interrelations between processes are given for bank erosion by failure.

In the left top, the morphology is given. This is not included in the list of processes given above. However, the change in morphology is the result of the interaction between all the processes and also influences these processes. This means that the change in morphology is a continuous process in which all processes induce change, which effects the other processes. In the interaction between the processes, different loops can be distinguished. Some of these loops are given in colours in Figure 2.3. The first loop of processes is given in blue. Here, the morphology together with river discharge, the bed roughness and vegetation determine the distribution of the flow. Flow velocities together with the bed roughness result in shear stresses. The shear stresses force the sediment, if available, to move. Further, does the bed-slope effect also have an effect on the movement of the sediment. The movement of sediment and the input of sediment result in the change in morphology, or the morphodynamics.

Another loop is given in red. The sediment transport gives change in bed composition. The bed composition, together with vegetation (which has the ability to hold the sediment), determine again the availability of sediment, which could limit the sediment transport. Outside of this loop (given in yellow), does the bed composition also influence the bed roughness. Bed roughness has a direct effect on the bed shear stress, but also via the flow distribution. This means taht bed composition influences sediment transport via multiple paths. In green a relatively short loop is given, in which bed-slopes (as part of the morphology) have an effect on the morphology via the sediment transport.

Vegetation is a process that does not completely fit in this scheme, because the main processes for the existence of vegetation, such as climate, are not included in the scheme. Only a limiting factors for vegetation is included, which is the distribution of flow. Very strong flows can remove vegetation and the areas that are always submerged are will have no or different types of vegetation than other areas.

These schemes show that the different processes are related trough different paths, which is what makes the dynamics of rivers so complex. With large variations in the system processes (which are mainly found in the sediment input and river discharge) and the positive feedback between the processes, the system remains dynamic with hard to predict changes due to the different interrelations between the processes.

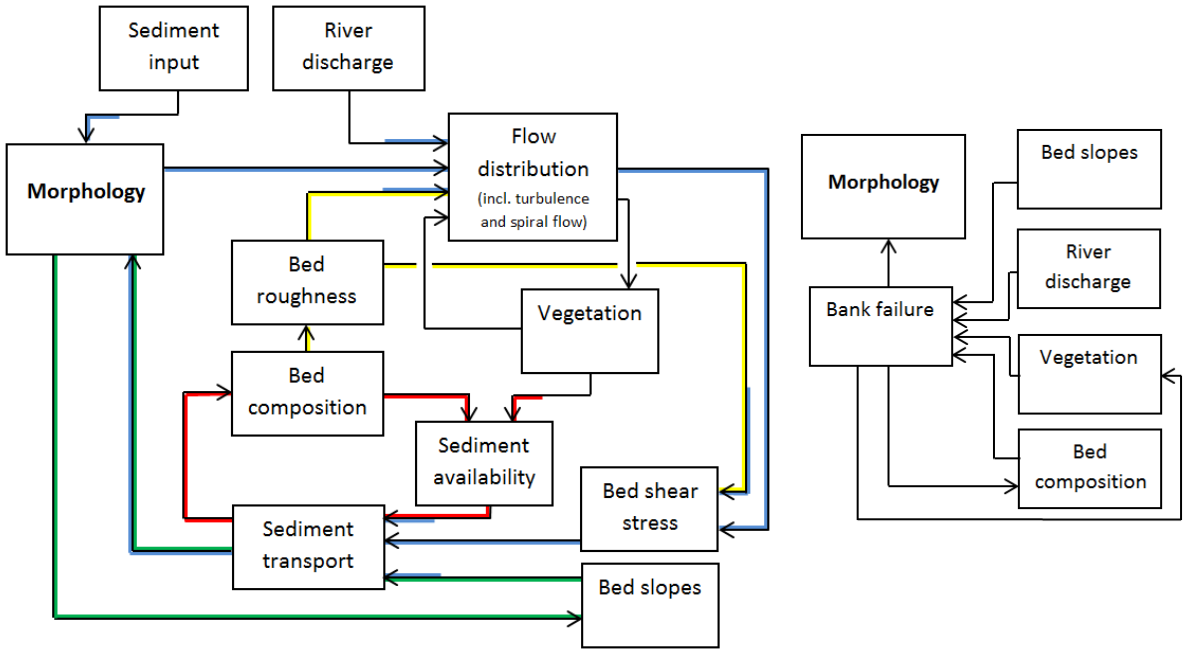

Figure 2.3: Two schemes showing all the interrelations between the physical processes in morphodynamics of braided rivers, with in the right scheme only the interrelations with the physical process bank failure and in the left scheme the interrelations between all the other physical processes (based on Ashworth and Ferguson (1986)). The blue, red, green and yellow paths are examples of loops which show that changes in processes finally affect the processes themselves which keeps the system dynamic.

Chapter 3

System analysis

The Ayeyarwady is the main river of Myanmar, flowing from the North to the South of the country. Main purposes of the river are irrigation, transport and fishing. Industries for timber, rice and sugar, but also for sand mining, cement, oil and gas are located around the river. In addition, it fulfils in daily needs, such as washing. This all underlines the importance and economic value of this river. In the first section of this chapter general information can be found about the river and climate in Myanmar. In the second section, the research area of this study is described in more detail.

3.1 The Ayeyarwady River basin

The country Myanmar is enclosed by mountain ranges, creating a midland at lower altitude. The 2170 kilometres long Ayeyarwady River (World Bank, 2015) begins at the confluence fo the the N Mai Kha River and Mali Kha River, and flows through the lower midland to the Andanman sea. The river is characterised by the large water level differences (Commandeur, 2014) and abundance of non-cohesive sediment (Myanmar geosciences society, 1977) . Straightened, meandering and braided planforms can all be found in the river, leading to a large delta. The river connects the two main cities, Mandalay and Yangon, with each other, with the countryside and with China. The research area of this study is located next to Mandalay, located in the red box in Figure 3.1. The complete braid plain between Singu and Sagaing is of influence on this study area.

Figure 3.1: Map of Myanmar showing the Ayeyarwady, main cities and research area

3.1.1 Climate and discharge

Myanmar has a monsoon climate, which has large effect on the river system. The southwest monsoon, existing from May to October, is the wet and warm season. This season contains almost the yearly amount of rainfall (1760 millimetres) and is followed by the more dry and cold monsoon. This northwest monsoon, lasts over the period of half November to February, when the tem-

perature drops to approximately 20 degrees. After this period the temperature slowly rises again to around 30 degrees, when in May the southwest monsoon starts again (Hadden, 2008). The large rainfall differences for the different seasons cause high discharge and water level differences in the Ayeyarwady. In Figure 3.2 this is clearly visible. From November until July, discharge are much lower and also show less variation, whereas in the wet season very large peaks up to almost 30,000 m^3/s can be found. However, what this graph does not show, is the variation within the year. During the year, many discharge peaks can be observed, which could all be of influence on the dynamics of the river. In Figure 3.3, the discharges for three different years are shown to display the yearly variations. Figure 3.4 shows the development of the average discharge over the years, where a decreasing trend is visible. This decrease can be observed in as well the dry as the wet season. Whether this trend is correct is doubtable, since it is produced from a single discharge-water level relation over the whole period. The discharges are all measured at Sagaing and provided by the DMH (departmant of meteorology and hydrology).

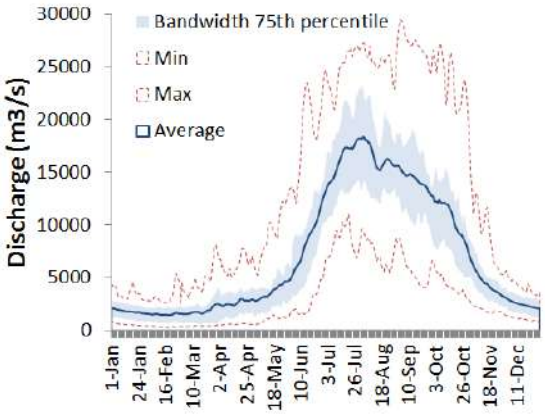

Figure 3.2: Average, minimum, maximum and bandwidth 75th percentile of discharges at Sagaing (DMH, adjusted by I. Niesten)

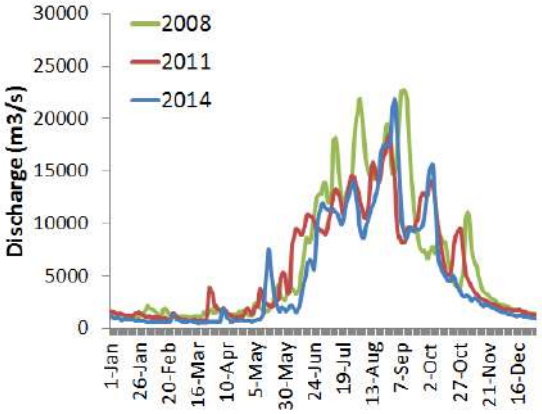

Figure 3.3: Discharges at Sagaing for the year 2008, 2011 and 2014, showing the large variations within the year (DMH)

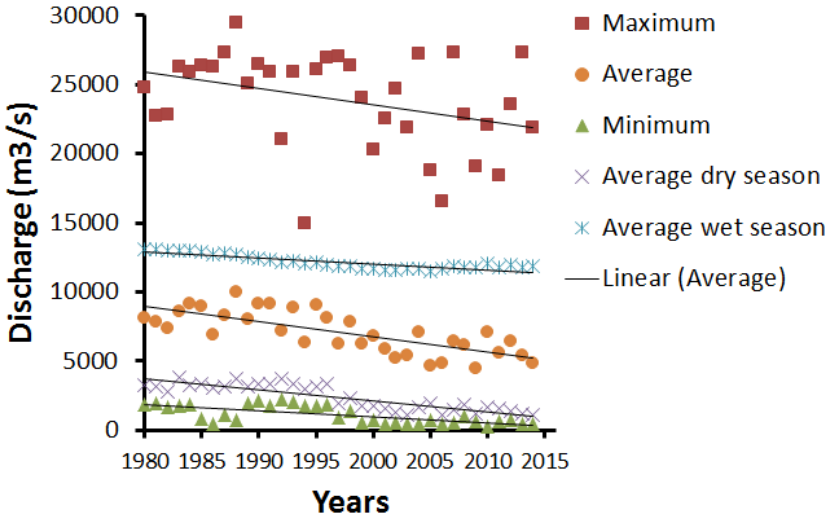

Figure 3.4: Decreasing trend in discharge at Sagaing (DMH). Graph based on daily data, where the wet season is from June to October and the dry season from November to February.

3.2 The research area: the Mandalay river region

This study focusses on the area in the red square in Figure 3.5. The reason to focus on this area, is availability of data. For the Amarapura floodplain development project, depth soundings end height measurements of the islands and floodplains were made. Sediment samples were also acquired, and water levels and discharges are also available. In this section the available data will discussed. In addition to the measurements, satellite imagery is also available. This will be discussed in the remaining part of this chapter.

Figure 3.5: SNG satellite image (dry season 2016) of the research area (red square)

3.2.1 Description of the research area

From around 200 kilometres upstream of Mandalay, the Ayeyarwady follows a defile, which is the reason why this is a relatively straight reach. From approximately 100 kilometres upstream of Mandalay up to Mandalay, a braid plain can be found. The southern part of this braid plain, between Min Kun and where the river turns right, is the research area (visible in Figure 3.5). This area is influenced by the complete braid plain upstream, of which a small part is also displayed in the Figure 3.5. Figure 3.6 shows the area from an upstream perspective. Here it is clearly visible that the research area is enclosed by the city Mandalay and a mountain ridge, limiting the movement of the river to the area in between. Different channels can be distinguished here, with three islands in between.

Studies in in this area show that the presence of sand was the dominant material in the bed, but also a small amount of silt (up to 5%) and gravel (up to 2%) were found (MBCCDL, 2016). The high percentage of sand is necessary for the dynamic behaviour of the river. However, no sediment samples were taken from the bank. At some locations, steep banks caused by bank erosion were observed in the field, as visible in Figure 3.7. Such steep banks suggest some sort of cohesion. Figures 3.8 and 3.9 are both taken at banks, showing the presence of clay and of sand at different banks. With the presence of clay, the sediment type is the cause of the cohesion, where with the appearance of sand, vegetation could have been the cause.

Figure 3.6: Google Earth (version 7.1.5.1557) image of the project area with the view in downstream direction. On the left the city of Mandalay is visible and on the right the mountain ridge. In between the river system is visible, including floodplains and islands

Figure 3.7: A bank of several metres high showing the erosion of banks (January, 2017)

Figure 3.8: Sand found at the bank (January, 2017)

Figure 3.9: Dried clay or mixture of sand and clay found at the bank (January, 2017)

3.2.2 Observations from satellite imagery

In this section, the research area is analysed from satellite data. Data was used of Landsat 4, 5, 7 and 8, which covers the years 1889 to 2016. From Landsat 3 also one useful measurement was available of the year 1975, and one of the year 1977. The data was processed using the Google Earth Engine. Processing existed of two parts. The first part was the creation of cloud free images from all the data available of every dry season. These average reflectance composites are used throughout the whole report and show the average channel pattern as can be observed during the dry season. The assumption is made that during the dry season the water images have a similar wet surface, where there might be some differences when water levels are not te some. The second part was the automatic detection of water according the method of Donchyts et al. (2016b), which is useful for the visualization of water masks in different years. The processing of the data is explained in more detail in appendix A. In the next paragraphs, satellite data is used for observations on system scale. An analysis of mega-scale morphological processes is also done to create an initial understanding of the changes in the system. A summary of the changes is given in this chapter. A detailed description of a sequence of processes is given in appendix B.

Water surface in the wet and dry season

The discharge in the Ayeyarwady varies significantly, leading to large water level differences. From measurements at the water station Mandalay water level differences within a year up to 10.5 metres can be found. In Figure 3.10, the water masks of the river in the wet season (in blue) and in the dry season (in red) for the year 2000 are visible. This year is displayed, because highest quality water mask could be computed here of the wet season due to least cloud cover. With the assumption that water surfaces are similar during during the dry season, this image is still representative to show the difference in water surface between the wet and dry season. All the islands in between the channels are flooded, and also next to Amarapura (see Figure3.5) a large inundated floodplain can be found. The most extensive floodplain is the one on the left side of the river, north of Mandalay (encircled in white). Including this floodplain, a river width up to 12 kilometres can be found.

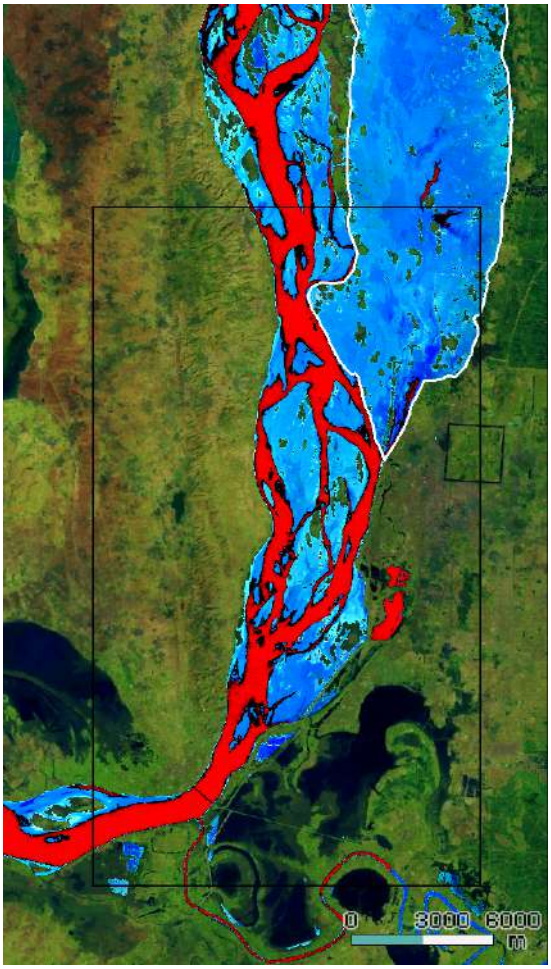

Figure 3.10: Water masks presenting the high (blue) and low (red) water in the year 2015 to show the floodplains, with the black box denoting the research area and the white line to show the large floodplain north of Mandalay

Fixed locations of the river

In the research area the Ayeyarwady is braided with multiple shifting channels and moving bars and islands. It is important to realize that the shift of channels and movement of bars and islands occurs mostly during the floods where the islands and floodplains are fully submerged. Satellite data can be used to find the regions where the river is active and where it is not, by putting the water masks of the different years on top of each other. This is done in Figure 3.11. This figure shows that at the latitude of Min Kun the river is fixed to its location, after which the river trifurcates. Visible as well is that some parts of the islands, but also the floodplain at Amarapura have not been eroded since 1989, even though they are submerged every year during floods. At some parts of the islands quite dense vegetation and even trees can be found, which contributes to the erosion-resistance of these islands. Looking at a map of the year 1914 (see Figure 3.12), assuming the map is correct, the system of islands was completely different. The islands have different shapes and different locations. This means that the soil type is probably not the cause of the erosion-resistance, but that this is solely caused by vegetation.

Mega scale morphological processes

Looking at the complete sequence of low water images, it is visible that the river develops in downstream direction. Bars and islands all move in downstream direction, which happens predominantly during the wet season. In Figure 3.13, five images of the river are shown, displaying the development of the between 1988 and 2016. It contains the research area plus an extension in northern direction of approximately four kilometres. This 'extension' is also displayed, because

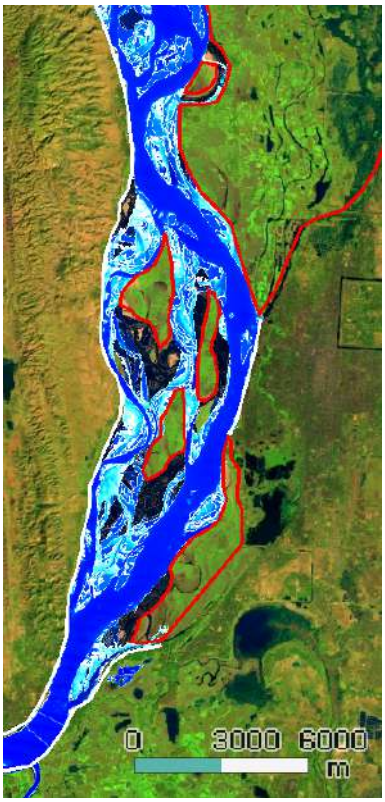

Figure 3.11: A determination of the parts of the river that are fixed to their location: locations that have not been water the past 28 years, are assumed to be hardly or non-erodible.

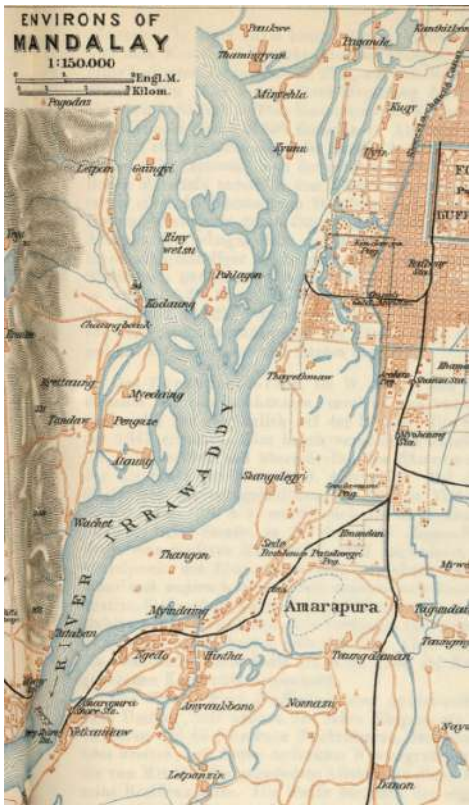

Figure 3.12: Map of Mandalay of the year 1914 showing the different locations of channels and islands (Baedeker, 1914)

it is of importance for the development of the river in the research area as well. In the figures, the borders of the non-eroded floodplains and islands are encircled in red and the non-erodible banks in white. The images area divided in four reaches, all showing a characteristic development. From North to South, these reaches are: the inflow reach, the island heads or trifurcation reach, the middle reach and the confluence reach. All these regions are discussed separately in the coming paragraphs and in the last paragraph the relation between these regions is discussed.

The inflow reach is an active region, influenced by the complete braid plain upstream of it. The main channel shifts over a width of approximately five kilometres, which is visible in the upper part of Figure 3.13. This shifting of the channel is caused by the bars passing by. The moving bars cause erosion at the opposite bank in the channel, more or less pushing the channel into the other bank. After passing of the bar, the banks can move back by accretion. The width of the channel remains approximately constant while the channel shifts, which is the consequence of a combination of processes. Most important of these processes are the hydrological variations, bed-slope effects, spiral flow, sediment transport by primary flow and possibly also bank erosion. The effect of these processes on the channel width are discussed in chapter 4.

The bars move through this reach with a speed around 600 metres per year, changing the channel pattern continuously. At the end of this reach, the easily erodible region narrows, making the channels come together. Especially during high water this results in a local increase in flow velocity. This has as consequence that the bars are largely eroded at this location and a deep stable channel is formed.

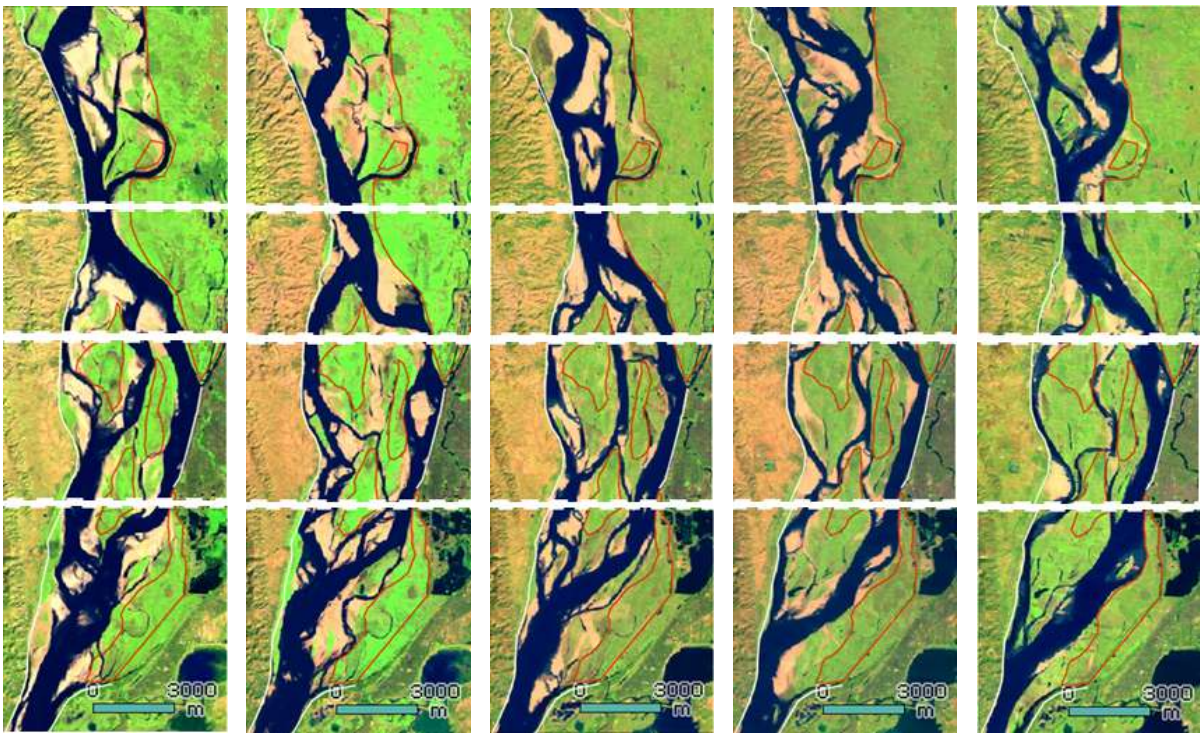

(a) Year 1988 (b) Year 1995 (c) Year 2002 (d) Year 2009 (e) Year 2016

Figure 3.13: Large scale moprhological processes, with in white the non-erodible boundaries and in red the boundaries of non-eroded floodplains. The observed area is divided into four reaches: the inflow reach, the island heads or trifurcation reach, the middle reach and the confluence reach.

The trifurcation reach is where the main channel trifurcates around the heads of the two northern islands in on average three channels. At the beginning of this reach, the region with erodible sediment widens again. This is also the reason why the why channel system widens again and trifurcates. In this widening of the system, the sediment of the eroded bars in the inflow reach can deposit again. The shape of the trifurcation is mainly determined by the location where bars are formed with the deposited sediment. In Figure 3.13b is for example visible that the left channel is forced to the middle of the reach by a large bar on the left. Where the islands heads erode in time, growth of the islands in upstream direction is only possible by collision of these new created bars with the islands. The bars not colliding with the islands pass by to the moprhological most active channel of the middle reach.

The inflow direction in this reach changes with the change in channel pattern in the inflow reach. Together with the development of bars, this changes the positioning of the trifurcation and so the distribution of discharge over the three channels. This is of major importance for the change further downstream.

The middle reach is a relatively stable part in the research area. The channel next to Mandalay is the most active channel, with side bars and mid-channel bars passing by. The moving bars cause narrowing, widening and shift of channel. The right channel has been larger in the past. With the decrease in width, the activity in this channel also decreased.

The confluence reach is largely influenced by the distribution of flow over the channels at the trifurcation. The large confluence shifts from east to west, where it is pushed away by the channel with largest discharge. The confluence develops in downstream direction, but shifts of the separate channels can cause the creation of a new confluence at the beginning of the

reach. The shift of the channels here is also caused by the creation of bars on one side of the channel, pushing the channel in the other bank. The newly created confluence will also develop in downstream direction. This process repeated itself two times in the period between 1975 and 2016.

The connection between the reaches is important in the development of the river. It is clear that disturbances move in downstream direction. All the downstream moving bars and shifting channels in the braid plain upstream of the research area determine the positioning of the trifurcation. This influences the distribution of discharge over the channels with consequences as the closure of channels, the development of different type of bars and the the shift of the confluence. In appendix B, a detailed description is given of such a sequence of morphodynamics in downstream direction.

Chapter 4

Sensitivity analysis

In this chapter some of the morphodynamic driving physical processes in braided rivers, as described in chapter 2, are tested in a sensitivity analysis. This analysis is performed with the physics-based numerical model Delft3D. This chapter begins with a summary of the input of the used model (a more detailed description of the model and the input of the model can be found in appendix C). This is followed by an explanation of the tested physical processes and the method of how these processes are tested. This is followed by the results, which contains a qualitative analysis on the bed topography and a quantitative analysis on the depths and widths of the channel. The chapter ends with a conclusion of the found results.

4.1 Model set-up and tested parameters

In Figure 4.1 the initial bed of the model is given. This is based on data of the Amarapura floodplain urban development project (MBCCDL, 2016) and SRTM (2010). The SRTM is not of the same year as the rest of the data, but is only used for the morphological relatively (compared to the rest of the research area) inactive floodplain north of Mandalay.

The boundary conditions are based on the DMH (2014) data as given in chapter 3 and on a RVO feasibility study (2015). At the upstream end a discharge time series is used and at the downstream boundary a QH-relation (discharge-water level), given in respectively Figure 4.2 and 4.3. The input of sediment is an equilibrium calculated by the model, in which the sediment input is approximately the same as in the sediment transport in the first row of cells in the model.

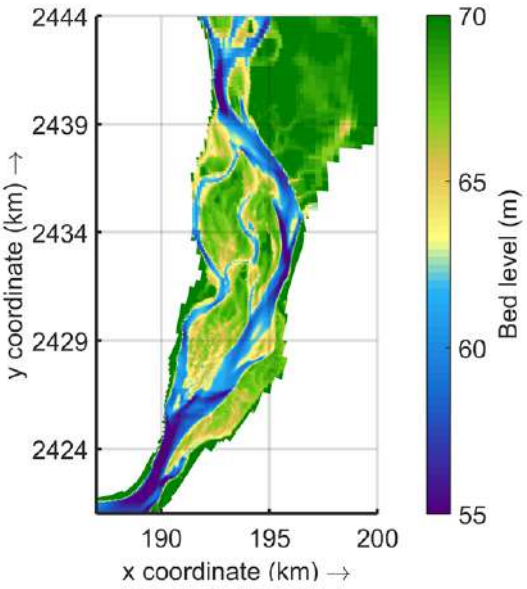

Figure 4.1: Initial bed level based on data of MBCCDL (2016) and SRTM (2010)

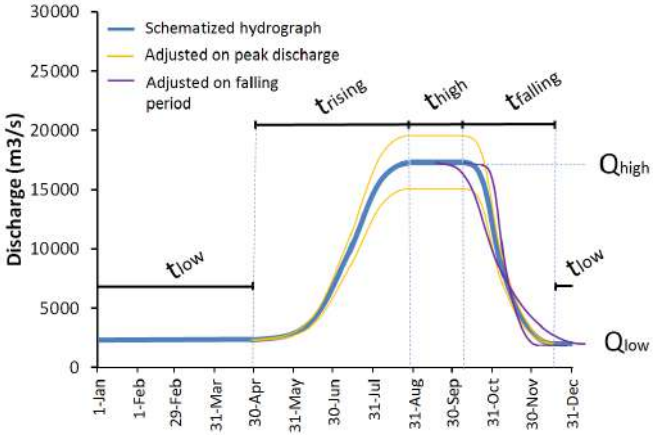

Figure 4.2: Used hydrograph (blue) and the adjusted hydrographs for variation in peak discharge (yellow) and period of the falling stage (purple)

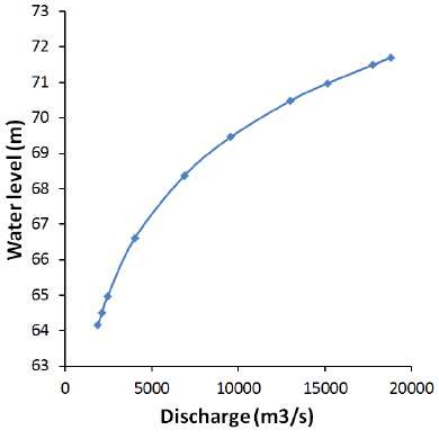

Figure 4.3: QH-relation as downstream boundary derived from the Sobek model from the study RVO (2015)

The used sediment transport formula is the general formula in Delft3D, which reads:

$$s = \alpha D_{50} \sqrt{\triangle g D_{50}} \theta^b (\mu\theta - \xi\theta_{cr})^c \tag{4.1}$$

in which:

$$\theta = \left(\frac{q}{C}\right)^2 \frac{1}{\triangle D_{50}} \tag{4.2}$$

where α, b, c, μ and ξ are user defined variables $[-]$, D_{50} the median particle diameter $[m]$, $\triangle$ the relative density $[-]$, θ the shields mobility parameter $[-]$ and q the specific discharge $[m^2/s]$. To write this equation in the form of equation 2.5, coefficient c is set to 0. In this way, b determines the power above the velocity in this formula. Chosen is to use $b = 2$ and $\alpha = 20$. $\alpha = 20$ is based on sediment transport passing Sagaing. The available data for sediment transport at this location is including wash load. Since wash load does not contribute to the morphology, $\alpha = 20$ is based on an estimation of which part of the total sediment transport (including wash load) contributes to the morphodynamics (C.J. Sloff, personal communication, 2016). . Due to the use of a morphological factor of thirty, the sediment transport is increased with approximately twenty percent at the upstream in the research area, decreasing to no extra sediment transport at the downstream end. This increase is caused by the rapid increases and decreases of the discharge. This does influence the results, but without data on sediment transports it is unknown whether this influences the estimated sediment transport negatively. In addition, the simulation in this sensitivity analysis are only used for comparison and for all these simulations the same overestimation of sediment transport is found. More about the choice of the sediment transport formula and the overestimation due to the use of the morphological acceleration can be found in appendix C.

For the spiral flow and bed-slope effects equations 2.7 to 2.10 are used. Default values are used for the calibration parameters in these formulations.

4.2 The tested parameter set

The set of parameters tested in the sensitivity analysis is derived from the described processes in chapter 2, and are given in Figure 4.4. The choice of the parameters will be explained in the next two sections. In the blue box the system forcing processes are given and in the red box the internal sediment transport processes are given. In the black dashed box the magnitudes of the parameters in the basis model can be found. Every run, one of these parameters is changed to a

value outside the black dashed box. In this way, the effect of every parameter can be explained by comparing the differences between the new run and the reference run (except for the direction of inflow, which has to be compared with the extra sediment transport). The complete input for each run is given in appendix C.4. Some of the processes from chapter 2 are not tested in this analysis. The different reasons for this will be explained in section 4.2.3.

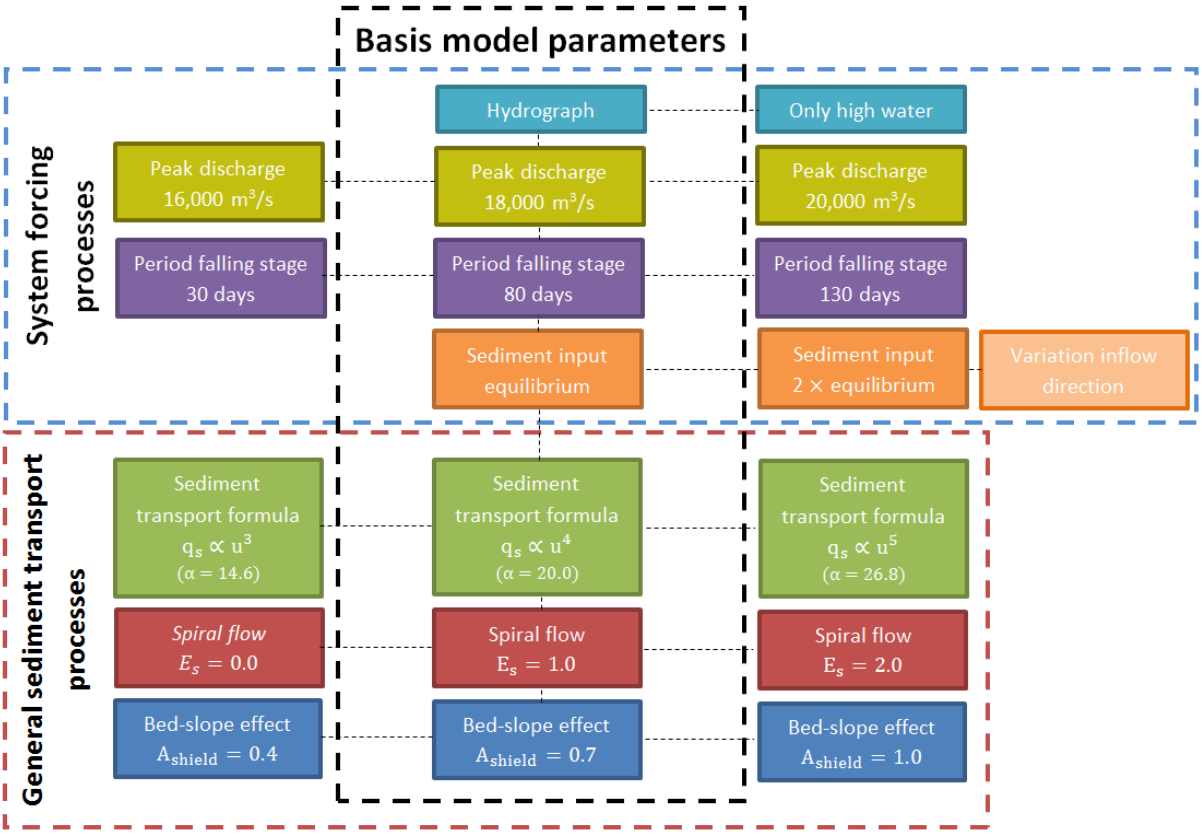

Figure 4.4: The basis model and the values for the tested parameters, split into system forcing processes and internal sediment transport processes

4.2.1 The system forcing processes

Of the system processes, the effects of hydrological variations and the effects of sediment input are tested. The first tested parameter (top parameter in Figure 4.4), is the difference of using a constant high discharge (like Schuurman and Kleinhans (2015) and Jang and Shimizu (2005) used) instead of a hydrograph. This should show how the different stages are important for the development of the river. Because morphological change is most significant during high water, the duration of the run with a constant high discharge is comparable with the sum of the periods where the islands are submerged in the reference run.

Differences within the hydrograph are also tested. The made adjustments in parameters are in the peak discharge and in the period of falling stage. The peak discharge is increased and decreased with $2,000\ m^3/s$. A higher peak discharge will probably lead to a more rapid movement of islands, bars and channels, but more interesting is to investigate if this also has an effect on the shapes of these features. For the falling stage periods of 30 days, 100 days and 130 days are tested. With a change in the duration of the falling stage, the duration of high and low water are also changed to keep the total period of the four stage one year. This is done in a way that the period in which the islands are submerged remains the same duration. The new hydrographs for the change in peak discharge and period of the falling stage are also given in Figure 4.2.

In the analysis of the morphodynamics from satellite imagery in section 3.2.2, it is explained that the bars move into the system with shifting of the channels as result. It was possible to simulate passing bars and a shifting channel at the inflow boundary, but problems arose by making these simulations comparable with the reference run. The effects of the passing bars and shifting channels in this different run is are discussed in chapter 5. For this sensitivity analysis is chosen to test the effects of the passing bars (extra sediment input) and shift of the channel in two different runs. In the first run, two times the amount of sediment is put into the model (compared with the reference run) and in the second run, the location of inflow is varied over the width (by changing the discharge over three separate boundaries at the upstream end). To keep the sediment input the same while using different flow boundaries, it was necessary to fix the amount of sediment transport as concentration. Because the model calculates sediment input in virtual cells just upstream of the first cells in the model and the first location to measure sediment transport is between the first and second row of cells, it not possible to put the exact same amount of sediment in the model using fixed concentrations, as with the model option to calculate the amount of sediment input. For this reason, it is chosen to compare the run with changing flow with the run with extra sediment input. More details about the change of inflow and the options to change the amount of sediment can be found in appendix C and the Delft3D-FLOW manual (2016).

4.2.2 The internal sediment transport processes

With parameter five, the power above the velocity in the sediment transport formula is changed. To keep the the runs comparable, the amount of sediment transport has to remain the same. Calibration of the different formulas is done with calibration parameter α. This is discussed in section C.2.4. The values of α are also given in Figure 4.4. For the bed-slope effect and the spiral flow, the change of parameters is rather trivial. The calibration parameters, as given in equations 2.7 to 2.10, are changed to values as given in Figure 4.4.

4.2.3 Not tested physical processes

Some of the processes described in chapter 2 will not be tested in this sensitivity analysis, for which different reasons exist. Variation in bed roughness model is for example not done, because the use of a different roughness model was already used in the consideration and derivation of a different sediment transport formula (see appendix C.2.4). This would mean that the roughness model would be changed in two different ways. This effect is, however, only on the sediment transport, while it bed roughness also influences the flow. Schuurman et al. (2013) did investigate the sensitivity of this process and found that the effect of it on the morphodynamics is large. Using a depth dependent model resulted in larger movement of the bars. Therefore, it is recommended to take this parameter into account for further study.

Further, no distinction is made between bedload and suspended load. Adaptation lengths (the length a sediment particle is taken with the flow without interaction with the bed) of the bed load and suspended load are by definition not equal, but when both the adaptation lengths are smaller than the grid size, no differences will be found between simulations with only bedload or with both bedload and suspended load. This was the case in this model. Vegetation and bank erosion by failure cannot be tested in model, since processes of these are not included in the software. Bank erosion by fluvial erosion is included in the sediment transport by primary flow. The last not mentioned process is turbulence, which is not tested, since effects of turbulence cannot be found with a 2D depth-average model on this scale.

4.3 The comparison method

To be able to tell something about the sensitivity of the system to the different processes, the results of the different runs have to be compared objectively. Egozi and Ashmore (2008) summarized different measures to compare braided rivers. They explain measures such as braiding intensity indices, bar indices, channel count indices and channel length or sinuosity indices. However, these measures tell something about the whole system, and not about local changes. Since the system in Mandalay has generally three channels and three islands, these measures will not be very useful. Dynamics can be found in the moving side and mid-channel bars and the shift of channels (as explained in chapter 3). In this sensitivity analysis, the different processes will be tested on those changes.

To compare the different runs, a specified moment in time has to be chosen. The model needs approximately one or two years of morphological spin-up to adopt to the different situation in the model compared to the real river. This means that the simulation period cannot be too short. In addition, from the first model runs is found that the results were influenced by the upstream boundary (this will be discussed further in chapter 5.2). The longer the simulation, the further this influence reaches into the system. In Figure 4.5, showing the reference run after a period of ten years, this is already visible. At the inflow, two long almost straight channels are created. This is very unlikely to happen, looking at the satellite imagery of the past thirty years. Because this study focusses on the area starting at the first bifurcation, it is important to look at a period where the effect of the boundary did not reach this part. It is chosen to compare the runs after a period of ten years. In appendix D, the bed levels after a simulation time of ten years of each run are given. Taken into account has to be that a simulation of ten years does not have to correspond with ten years development of the river, since actual sediment transports are unknown and not so not implemented in the model.

Comparison of the runs will exist of three parts, namely:

- width and distribution of depth over this width (hereinafter revered to as width-depth relation)
- channel width change rate
- qualitative comparison on shapes of channels and islands

Satellite data does not contain enough information to explain all morphodynamics. With the qualitative analysis, the focus will be on shapes of the islands and channels and which processes play a role in the development of these shapes. The quantitative analysis of the width-depth relation in channels is performed, because the cross-sectional shape is important for the dynamics of the rivers. Steep banks for example increase the probability of bank failure. It is also interesting for engineering practice, looking at for example navigable depth. Investigating the yearly change in channel width tells something about the dynamics of the system, which is an essential property of a braided river.

Both the width-depth relation and yearly channel width change are determined for the cross-sections as shown in Figure 4.5. In the right channel thirteen cross-sections can be found and in the left channel twelve. The cross-sections are located such that for all runs the channel width could be determined properly, without disturbances of side channels. The widths and depths are determined for a discharge of $2,000\ m^3/s$. This relatively low discharge is chosen to have a clear distinction between all the channels. To ensure that the water levels were stable, simulations were performed with fixed beds under a constant discharge for 15,000 minutes. Water levels turned out to be stable after approximately 10,000 minutes. The depths in the channels were calculated by Delft3D for every cell. For each cross-section, the corresponding grid cells were known. For these cells depth statistics were calculated (mean, median, maximum, 25 percentile

and 75 percentile). The widths are defined as the the distance between the ends of the two wet cells furthest apart from each other in the cross-section. Because some cells do no get completely dry in the model, a threshold for the water depth for wet cells is chosen at 0.3 metres. With the determination of the width change, widths were assessed for every year during the ten year simulation. For some years, two channels were found in some cross-sections. The distance between the two furthest wet cells did in those cases not represent the width of the channels, with large width change as consequence. Where large changes in channel width were found, the real channel widths were checked and corrected if needed by hand. For these cases the width was chosen of the channel which remained in the cross-section the whole simulation.

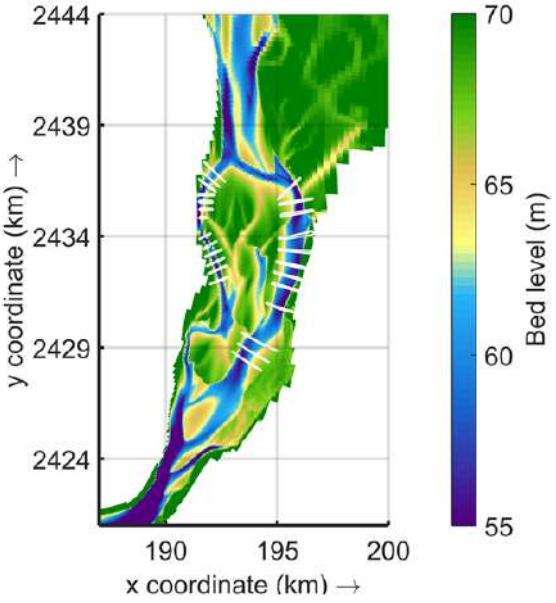

Figure 4.5: Locations of the cross-sections on top of the bed level of the reference run after a simulation time of ten years

Figure 4.6: Locations of the cross-sections on top of a satellite image of the year 1994

To check the performance of the model, the quantitative methods were compared with data. For the width-depth relation, the only available data is the initial bed. A comparison can be made between width-depth relation after ten years of simulation and of the initial bed. Of course the distribution of the depths over the channel is different, but the assumption is made that similar width-depth relations can be found on average over the channel length. This would not hold if the discharge distribution over both channels changed significantly, but this is not the case.

The change in channel width can be checked with the change in channel width on the satellite imagery. The same cross-sections were used for the satellite imagery as for the model. These cross-sections were printed on the images with the GEE and measured by hand. The yearly images of the dry season from 1994 to 2014 were used. The channel system before 1994 was too different to compare with the recent system at the same cross-sections. A Figure of 1994 with cross-sections is showed in Figure 4.6. In this Figure is also visible that there are some difficulties with the determinations of the widths on the satellite imagery. Some cross-sections are shorter than the river width and at many locations multiple channels can be found in one cross-section. Because width determination is done by visual inspection, this can easily be solved. Where the channel was not exactly located on the cross-section, the cross-section was extended, and where multiple channels were found, widths of the same channel were measured over time. Another problem with the width measurements from satellite imagery, is that the discharge on the different images is not the same. To solve this, a discharge-width relation is determined with the initial bed in the model. The assumption is made here that the slopes of

the banks remained on average over the channel the same. because the discharges are known, the width can all be translated to a width for a discharge of $2,000\ m^3/s$. The QW-relations, the representative discharge for the satellite images and the corrections for the measured widths are given in appendix E.

4.4 Width-depth sensitivity of the channels

The width-depth relation of the channels is a measure for how the system has developed, so the morphology. In Figures 4.7, it is visible how the width, but especially depth, can vary for the different tested parameters at a discharge of $2,000\ m^3/s$ (after the simulation time of ten years with the complete hydrograph). Because the bed has changed during the simulations, it is logical that a different depth-profile can be found in the different figures. However, it can be expected that cross-sectional shapes should remain the same over the average of the channel, since width-depth relations are dependent on stream power and sediment input. The shape of the cross-section can be described with the width and the distribution of the width over this channel. Looking at the depth profile using the initial bed in Figure 4.7b, it seems unlikely that the channel gets shallow as in Figure 4.7a or deep as in Figure 4.7c. The difference in width is hardly visible on these figures, but are significant. The average widths from Figure 4.7a to 4.7c are respectively 766 metres, 830 metres and 918 metres. These Figures also explain why it is necessary use enough cross-sections for the measurements. With the large variability in depth over the length of the channel, mistakes could easily be made.

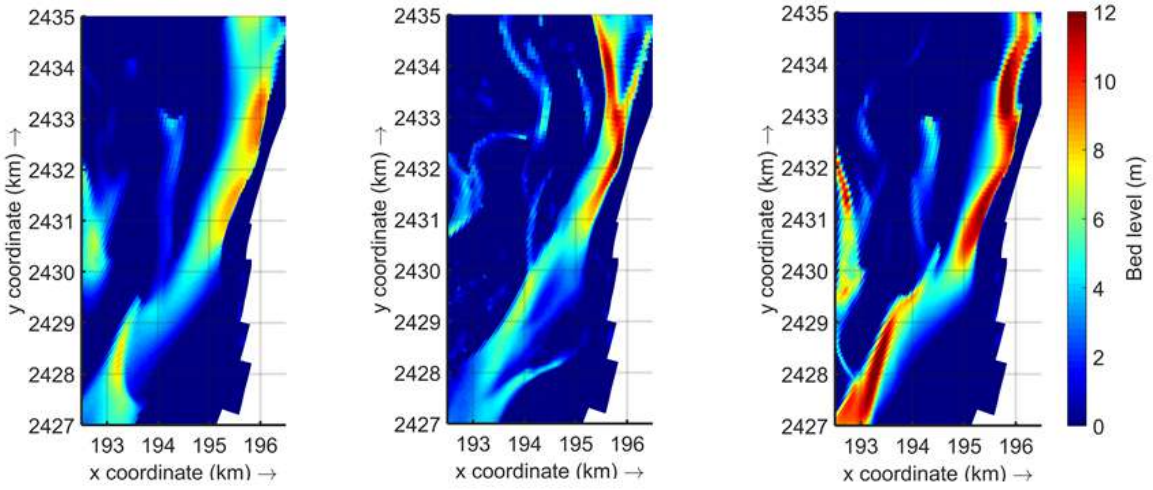

(a) Bed-sl. eff. $A_{shield} = 0.4$ (b) Initial (c) Spiral fl. $E_{spir} = 2.0$

Figure 4.7: Depth profiles of the left channel, showing large differences in depths between run with different parameters (after ten years simulation) and the initial condition

To investigate the widths with corresponding depth distributions Figures 4.8 and 4.9 are used. In Figure 4.8 the mean and median depth are given for the mean width for the initial bed, the reference simulation and the simulations for all tested parameters. This is done for both the left and the right channel during a discharge of $2,000\ m^3/s$. In the graphs the low magnitude of each parameter is given with a full coloured dot and the high magnitude with only an outline of the same colour. A vertical line is drawn through the reference run. The expectation is that the tested values of each parameter (the filled and the one with outline) lay on opposite side of this vertical line. For the right channel this is not the case and no correlation can be found between the width and depth. This is caused by the large variation in discharge in this channel, as shown in table 4.1. For the left channel the variation in discharge is much smaller compared to the average discharge in this channel. This has lower scatter as result in the relation between the mean width and mean depth (only mean depth will be discussed further, since the median

and mean show similar results). In figure 4.8a also a fit for the relation between mean width and depth is given and is visible that the mean depth slowly decreases with an increase in width. With a depth around 100 times lower than the width, a slope of the fit (for the relation between mean and depth) of -0.008 m/m seems reasonable. In this way the cross-sectional area remains approximately the same for different simulations.

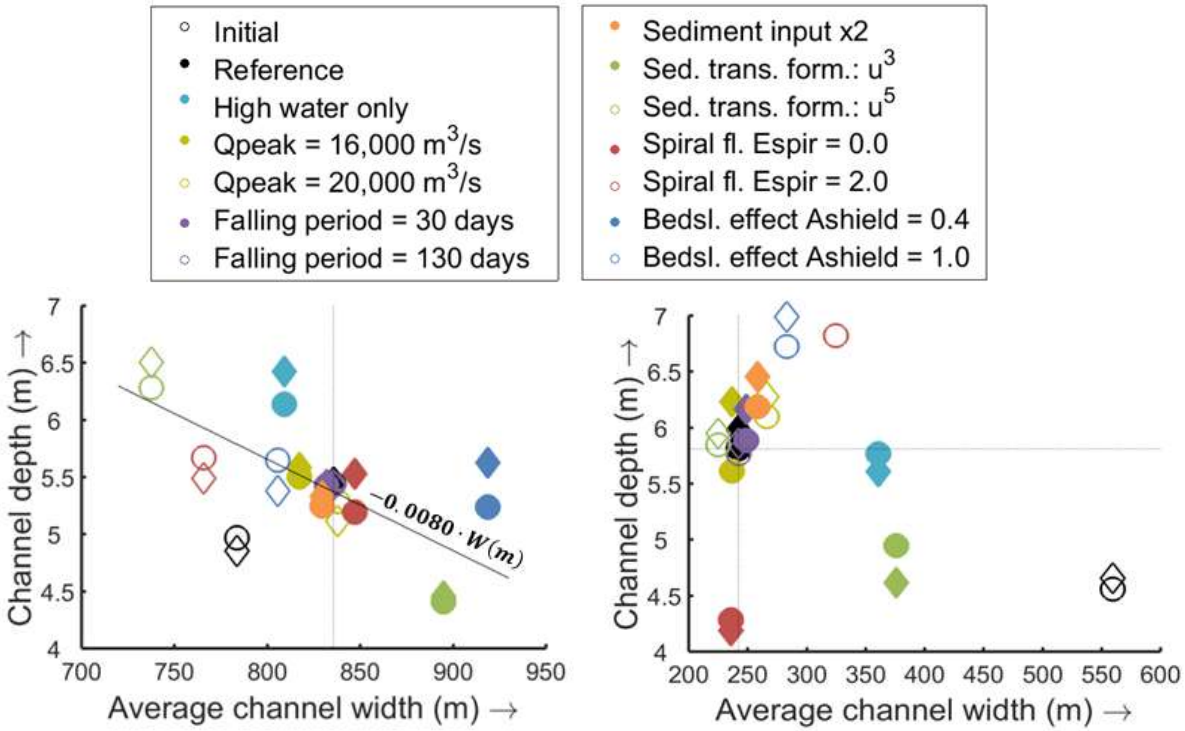

(a) Mean and median left channel

(b) Mean and median right channel

Figure 4.8: Relation between the average width and the mean and median depth for all the simulations in the sensitivity analysis. The results are averaged over all the cross-sections in the left and right channel separately at a discharge of $2,000\ m^3/s$. The fit for the relation between the average width and mean is given for the left channel including slope. For the right channel no correlation is found.

In Figure 4.9, the 25th and 75th percentile of the depth and the maximum depth are given in relation to the mean width. The fit for the 25th percentile has a slope of most zero. This means that, independent of the width of the channel, 25 percent of the channel is shallower than 3.3 metres. With decreasing with, this shallow area gets smaller. So, to maintain a similar cross-sectional area, another part of the channel has to become deeper. This is visible in the fits for the 75th percentile and the maximum depth, which increase with a decrease of the width. This means that the variation in depth is larger for smaller widths. This results in steeper gradients in the bed (in cross-sectional direction). From this explanation is already clear that bed-slope effects will have a large influence on the width and depth of the channel. Large bed-slope effects result in shallow wide channels, where small bed-slope effects allow steep banks, so result in narrower and deeper channels.

The other two internal sediment transport processes also have a high influence on the width of the channel and distribution of depth in the channel. As sediment transport responds highly non-linear on the flow velocity through formula 4.3, sediment transport in the channels (high flow velocity) and on top of the submerged bars (low flow velocity) is highly sensitive to n. With larger n, the difference between the sediment transport in the channels and on top of the submerged bars gets larger. This has deeper and therefore also narrower channels as results.

Lower values for n have the opposite effect.

$$s = m \cdot u^n \tag{4.3}$$

Spiral flow also has a deepening effect on the 'straight' channel, because the deepest part of this channel shifts from bank to bank. In these type of 'bends', spiral flow can be found. Where the spiral flow deflects the sediment transport towards the inner bend, the deep parts of the channel get deeper and the shallow parts get shallower or wider.

The effect of the upstream boundary on the width and depth in the channels is much lower than for the internal sediment transport processes. Only sediment input was expected to have an influence the depth of the channel. The disturbances in morphology caused by the sediment input travelled approximately 600 metres per year in downstream direction, which was not enough to have an impact on the morphology in the observed channel.

In Figures 4.8 and 4.9 also the average width and different statistics for the depth are given for the initial condition, which are used to check the results. This initial condition presents the actual measured situation of 2016. For the right channel this situation showed a much wider and shallower situation. This channel opened during the simulations, which explains this difference. For the left channel the average width of the initial conditions is within the range found after simulations. However, the mean, 75th percentile and maximum depth lay far several metres from the fits found for the width-depth relations. This probably has to do with the continuously changing conditions in the distribution of discharge over the channels. This also shows how important the morphology around the bifurcations is for the development of the whole system.

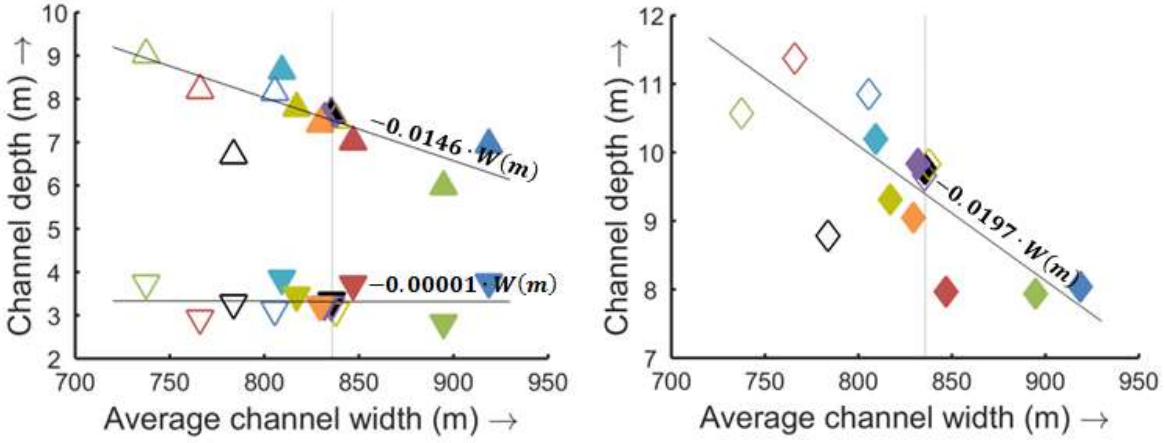

(a) 25th percentile and 75th percentile depth

(b) Maximum depths

Figure 4.9: Relation between the average width and the 25th percentile of the depth, the 75th percentile of the depth and the maximum depth are given for all the simulations in the sensitivity analysis. The results are averaged over all the cross-sections in the left channel at a discharge of $2,000\ m^3/s$. The fits with their slopes of the relations between the width and the depths are also displayed.

Table 4.1: Discharge distribution over the different channels for the different simulations

	Right (m)	Left (m)	Middle (m)
Initial bed with $Q = 2000\ m3/s$	182	1705	51
Reference run	476	1524	
Only high water	403	1597	
Peak discharge $Q = 16,000\ m3/s$	458	1542	
Peak discharge $Q = 20,000m\ 3/s$	540	1460	
Falling stage 30 days	481	1519	
Falling stage 130 days	503	1497	
2x sediment input	677	1323	
Sed. trans. formula: u^3	474	1526	
Sed. trans. formula: u^5	465	1535	
Spiral fl. $E_{spir} = 0.0$	319	1679	
Spiral fl. $E_{spir} = 2.0$	419	1581	
Bedsl. Effect Ashield =0.4	281	1718	
Bedsl. Effect Ashield =1.0	553	1446	
Average	465	1534	
Standard deviation	96	96	

4.5 Width change rate sensitivity

The width-change rate is a measure for the dynamics of the system. In the top of table 4.2 the width change rate (m/year) is given for two periods of satellite images. Two periods are displayed, because the width-change rate has decreased over time. In the other part of the table the width change rates of different model simulations are given. Not all processes discussed in this chapter have been tested, since this analysis was very time consuming. Only the processes which had a large effect on the width have been tested. In addition, the overall increase of the sediment transport by a factor three is tested (shown in bottom of the table). This is done to cover the uncertainty in the estimation of the sediment transport. In table 4.3, the relative width change rate [-] is given, which is performed for the same periods of satellite images and the same model runs. The relative width change rate excludes the effect of the width of the channel on the change in width. The relative width change rate is calculated according equation 4.4. In figure 4.10, the development of the average width in time for both channels from satellite imagery and for the reference simulation is given. It is visible that the widths at the beginning of the simulation and at the last satellite image have a difference of 340 and 80 metres for the left and right channel respectively. Between the last used satellite image (2014) and the start of the model is a period of two years. In these two years these differences can be bridged, but it is also likely that differences in discharge at the satellite images and in the model cause this difference in width.

$$relative\ width\ change\ rate = \frac{\mathrm{d}W}{\mathrm{d}t}\frac{1}{W} \tag{4.4}$$

In table 4.2 is visible that the width change rate of the right channel in the simulations is approximately a factor 1.5 lower than found on the satellite imagery. This is caused by a decrease in channel width. This is in agreement with the found results for the relative width change rate, where results are almost equal for the reference run. The processes that have largest influence on the relative change in width in this channel are the bed-slope effect, changing inflow direction and higher sediment input and higher overall sediment transport. With a decrease of the bed-slope effect, the small channel becomes deeper and thereby more stable. With changing inflow direction and higher sediment input the cause is most likely the formation of a bar in

front of the channel with lower (sediment) inflow in the channel as results. A higher overall sediment transport scores lower because the channel gets stable in an earlier state due to the influence of the upstream boundary.

For the left channel the width change rate is significantly lower, both for the absolute change as the relative change. Variation in the different parameters, except increasing the overall transport, does only result in a relative width change rate of 0.03 higher. For the internal sediment transport processes (the sediment transport by primary flow and deflection of sediment transport by bed-slope effects and spiral flow) this is logical, since these induce change when something in the system has changed. Without any perturbations upstream, these will not lead to a larger change in width. With larger peak discharges the channel became stable in an earlier state, with as consequence almost no change in the width of the channel in the final years of the simulation. Acceleration the morphodynamics by increasing the overall sediment transport does increase the relative width change rate with 75 percent, but also here the change rate is still 30 percent lower than observed from satellite imagery. What seems to be missing in the model compared to the satellite images, are the pulses of sediment or bars which are 'pushed' through the channel as sort of disturbances. Due to these bars or sediment pulses accretion, at the banks occurs. This is followed by erosion or a shift of the channel. This process is displayed in the satellite images in Figure 4.11. The width at dashed line 1 decreased with around 300 metres between 2003 and 2004. This bar erodes again, causing an increase of that same width in the upcoming two years. At dashed line two a large bar is located in 2002. This bar erodes in the two years afterwards. At dashed line 3 a decrease in width of 150 metres can be found between 2003 and 2004, followed by two years of increasing width. Such a widening can also be found at dashed line 4 after 2002. This process can be simulated with the model by putting in an overload of sediment at the upstream end. But, since it takes time for the sediment to propagate trough the system, this process can be observed after simulations longer than fifteen years.

Table 4.2: Average (absolute) width change per year of the channels for satellite imagery and model simulations

Width change rate (m/year)		Right channel	Left channel	Both channels
From satellite	1995-2014	94	140	116
	2002-2014	74	119	96
Reference run		52	68	60
Larger Qpeak	$Q = 20,000\ m^3/s$	54	71	62
Changing infl. dir.	and sed. input	50	90	69
Bed-slope eff.	$A_{shield} = 1.0$	40	77	57
Spiral flow	$E_{spir} = 2.0$	56	74	65
Sed. trans. formula	u^3	63	80	71
Higher sed. trans.	3x	53	110	80

Table 4.3: Average relative width change of the channels for satellite imagery and model simulations

Relative width change rate (-)		Right channel	Left channel	Both channels
From satellite	1995-2014	0.30	0.24	0.24
	2002-2014	0.28	0.20	0.28
Reference run		0.28	0.08	0.18
Larger Qpeak	$Q = 20,000\ m^3/s$	0.25	0.09	0.17
Changing infl. dir.	and sed. input	0.20	0.11	0.16
Bedslope	$A_{shield} = 1.0$	0.18	0.10	0.14
Spiral flow	$E_{spir} = 2.0$	0.24	0.09	0.17
Sed. trans. formula	u^3	0.27	0.10	0.18
Higher sed. trans.	3x	0.21	0.14	0.18

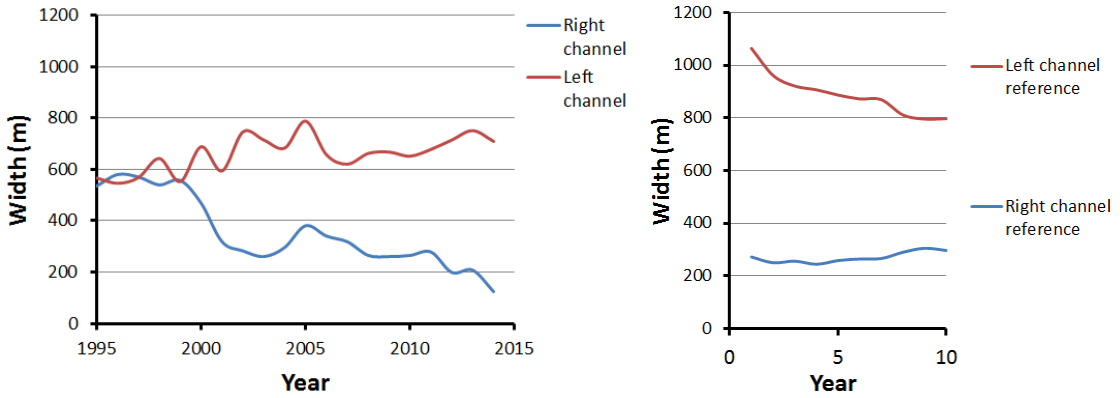

(a) Satellite images

(b) Reference model simulation

Figure 4.10: The development of the width of the left and right channel observed from satellite imagery and found with the model simulation

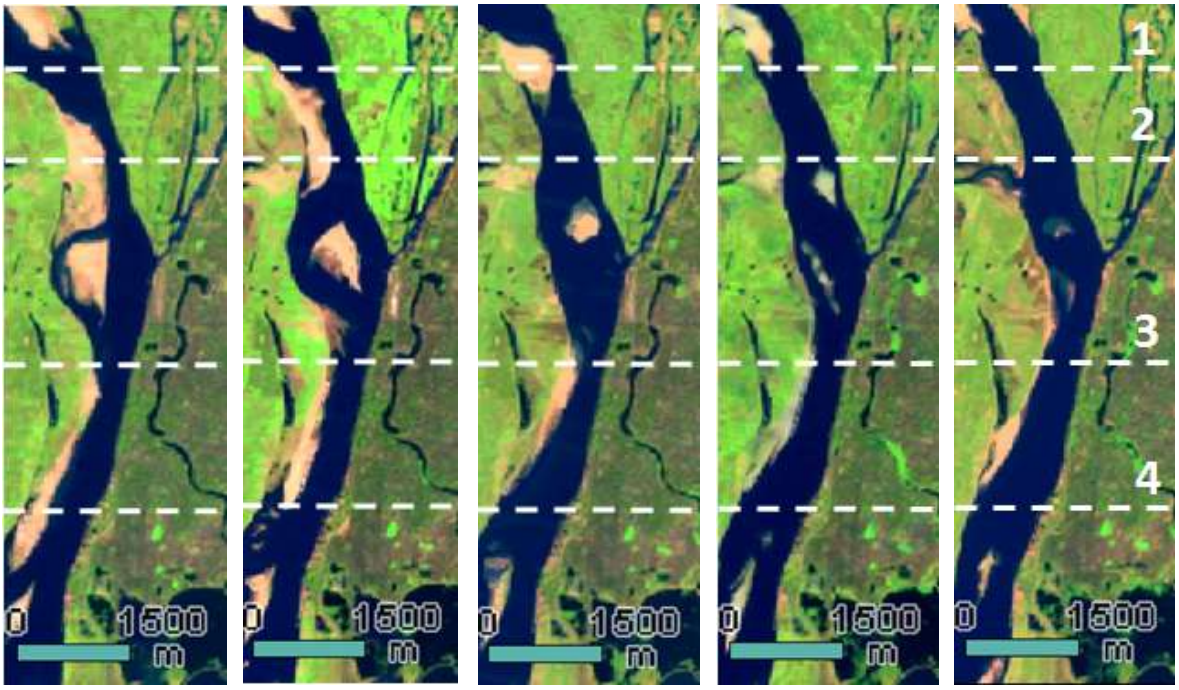

(a) 2002 (b) 2003 (c) 2004 (d) 2005 (e) 2006

Figure 4.11: Change in channel width due to the movement, attachment and de-attachment of bars. The dashed lines are given to show the change in the corresponding cross sections.

4.6 Qualitative analysis bed topography

In this section comparisons are made based on bed level between the different runs after a period of ten years. In appendix D the bed topographies of the complete research area are given for all the runs. In this section is zoomed in on the significant differences in shapes of channels, islands and bars. The locations which is zoomed in to, are also given in appendix D. Where necessary, additional plots are shown to explain of the differences.

4.6.1 Difference only high water and hydrograph

In Figure 4.12 can be seen that the absence of the different stages of the hydrograph leads to large shape differences in bed topography. The channel encircled with red became significantly narrower and shallower without hydrograph (bed level difference approximately 5 metres). Further downstream (not included in the Figure but visible in appendix D) a similar closure of a channel can be found using only a constant high discharge. This means that during another stage then high water, erosion has to be found in these kind of channels. In Figure 4.13 is visible how the bedload transport during the rising stage results in erosion in the channel. The increased discharge is pushed through the too small channel, creating a gradient in flow velocity up to the smallest part of the channel. The rise in flow velocity causes a rise in sediment transport. Because the rise in sediment transport is along the flow line, this leads to erosion. The period of erosion during the rising stage is the reason why this channel remains using a hydrograph, while it disappears using only a high discharge.

Another difference between using a hydrograph or a constant discharge is the two small channels on top of the islands (visible in Figure 4.13). The existence of the left of these channels is caused by the opening in the bar in the inflow channel. In other simulations as well, this channel is just found when this opening in the bar is present. In addition, does the parameter n in sediment transport formula (equation 4.3) play an important role. With large n, a small rise in flow velocity gives much larger sediment transports. Where small deviations in the bed occur, this can cause the incision of new channels. Also with fluctuations in water levels, a subtle interaction between the different magnitudes and locations of sediment transport can cause the incision of new channels.

The shape of the islands in Figure 4.12a (so with a complete hydrograph), also shows large differences with the shape in Figure 4.12b. A large sidebar is attached to the islands (encircled in orange), which moved from the head of the islands, in time, to the location where it can be found in Figure 4.12a. The movement of this bar can also be explained with Figure 4.13. It is visible that both in the rising stage as in the high water period, the sediment transport is higher on top of the bar than right behind it. This is caused by the divergence of the flow in the deeper area just behind the bar. This flux in sediment transport causes the movement of the bar. How this bar grows is not given in these figures. The growth of the bar predominantly happens during low water. During that period, the flow is concentrated in the deep part of the channel visible in Figure 4.12b. This results in lower flow velocities on the right side of the channel, so on the side of the bar. This causes sedimentation in this area and so growth of the islands.

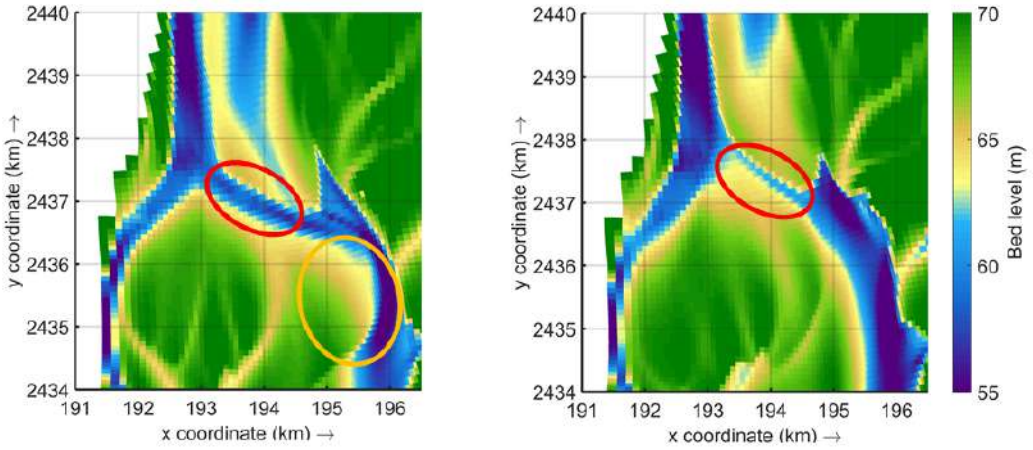

(a) Simulation with hydrograph

(b) Simulation with constant discharge

Figure 4.12: Bed levels after a simulation of ten years with hydograph and for a simulation with constant high discharge with a duration similar to the sum of the duration of the periods of high water in the hydrograph

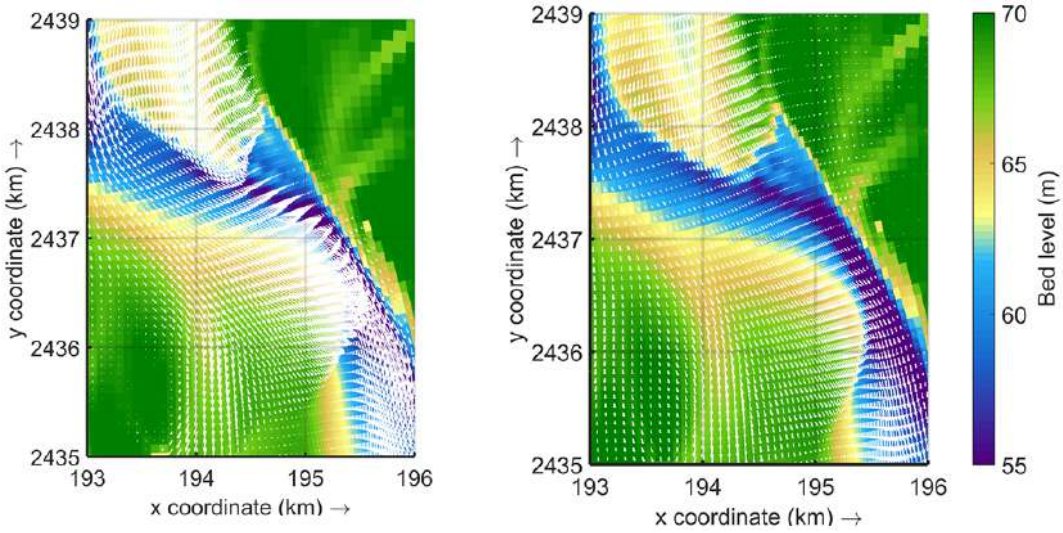

(a) Rising stage

(b) High water

Figure 4.13: Bed load transport on top of the bed level in a subsequent rising stage and high water

4.6.2 Different peak discharges

In Figure 4.14, the bed levels after simulation with different peak discharges are given. As expected, the differences are predominantly in the extent in which the bed is developed. Going back in simulation time with the simulation with the largest discharge, shows bed topographies which are similar to the bed topographies found for lower peak discharges. Only notable, is that the difference in development more upstream is smaller than downstream. This is probably because the river system narrows in downstream direction. This means that further upstream, the discharge is spread over a larger width. This causes lower differences in flow velocity, and so smaller differences in sediment transport.

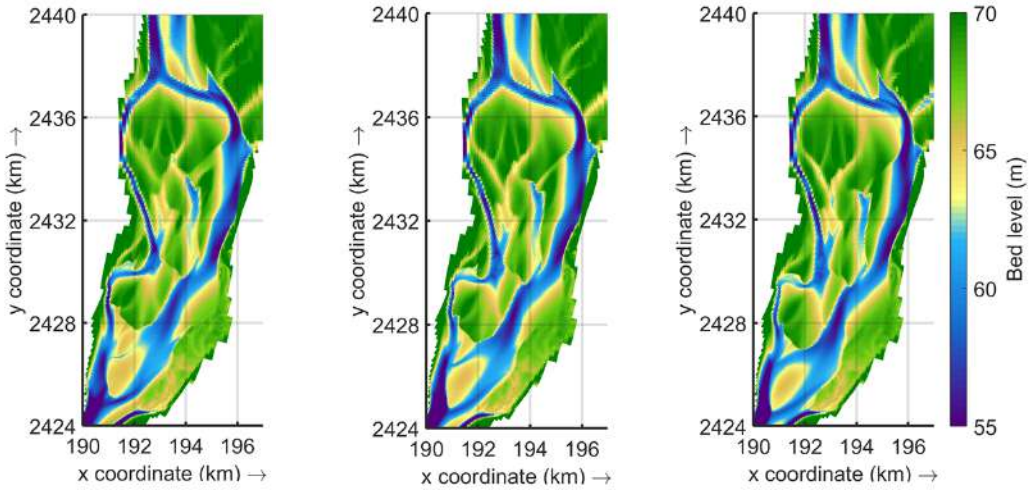

(a) Peak discharge of $16,000 m^3/s$

(b) Peak discharge of $18,000 m^3/s$

(c) Peak discharge of $20,000 m^3/s$

Figure 4.14: Bed levels of simulations using different peak discharges

4.6.3 Different duration falling stage

The duration of the falling stage had no significant influence on the morphology. Looking at the bed level differences between the model with a duration of the falling stage of 30 days and the model with a duration of the falling stage of 130 days, as given in Figure 4.16, it is visible the most significant difference is that bars moved further downstream having a shorter falling stage. This, however, does not have to do with change in the falling stage. This change is caused by the variation in the duration of the high water to keep the period of the hydrographs one year. Looking solely at sediment transport rates, as done in Figure 4.15, it can be seen that the graph of the bedload transport has a similar shape as the hydrograph. Variation in the duration of the falling stage does not have different peaks as result.

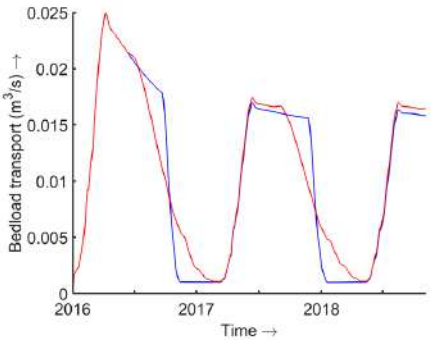

Figure 4.15: Instantaneous bedload transport in the Mandalay channel for simulations with a 30 days falling period (blue) and 130 days falling period (red)

The total amount of sediment transport is almost similar. The small difference in cumulative sediment transport during the first year results in a small bed level difference between the two simulations. This causes a slightly different peak in bedload transport for the year after, but no significant changes can be found. However, in other simulations (different from the model as used in the sensitivity analysis) large peaks were found in sediment transport during the falling stage. It is possible that for these simulations the duration of the sediment transport does have a significant effect on the bed development.

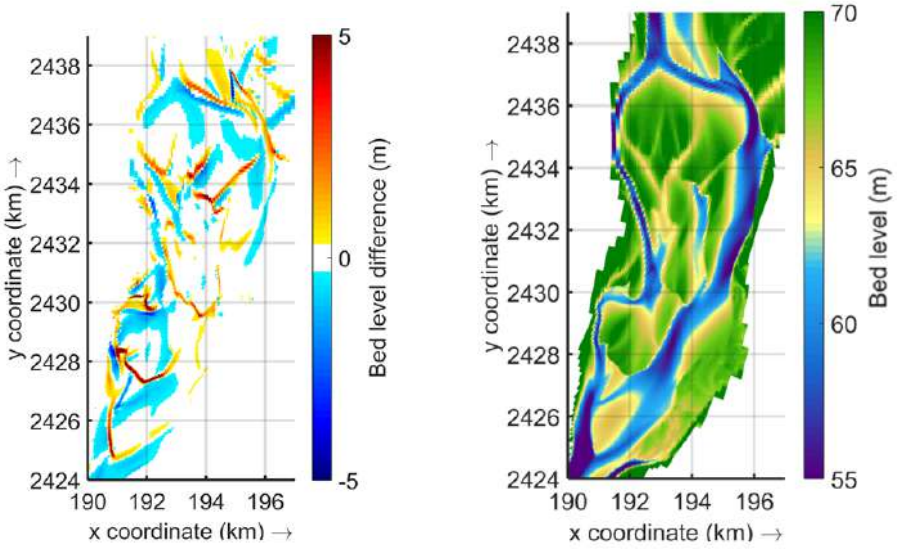

(a) Bed level difference (b) Reference run

Figure 4.16: Bed level difference of the simulation with a falling period of 30 days and 130 days and the bed level of the reference run

4.6.4 Different sediment input and inflow direction

For a simulation of ten years, extra sediment input resulted in differences larger than one metre only in the upstream part of the research area (area above y =2434 km, visible in Figure 4.17a). This is in agreement with the observed speed of bars on satellite imagery of approximately 600 metres/year. Further downstream only minor differences could be found. The longer the simulation, the more downstream the effect of the inflow boundary is noticeable. This means that it takes a long simulation time before sediment input affects the whole area. This means also that the uncertainty in the sediment input would not influence the area far enough from the boundary within a certain time. However, in this simulation only the amount of sediment transport is varied and not the location of input. When bars move into the system, as described in section 3.2.2, this has a direct effect on the flow distribution. Since the flow disturbances propagates much faster through the system than the sediment, it impacts the morphology further downstream in an earlier state. This is shown with the simulation where the inflow location at the boundary is varied. With this simulation it was only possible to simulate four years with an equal sediment input as for the simulation with extra sediment input. After this period a instability occurred with unrealistic large sediment input as result. The exact cause of this instability is unknown, but probably has to do with a too rapid change of inflow conditions compared to the time for the water level and bed to adapt to it. The difference in bed levels between the reference run and the run with changing inflow direction and extra sediment is shown in Figure 4.17b. It is visible in this figure that the effect of the changing flow direction in combination with extra sediment input already reaches further downstream after four years than the effect of only extra sediment input after ten years.

Differences in bed level found with extra input are shown in Figure 4.18. It is visible that channels are less deep and that bars get wider and higher. The effect on the large islands is less significant. Also the small channels on top of the islands show minor differences.

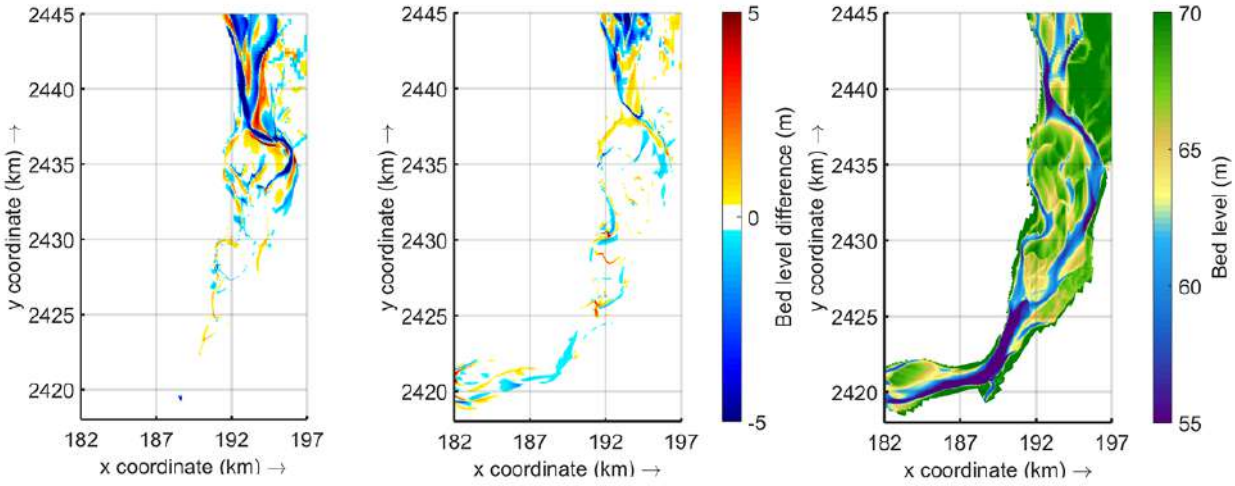

(a) 10 years simulation (b) 4 years simulation (c) 4 years simulation

Figure 4.17: Bed level differences between the run with equilibrium sediment input and the run with 2 times equilibrium sediment input (left), bed level differences between the run with run equilibrium sediment input and 2 times equilibrium sediment input with changing inflow direction (in the middle), bed level as reference to determine the reach of the disturbances with different input in the left and middle figure.

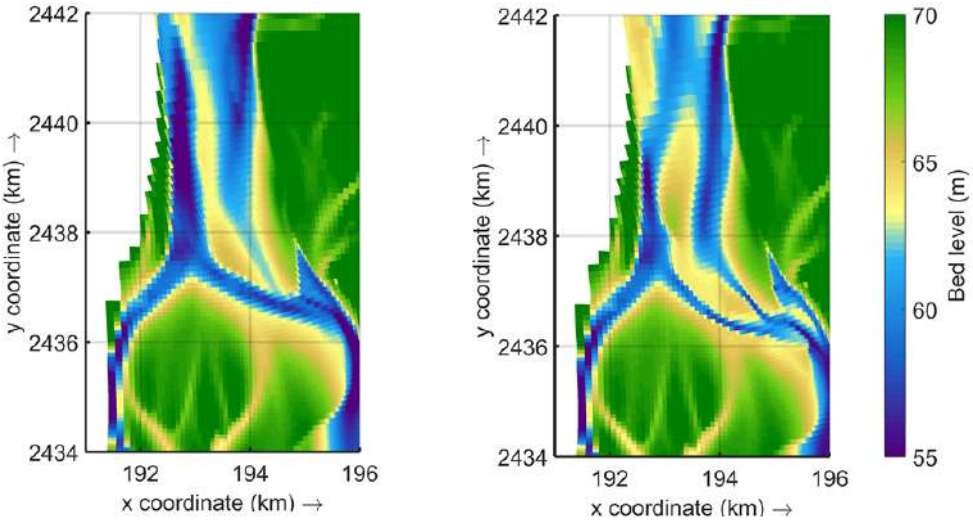

(a) Equilibrium sediment input (reference run)

(b) 2 times normal sediment input

Figure 4.18: Bed levels of a simulation with and without extra sediment input

4.6.5 Different sediment transport formula

It is explained that the parameter n in the sediment transport formula of equation 4.3, has a large effect on the difference between sediment transport in the channels and on top of the submerged islands (or bars). This does not only affect the widths and depths of the channels, but also the height and velocity of the bars. In the Figures 4.19a to 4.19c is visible that bar height decreases for lower n. Further can be seen, that in these figures corresponding shapes of islands are denoted with a number. These show that after the simulation time of ten years, the corresponding shapes are located further downstream for lower n. The different values of n were a result of uncertainty in the bed roughness in large sand-bed rivers (see appendix 2). When the magnitude of sediment transport is known (which is in this study not the case), bar speed

can be calibrated by changing the power above the velocity in the sediment transport formula while keeping the total transport the same. In this way, more can be learned about the actual bed roughness model.

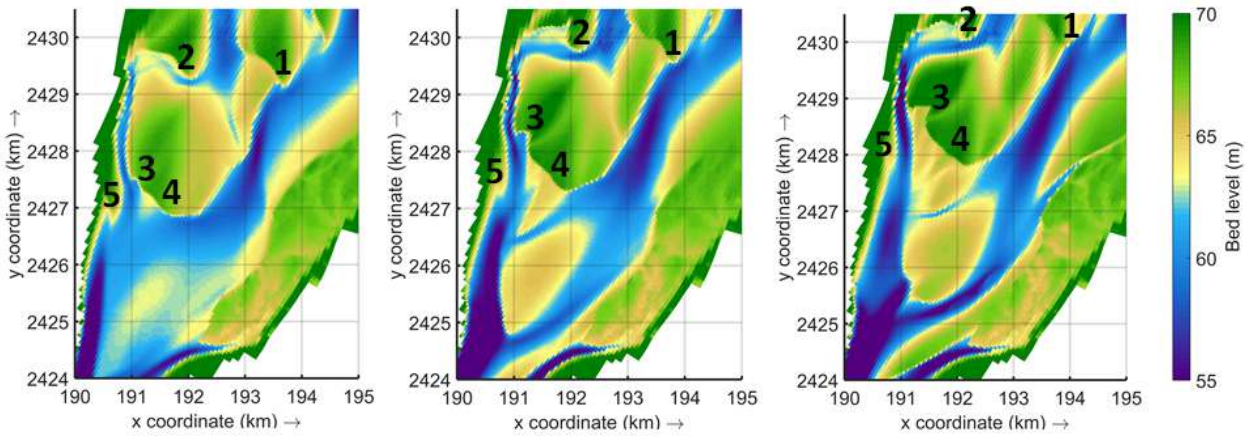

(a) $S \propto u^3$ (b) $S \propto u^4$ (reference run) (c) $S \propto u^5$

Figure 4.19: Bed Level after simulations with a different power above the flow velocity in the sediment transport formula

4.6.6 Different magnitude of spiral flow

Spiral flow has a significant effect on the bed topography of the river with its many flow curvatures. The most obvious difference with a large spiral flow compared to no spiral flow, is the shape of the bend given in red in Figure 4.20. According to theory, the spiral flow deflects the sediment transport to the inner bends, increasing erosion at the outer bend and deposition in the inner bend. This created two sharp bends with large point bars. More interesting, is the incisions of the new channel with larger spiral flow (encircled with orange). Most likely is that the flow is subject to high resistance in the right direction and looks for a shorter route (this is similar to a meander cutoff). Due to the spiral flow, the bends get sharper and the route for the flow longer, which is the cause of the larger resistance. Also in other cases, the spiral does not directly result in the incision of channels. Indirect causes, due to change of the bed, more often result in the incision of new channels.

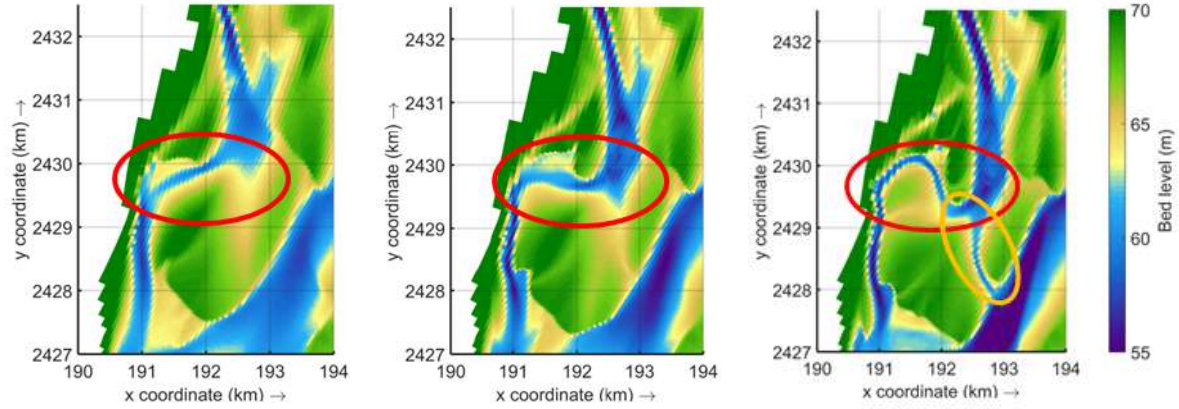

(a) No spiral flow ($E_{spir} = 0$) (b) Default spiral flow (reference run, $E_{spir} = 1$) (c) Two times larger magnitude spiral flow ($E_{spir} = 2$)

Figure 4.20: Bed levels for simulation with a different magnitude of the spiral flow

4.6.7 Different magnitude bed-slope effect

The effect of bed-slopes effects on the morphology is relatively straight forward. With a larger bed-slope effect (meaning a lower value for $A_{shields}$ in the model), banks and bars become flatter and the channels become shallower. With a smaller bed-slope effect banks and bars become steeper and channels become narrower and deeper (as Schuurman et al. (2013) also described). A large bed-slope effect also has a smoothing effect on the bed topography. This is clearly visible in Figure 4.21. In the left figure, which shows the results with a higher bed-slope effect, the islands are more smooth. In the other two figures two small channels are located. The bed-slope effect also has a large effect on the first bank on the left in Figure 4.21a. The appearance of more small channels or incision with a lower bed-slope effect is logic, since it allows smaller and narrower channels.

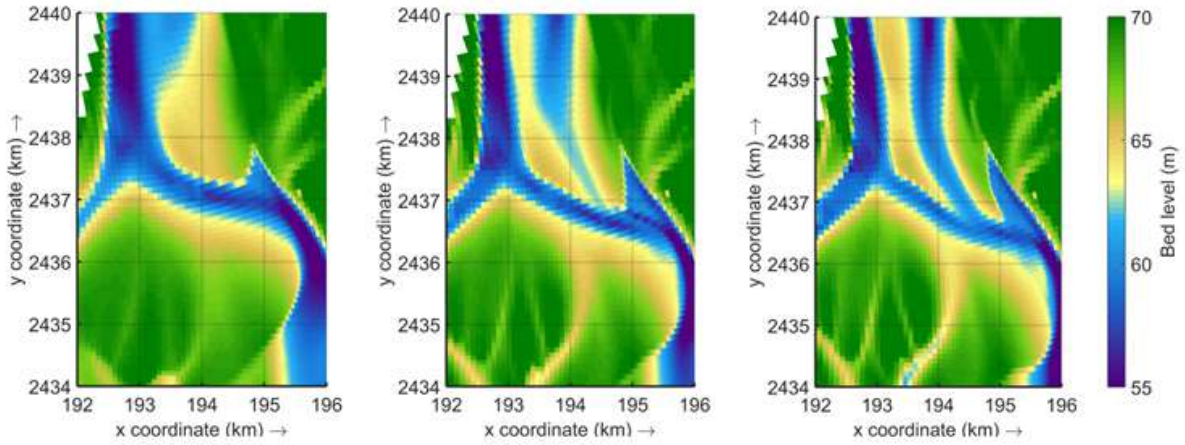

(a) Large bed-slope effect ($A_{shield} = 0.4$)

(b) Default bed-slope effect (reference run, $A_{shield} = 0.7$)

(c) Low bed-slope effect ($A_{shield} = 1.0$)

Figure 4.21: Bed levels for simulation with different magnitudes for the bed-slope effect

4.7 Conclusion sensitivity analysis

The effects of the physical processes tested in this sensitivity analysis can be split in effects on the morphology and on the dynamics. For the morphology the variations in discharge are of main importance. Due to the interaction of sediment transport magnitudes and locations at the different water levels, channels perpendicular to the flow direction with high water can maintain. This also causes different shapes of bars. The internal sediment transport processes have the largest influence on the width and depth of the channels. These processes also influence the shape of the bars. The bed-slope effect forces the bars to be lower, as it is negative feedback on bar growth. Spiral flow increases curvatures in the channels (creating differently shaped bars) and can cause meander cutoffs. With the use of different sediment transport formulas, the sediment transport on top of bars can be influenced, determining the height of these bars. It also plays a role in the dynamics of the system. Larger sediment transport on top of the bars has larger velocities of these bars as consequence. With higher peak discharges the velocity of these bars is also increased. Most important for the dynamics are the pulses of sediment that move through the system. These result in channel widening and narrowing, but also shift of the channel.

Chapter 5

Physical process evaluation based on combined satellite imagery and model observations

In Figure 5.1, the development of the bed is visible for a simulation of twenty years. It is clear that some significant changes of the channels and islands occurred. Some of them are similar to what can be observed on satellite imagery, others are more unlikely. The predictive value of the model is hard to asses, but has to be limited since not all important physical processes discussed in chapter 2 are implemented in the model (bank erosion, vegetation and to a limit extent turbulence). Even though the predictive value is limited, the model returned similar morphodynamics as found on satellite imagery, for which the underlying processes can be explained. The effects of certain processes were described in the sensitivity analysis. In this chapter another approach will be used, where observations from satellite imagery and model results are combined. The analysis starts with the reference model as used in the sensitivity analysis from the previous chapter. Where the satellite imagery and the model show similar morphological development, the model will be used as tool to explain which processes play a role in these developments. Where the model and satellite imagery show different results, an analysis is performed of how these differences could occur. This could mean an adjustment to the model to test which processes play a role in these differences, or an analysis on processes that are or not included in the model. The set-up of each model used in this chapter given in appendix C.5.

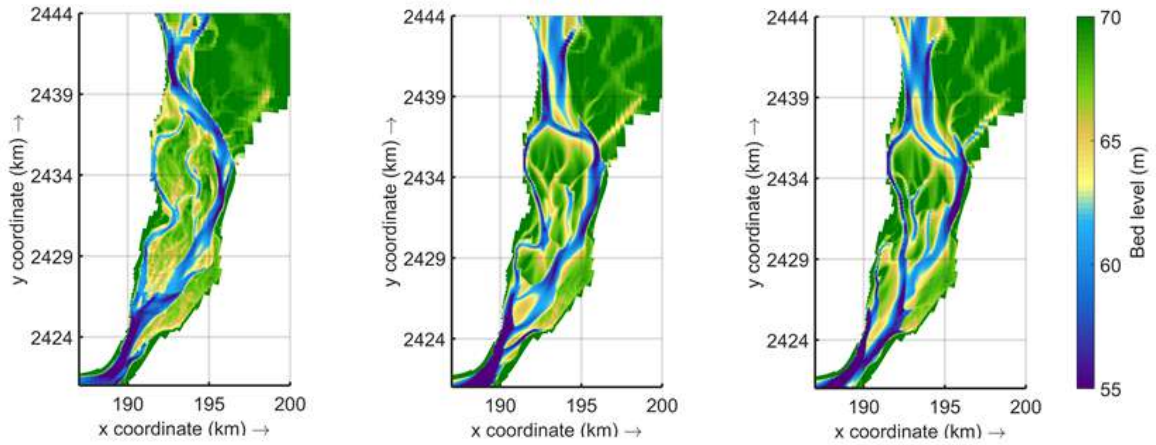

(a) Initial (b) 10 year simulation (c) 20 year simulation

Figure 5.1: Bed development of a simulation of twenty years (model 1, appendix C.5)

5.1 Incision of side bar

In Figure 5.2a to 5.2c, the process of incision in a side bar is displayed on satellite imagery. From only satellite imagery, it is not to possible to tell what the reason could be for such an incision. In the model occurred a comparable incision, which is displayed in Figure 5.2d to 5.2f. During the beginning of the falling stage, an increase in flow velocity and sediment transport can be found in the main channel. Due to the difference in flow direction on top of the bar and in the main channel, deceleration of the flow occurs on top of the bar in the inner part of the bend. This has deposition as consequence, giving an increase in bar height on that side. In this way, the lower part of the bar will be enclosed by the floodplain and by the higher part of the bar. With the main flow straight on this new channel, the flow will be pushed through it. When the water drops even further, the flow will be concentrated in this channel. This leads to an increase in sediment transport with erosion as consequence. In Figure 5.2e and 5.2f this erosion is visible. During two falling stages a whole new deep channel is created. This incision is mainly caused by sediment transport by the primary flow, where the erosion during the falling stage has an accelerating effect.

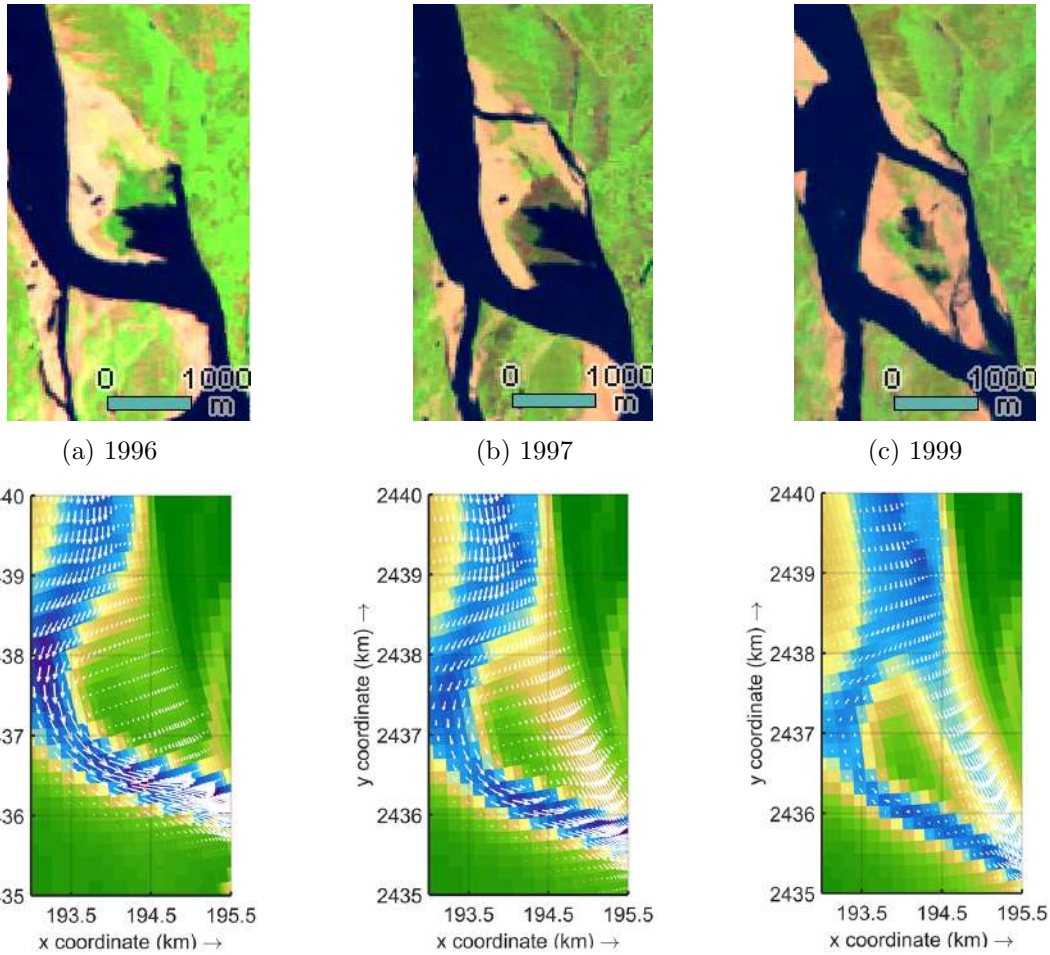

(a) 1996 (b) 1997 (c) 1999

(d) Beginning falling stage (e) End falling stage (f) End next falling stage

Figure 5.2: Incision of a side bar from satellite imagery and model simulations. In the figures of the model simulations bed level and sediment transport are given (model 2, appendix C.5).

5.2 Morphodynamics at the inflow and trifurcation reach

The morphodynamics in the inflow and trifurcation reach showed the largest variability, due to the large differences in incoming bars. This causes a variability in channel pattern, which is displayed in the three satellite images in Figures 5.3a to 5.3c. To simulate this with the model, large variability had to be found at the boundary. This variability must be found in the sediment input, which determines the creation of bars. The created bars will force the channels to shift, giving change in the channel pattern. In Figure 5.3d, the results of a ten year simulation with the model with input as used in the sensitivity analysis is displayed. Here, a straight inflow reach is created, which is very unlikely to happen. Increasing the sediment input, which is done for the simulation of which the results is shown in Figure 5.3e, already caused the creation of multiple bars (near the islands and on the sides of the channel). Still, the inflow channel is relatively straight. This means that only larger amounts of sediment input will not cause shift of the channel in the inflow region.

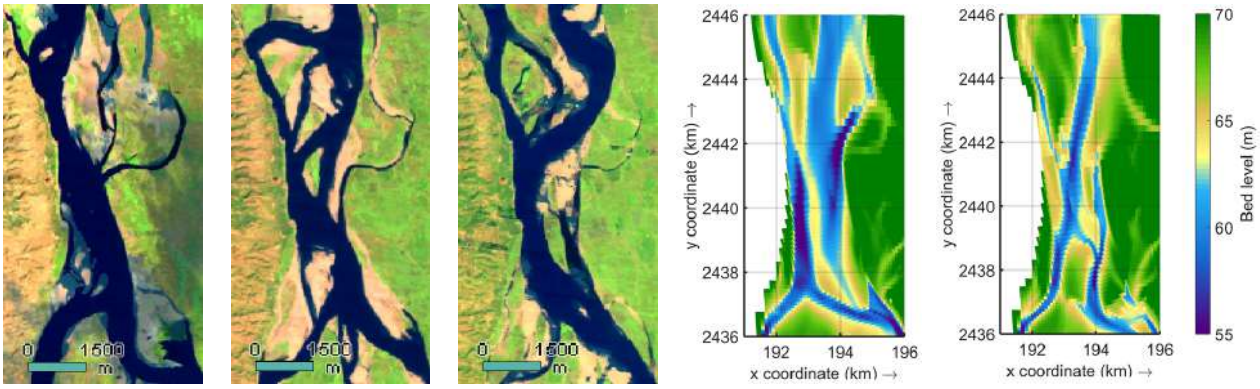

(a) 1996 (b) 2006 (c) 2016 (d) 10 years simulation (model 2, appendix C.5). (e) 10 years simulation, extra sediment input (model 3, appendix C.5).

Figure 5.3: Morphology at the upstream end of the research area on satellite imagery for three different years and for the reference model and a model with four times more sediment input

An attempt for larger dynamics with shifting channels at the upstream end of the research area, is done by extending the model in upstream direction. This showed to have no significant influence on the channel pattern. No bathymetrical data was available for the reach further upstream, so a bathymetry was created manually. The channel pattern and island shapes were based on satellite imagery, where heights and depths of the channels were estimated from the bathymetrical data of the original model. The initial bed and results of the simulations with the extended model are given in Figure 5.4. It was expected that bars would move downstream, causing change of the inflow channel of the research area (between y=2440 km and y=2445 km). However, as can be seen in Figure 5.4b, a similar result was found as with the original model (Figure 5.3d). For the shift of the channels and the creation of incoming bars, it is necessary to have pulses of sediment coming in. In the extended part of the model too low irregularities in the bed were created for the development of these sediment pulses. Maybe even more important, is the absence of a dynamic boundary at the upstream end. For the simulations in Schuurman et al. (2013) also no dynamic boundary was used, resulting in almost no changes in bar shapes and channel pattern.

To create sediment pulses and a shift of the channel, the sediment input was varied over the width of the boundary. This is done by dividing the upstream boundary in six parts, where de discharge was varied in time over the different boundaries. Where the water level is approximately the

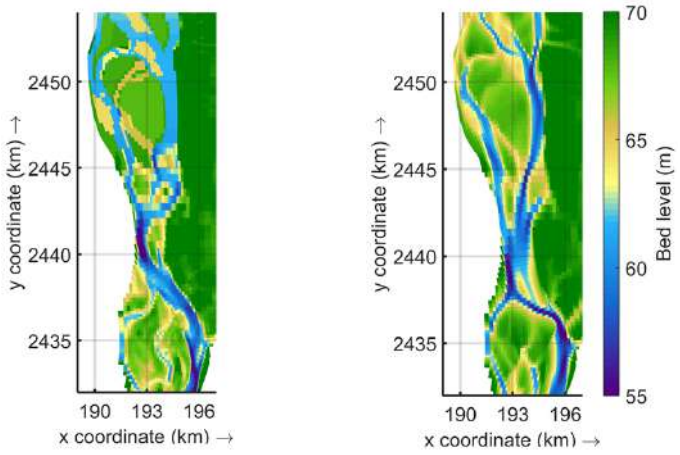

(a) Initial (b) After 10 years simulation

Figure 5.4: Initial bed level and bed level after a simulation of 10 years (model 4, appendix C.5).

same over the width, but the discharge is varied over the width, flow velocities were higher where the discharge was high. The model computed an overload of sediment at these locations. The flow carrying the large amount of sediment merges directly af the boundary with the flow with a lower velocity. This causes deceleration, with deposition of the overload of sediment as consequence. Shifting only the inflow over the boundary will result in a meandering planform (Schuurman et al., 2016b), but also adding this overload of sediment to the model resulted in braiding. From the overload of sediment bars were created, resulting in a shift of the channel. Using this method the location of the channel is not determined by the direction of inflow at the boundary, but by the bars that were created from the overload of sediment. This resulted in large variations in the location of the inflow channel, as found in Figure 5.5. This had dynamics in the complete research area as consequence, which turned out to be essential for the later mobility of the system. This is in agreement with the results of the flume study of Ashmore (1987). Although this method of shifting boundaries was very useful to simulate later dynamics in the system, it is hard to control the actual amount of incoming sediment. To have more control over the simulated scenarios, additional test have to be performed. More details about the input of this method can be found in appendix C.3.

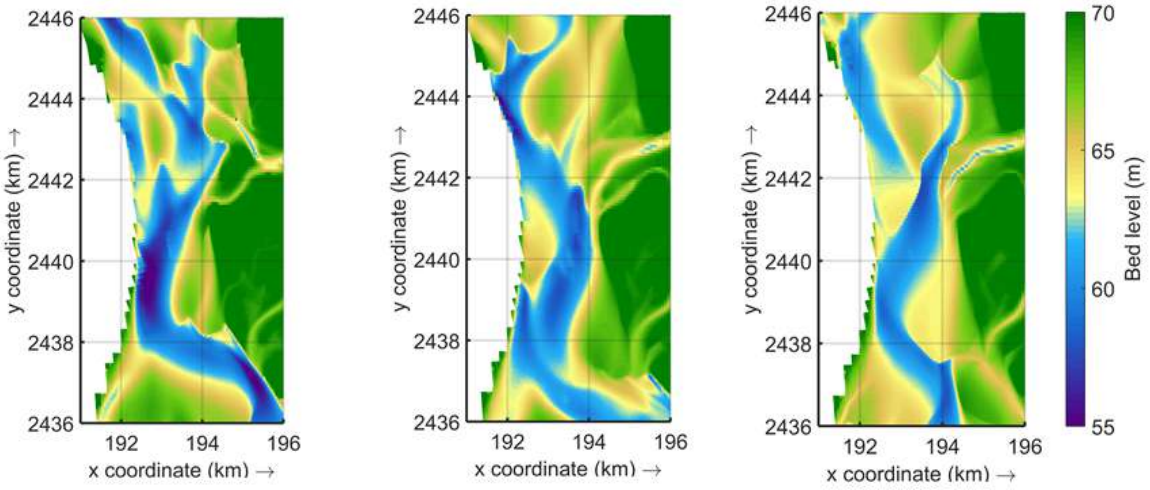

(a) 5 years simulation (b) 10 years simulation (c) 15 years simulation

Figure 5.5: Bed elevation of the inflow channel with shifting channel and moving bars (model 5, appendix C.5).

An example of an irregular channel pattern that is created by bars moving from the upstream end, is given in Figure 5.6a. A similar channel pattern is also found from satellite imagery, given in Figure 5.6b. From both satellite imagery as the model is visible that this channel pattern is forced by bars coming from upstream (for the satellite imagery this is also explained in more detail in appendix B). The results from the sensitivity analysis showed that the different stages in the hydrograph are important for the creation and maintenance of channels perpendicular to the main flow under high water conditions. The different stages in hydrograph were also necessary simulate a situation as shown in Figure 5.6a. During high water, deposition occurred in the channel to the right, making it narrower and shallower. This decrease in cross-sectional area of the channel system is the cause of a flow velocity increase during the falling stage, which results in high sediment transport in the channel. The increase in sediment transport locally in the channel has as consequence that the channel deepens and widens again during the falling stage, avoiding closure of the channel. In the meantime, the bar moved further and further till it reached the islands and closure of the channel could not be prevented any more.

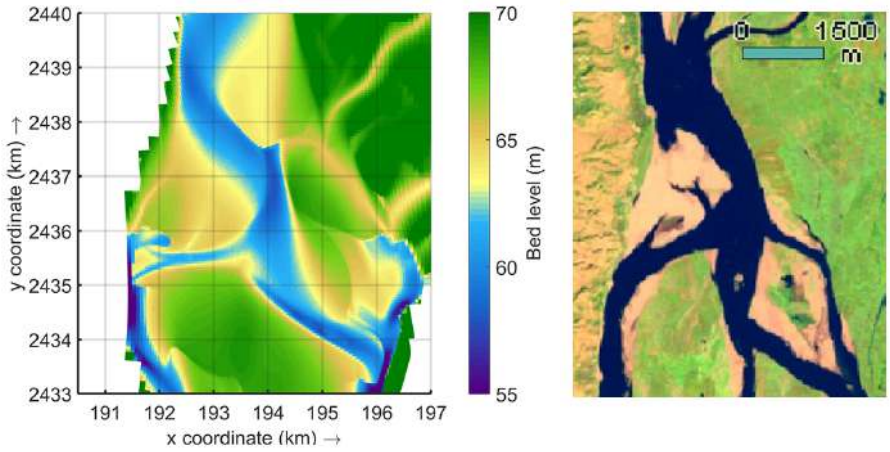

(a) Bed level in model (b) Satellite image of year 1999

Figure 5.6: Comparable unnatural looking shape from satellite imagery and model results (model 5, appendix C.5).

5.3 Movement of the islands

Figures 5.7a and 5.7b are satellite images showing the shape of the islands. It is visible that the islands moved in downstream direction the past ten years, but that the shapes remain similar. The heads of the islands remain peaked and the channels are located at approximately the same locations. In the model, the peaked shape of the islands is already changed after a simulation time of five years, as shown in Figure 5.7c. This is probably caused by the absence of (the effects of) vegetation in the model. Figure 5.8 shows an island head where sediment is kept together by the vegetation on top of it. How much the vegetation influence the erosion speed cannot be determined by comparing satellite imagery and the model, since the real sediment transport is unknown and not used for the model. However, it is likely that the vegetation has an effect on the shape of the island heads, since the shape in the model (without vegetation) deviates significantly from the shape on satellite imagery of the past years. The effect of the vegetation becomes even more evident when using a dynamic boundary with sediment varying over the width. In Figure 5.7d is shown how the islands deform in a simulation time of just ten years with dynamic boundary.

Vegetation does not seem to be the only island shape influencing factor, but the collision of bars with the islands also has a large influence. In Figures 5.9a and 5.9b is shown how a bar attached to the islands in the wet season of the year 2000. In the subsequent three wet seasons,

the sediment is spread out over the island heads. It can be seen that non vegetated areas move faster than the vegetated island heads. Although not visible from the imagery, the height of the bars/islands could also influence the speed of movement. In the model (Figure 5.9d) collision of a bar with the islands is also found in the model, for which a four times larger sediment input was necessary compared to the basis model of the sensitivity analysis. In the figure is visible that the shape of such a bar is also similar to what is found on the satellite imagery.

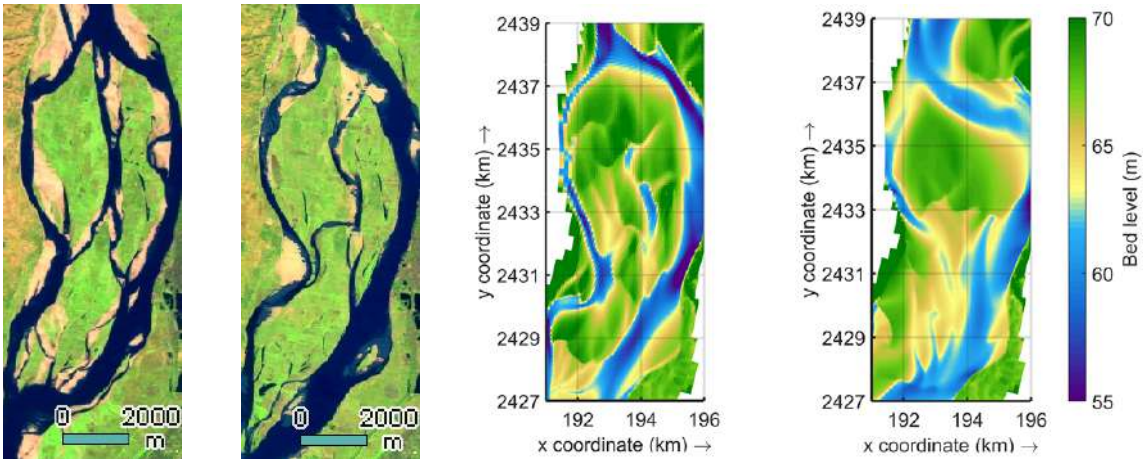

(a) 2006 (b) 2016 (c) Bed level after a simulation of 5 years (model 2, appendix C.5) (d) Bed level after a simulation of 10 years with dynamic boundary (model 5, appendix C.5)

Figure 5.7: Satellite images and model result showing the shapes of the islands. From satellite images only a limited deformation can be observed, but in the model large changes appear.

Figure 5.8: Picture of the left island head showing bank failure and the vegetation on top it (January, 2017)

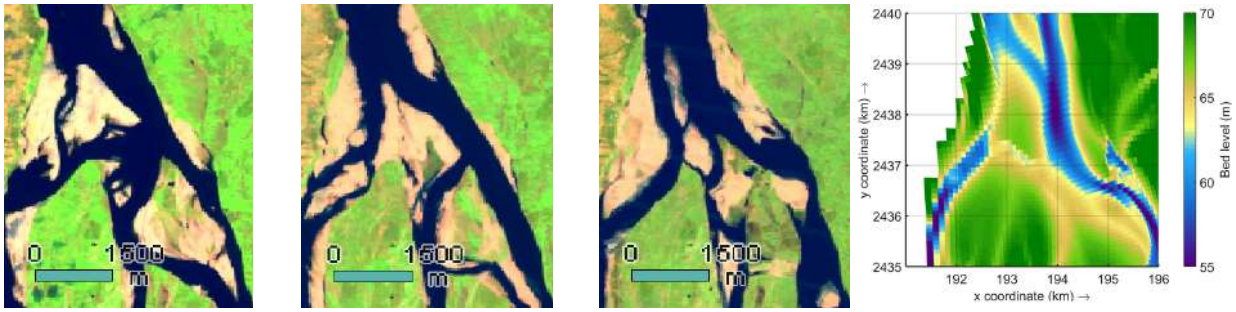

(a) 2000 (b) 2001 (c) 2004 (d)

Figure 5.9: Satellite images and model result showing the attachment of bars to the islands (model 6, appendix C.5).

5.4 Development of mid-channel bars

In section 4.5 of the sensitivity analysis was already concluded that the mid-channel bars do not develop in the model. A reason for the absence of these mid-channel bars could have been a too low amount of sediment input. However, even when large amounts of sediment were put into the model, the mid-channel bars did not develop. Another option is the absence of bank erosion in the model. Sarker et al. (2003) describe that mid-channel bars deflect the flow to the outer banks, leading to bank erosion. The process of widening by bank erosion and sediment coming available enhances the process of continuous bar development. An example of this is given in Figure 5.10. In this figure the movement of a bar is followed from 2015 to 2017. While the bar moves in downstream direction, it narrows the channel. It also forces the flow to the other side of the channel, with erosion of the bank as result. The bank of the year 2015 is also shown in Figure 5.10c. The movement of the bank is approximately 200 metres in just two years time. In Figure 5.11, a picture is shown of the situation in 2017. On the foreground, the moving bar is visible and on the background the eroding bank. It is visible that erosion due to failure plays a dominant role here. Similar types of bank erosion due to mid-channel bar movement can be observed more on satellite imagery, but cannot be found in the model. This is probably because bank erosion by bank failure is not included in the model. Without widening of the channel due to bank erosion, flow velocities remain too high and the bar will be eroded instead of moved to the widened part of the channel.

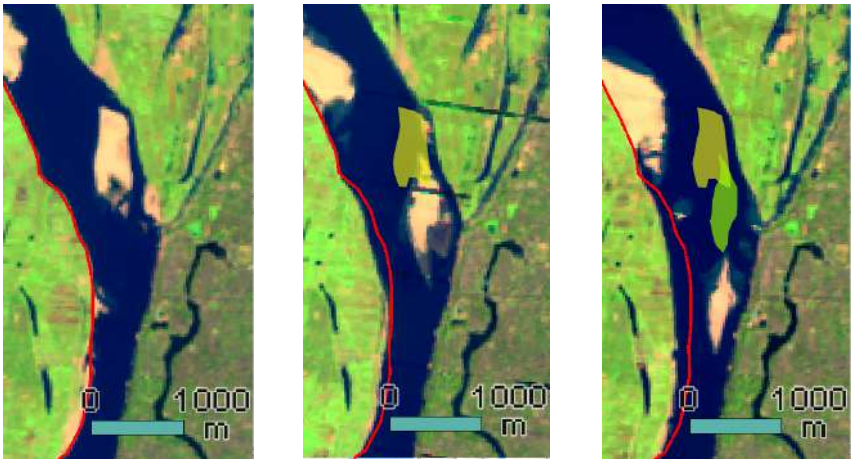

(a) 2015 (b) 2016 (c) 2017

Figure 5.10: Satellite images showing the interaction between bank erosion and the movement of a mid-channel bar. In red the right bank of the year 2015 is displayed and in yellow and green the path of the bar is followed

Figure 5.11: Picture with on the foreground a mid-channel bar and on the background the erosion of the bank by bank failure (January, 2017)

Chapter 6

Discussion

The consequences of sediment management and river training measurements in braided rivers remain challenging to predict, because the understanding of the underlying physical processes of the morphodynamics are still not sufficiently understood. The goal of this study was to investigate the most relevant physical processes influencing the morphodynamics and to asses the ability of the model to make predictions. This chapter starts the relation of the results of this study with the present literature, followed by a discussion on the input the model. In the subsequent two section the results of the analysis of this study are discussed. In the final section is explained how this model can be used for engineering purposes.

6.1 Relation to present literature

Van der Velden (2015) also did a case study on the Ayeyarwady River to investigate the morphodynamics, using both satellite imagery and a Delft3D model. Her research described the changes in planform of a period of fifteen years and the impact on the river system by possible river training measures for navigability. Where van der Velden (2015) focussed on a 177 kilometres reach, this study focussed on a much smaller reach of 30 kilometres. Together with the availability of more accurate bathymetrical data, it was possible to investigate the physical processes determining the morphology and dynamics in more detail. The increased understanding of these processes will be useful for further navigability studies, since the physical processes most important for modelling (navigable) depth were explored. The processes are the sediment transport by primary flow and deflection of sediment transport by spiral flow and bed-slope effects. In addition does the input of sediment showed to be the main driving factor for the dynamics, causing shift of the channels or fairways.

Schuurman (2015) also used the 2D depth-averaged Delft3D model to investigate the morphodynamics of braided rivers. In his studies he always used an artificial straight river reach, where a braided river developed from an almost flat bed. After a certain period, bars moved in downstream direction barely changing of shape. He mentioned that stabilizing of these shapes was caused by the absence of realistic changes in sediment input at the upstream boundary. In this study is shown that this is indeed the case. Changing the sediment transport formula could also have a reducing effect on the stabilization of the shapes of bars and channels. With a lower power above the velocity in this formula, the sediment transport on top of bars can be increased. This causes larger movability of the bars and less stable and deep channels.

Surian (2015) and Williams et al. (2016) both described in their summarizing studies that the comparisons between numerical models and other sources of information (physical models, data)

is still lagging, but could return valuable information. In comparison with Schuurman (2015), the Delft3D model is in study applied to an existing case. This gave the opportunity to compare the model results with the satellite imagery, which returned information about physical processes that might not be (correctly) implemented in the model. It showed that the process bank erosion by failure might be necessary for the development and shift of mid-channel bars. In addition, it showed that vegetation on the islands is a dynamics reducing factor and is of main importance for the stability of the islands.

6.2 Discussion model input

For the model, the choice is made to use a morphological acceleration factor of thirty to reduce the computational time. This resulted in an increase of the sediment transport at the upstream end of twenty percent, descending to no increase at the downstream end. This increase in sediment transport is caused by a more rapid decrease or increase of the discharge then the water level can adopt (the hydrograph is squeezed using morphological acceleration). This has unrealistic flow velocities as results, leading to unrealistic sediment transport. This effects dampens out further into the system. A decrease of sediment transport towards the downstream end has as result that the bed slope decreases. The celerity in which the bed slope decreases is not further investigated, but with the large fluctuations in discharge as found in the Ayeyarwady River, caution has to be given to the use of morphological acceleration.

The downstream boundary also showed to have significant impact on the results. It was found later that the used downstream boundary, a relation between discharge and the water level, overestimated the water level approximately four metres. Calibrations of the water levels with this new boundary resulted in a lower bed roughness with flow velocities fifteen to twenty percent higher (A. Commandeur, personal communication, 2017). This resulted in larger dynamics with more incisions of new channels and shift of existing channels, especially near the downstream end.

For this study, the only available data on sediment transport was including wash load. An estimation had to be done for the amount sediment transport interacting with the bed. This estimation showed to be in the right order, since velocities of bars were on satellite imagery and in the model were similar. However, more data on the sediment transport is a prerequisite. This would give more accurate results in general, but would also be valuable for the determination of the amount of sediment input.

6.3 Discussion satellite data analysis

The first understanding of the river dynamics was obtained using satellite imagery. The analysis of the satellite imagery showed that morphodynamics can be described very well from the sequence of satellite images, but that it can be difficult to asses from them which processes caused these developments. The description of the morphodynamics, together with the determination of the fixed banks, islands and the dynamic regions, gives a good support for the interpretation of model results. The use of average reflectance composite images showed to be very useful. Where in previous studies (Baki and Gan, 2012; Wang et al., 2014; Bhunia et al., 2016) only cloud-free imagery was available with unequal time slots, this method allowed to have yearly images under similar conditions. Disadvantage of the use of average reflectance composites is that the discharge on images is harder to asses, since the averaging process is rather complex.

For this study, the data of the satellite imagery has only been used for visualization purposes of water masks and the river planforms, but much more processing analysis are available for a more extensive analysis of the river region. As example, Pahlowan and Hossain (2015) used the

NDVI (normalized difference vegetation index) to explore the effects of vegetation on migration of banks. Other valuable analysiss could be the determination of bank line shift, determination of island and bar sizes, determination of island and bar velocities or the determination of the amount of suspended sediment. Doing this with a processing platform with scripted analysis, such as the Google Earth Engine, analysis can be performed easily on different regions.

6.4 Discussion sensitivity analysis

The sensitivity analysis has been an observation of the relative influence of the different processes. Comparison of results in previous studies on braided rivers is mainly done using reach scale measures as channel count indices, braiding intensity indices or sinuosity. To study the effects of individual processes, the focus had to be on local changes. It turned out to be difficult to find suitable measures for the comparison of the different results, due to the large dynamics of the system. In addition, drawing conclusion on the effects of the processes had to be done carefully. Varying the processes could have subtle changes upstream as consequence, which also affect the situation further downstream. This makes changes not only dependent on the change of the process, but also on the morphology further upstream. For engineering purposes it will also be necessary to look at local change. A possibility could be to use pattern recognition. Certain morphodynamics, such as the downstream movement of the confluence, repeat themselves. Recognizing these patterns can be useful for short term predictions or validation of models.

A sensitivity analysis on sediment transport by primary flow and deflection of it by spiral flow and bed-slope effects, was also performed by Schuurman et al. (2013). However, in this study different sediment transport formulas are considered and also the effects of hydrological variations were taking into account. Testing the effects of spiral flow and the bed-slope effect again, was to give the full picture and to observe the relative influence of the parameters. Another process tested by Schuurman et al. (2013) is the bed roughness. He stated that effects of this process were also significant. Therefore, it is recommended to take this process into consideration with further use of models.

The comparison of the results in this sensitivity analysis showed that the processes having largest effect on the morphology, are the presence of hydrological variation, the sediment transport by primary flow and the deflection of the sediment transport by spiral flow and bed-slope effects. The hydrological variations are implemented in the model relatively realistic in the upstream boundary, but the other processes are implemented as constitutive formulations. The functioning and accuracy of these processes has to be calibrated. For this study, only data was available for the initial bed. This made it impossible to check whether development with the bed using of these constitutive formulations was correctly. Calibration of these processes was only possible by comparison with satellite data, which has been rather arbitrary. For a larger accuracy, a possibility is to implement these processes differently. Schuurman et al. (2013) suggested for example to search for a physics-based approach for the bed-slope effects. To avoid the use of the constitutive relation for spiral flow, a solution could be to perform 3D calculations. This enables the model to have different directions of flow velocity in the bottom and top of the water column. In this research a sediment transport formulation was proposed based on a different roughness model. This shows that the sediment transport is not only dependent on the used estimator, but also on a correct representation of the other processes. Multiple sediment transport formulas must therefore be considered for the calibration of new models.

Looking at the process of hydrological variations, Schuurman et al. (2013) mentioned that using a constant high discharge instead of using a complete hydrograph did not matter for the final results of the simulation (only some channels and bars where reactivated). Simulations in this study show that the use of a hydrograph is essential for the existence of channels perpendicular

to the main flow direction during high water. The existence of these channels is also found on satellite imagery and does affect the shapes of bars as well. For the hydrological variations it is important have a peak discharge for which all islands and bars will be submerged. In this study is shown that varying the peak discharge does not have a significant influence on the shape of the channel and bars, but this also has its limit. It will be necessary to use a discharge high enough to have flow velocities on top the islands that induce significant sediment transport and so movement of the islands.

The effect of varying the falling period did not result in significant differences in morphology or sediment transport, while Coleman (1969) mentioned that the rapid decrease in water level could lead to local deposition and incision of channels. Several reasons can be given for this. A first reason is the absence of the process bank erosion by failure. With a rapid drop of the water level, the propability of instability of banks is larger. However, this cannot be found in the model. Another probability is that the local bed topography played a role in this. At locations of for example narrow channels, large erosion was found during the falling stage. Variation in the duration of the falling stage could in those cases be of influence. Investigating this could for example be useful for efficient dredging.

6.5 Discussion physical process evaluation based on combined satellite imagery and model observations

The evaluation of the model using satellite imagery showed to be useful as additional method to learn more about the processes then was done from the sensitivity analysis, but also about different processes than from the sensitivity analysis. Similar bed developments in the model as found on satellite imagery provided extra information on how these morphodynamics evolved. An example is the incision of a side bar, where increased sediment transport during the falling stage turned out to play a major role. Another example is the rotation of the large bifurcation to a very unnatural looking shape. For the creation of these type of irregular shapes both a hydrograph and bars moving into the system turned out to be necessary.

Differences between the satellite imagery and model results were also informative. It was found that straightening of the inflow channel had to be avoided, because this reduced later mobility of the system. A limited later mobility in model simulations was also found by Schuurman et al. (2013), Yang et al. (2014) and Surian (2015). A method was found to increase the dynamics at the inflow channel and consequently the rest the research area. Important was to create pulses of sediment, varying over the width of the upstream boundary. However, large uncertainties are there in the amount of sediment coming into the system (Jagers, 2003). This uncertainty will partly remain, but can be reduced by increasing the understanding of the effects of the sediment input and by measuring or determining the actual amounts of sediment transports. A better understanding on the sediment input can be created by doing physical experiments. Especially the effects of horizontal variation in the sediment input has not yet been studied. To determine the actual amount of sediment input, the most accurate possibility is to make measurements of the sediment transport. Because a large variability is there in space and time, it important measure at multiple locations with a limited time step. The measurements also have to capture at least five years to learn about the variability in the sediment discharge. In addition, it will be necessary to make measurements of the bathymetry in the meantime. In this way, transport on the bars and in the channels can be compared. This already shows that many measurements will be needed, which can be very costly. The sediment transport can also be estimated with a combined satellite and model analysis. From the satellite imagery bars sizes and velocities can be determined. Creating similar bar sizes and velocities could return information on the actual sediment transport. With the measured or estimated (with the model) sediment input,

scenarios can be determined and simulated to cover the uncertainty of forecasting the amount of sediment input.

What also can be done is to extent the model in upstream direction. The further the boundary of the model is located from the area to investigate, the later the effect of the boundary will reach the research area. With a longer model, the bars coming into the research domain are also as realistic as possible. However, only extending the model will also result in a simulation in which bars will not reshape (as found in (Schuurman et al., 2013)). A dynamic boundary, with variation over the width in sediment input, will be necessary to keep the model dynamic.

Also found from the comparison between model simulations and satellite imagery, is that the vegetation has a stabilizing effect on the islands. This decreases the dynamics of the system significantly. Because vegetation is not included in the model, it was visible that the islands moved differently and more freely than observed from the satellite images. This effect was even larger using the varying sediment input at the boundary. For a correct representation of the morphological change, it is therefore necessary to implement vegetation. Present options to simulate the presence of vegetation in Delft3D are a local increase of the density of the sediment or a locally lower availability of sediment. The use of these methods did not give satisfying results. Locally decreasing the availability of sediment can results in islands at locations where these are not desired. Locally increasing the density of the sediment with a factor two did not give significant differences in the erosion of the islands. In addition, this will also influence the long term response of the system. For more realistic results, it is recommended to create an option in Delft3D for the process vegetation. Especially in combination with methods to increase the dynamics (at the boundary), this will be necessary.

From the comparison between model simulations and satellite imagery is was not directly clear whether bank erosion due to failure is essential for the development of the morphology, even though from field observations was clear that is occurs at many locations. Movement of banks of the islands was also observed in model (where bank erosion due to failure is not implemented), which took place while the islands were submerged. The only significant difference found that indicates that bank erosion due to failure is important for the development in the river, is the absence of the development of mid-channel bars in the model. The fact that no significant differences are visible during the falling stage could also be a sign of the absence of bank failure. Where in other braided rivers as the Brahmaputra the erosion of banks has a significant influence (Baki and Gan, 2012), it is possible that this is of less importance in this river reach. This might be the case, since this river reach is enclosed between Mandalay and the mountain ridge. It is also possible that the bank erosion due to failure is simulated in the model by fluvial bank erosion, because of the absence of vegetation. This could be investigated in more detail using the Delft3D module which does include bank erosion. The difference between simulations with the two different models could show the effect of having bank erosion by failure. The model including bank erosion by failure could also tell something about the hypothesis of the absence of mid-channel bars. Bank line shifts found in this model can also be checked by determining bank line shift from satellite data. In the analysis of bank line shifts from satellite imagery, the presence of vegetation can also be taking into account.

6.6 Application of the model for engineering purposes

This study was done to increase the understanding on the morphodynamics of the Ayeyarwady River and to come a step closer to the design of suitable and sustainable river training measures. The most dominant processes are explored, which can be used for the improvement of the model results. It is clear from this study that the model cannot be used to predict the morphodynamics precisely. The main causes for the limited predictive value of the model are the uncertainty in

upstream input of the sediment and the absence of the process vegetation in model. The absence bank erosion by failure in the model also has a minor effect on this. The deviations in processes in the model and reality cause incorrect predictions of the morphodynamics. Where this causes relatively small deviations upstream, these deviations result in even larger differences in the predictions downstream.

Without giving precise predictions, the model can still be useful for engineering purposes. The comparison between the satellite imagery and model results showed that the model is able to simulate local morphodynamics correctly. This means that the model cannot be used to determine what time and which locations erosion or deposition can be found, but that it can be used to determine at which locations erosion or deposition can be expected at some moment in time. An advantage of the use of the model, is that different scenarios can be tested easily. Different scenarios could for example contain variations in the location and amount of the sediment input.

Because the model can be used to asses locations of risk for sedimentation and erosion, it can also be used to determine the impact or river training measures. Impact assessment can also be done for sediment management measures. Since the model can also be used as estimator for the amount of sediment transport, the amounts to dredge can also be determined.

Chapter 7

Conclusions and recommendations

In the first section of this chapter the conclusions of this study are given and in the second section the main recommendations for further study of the Ayeyarwady River.

7.1 Conclusions

The goal of this research was twofold. The first part was to explore the effects of the most relevant physical processes on the morphodynamics of the Ayeyarwady River and the second part was to investigate the ability of a 2D depth-averaged morphodynamic model to simulate the morphodynamics of the Ayeyarwady River. The physical processes that influence the morphodynamics can be separated between system forcing processes influencing flow and sediment transport and internal flow and sediment transport processes. The first group of processes is imposed by the system and contains the hydrological variations, the input of sediment in the system, the availability of erodible sediment, vegetation and the bed roughness. The second group is the consequence of the system forcing processes and contains the sediment transport by primary flow, deflection of the sediment transport by spiral flow and bed-slope effects, turbulence and bank erosion. All these processes are interrelated with each other in different ways, all having different influence on each other and on the morphology. Since the morphology also affects the different processes, a positive feedback exists. This positive feedback between all processes makes the change in morphology, or the morphodynamics, hard to predict.

The observed morphodynamics differ of character for the different regions in the research area, due to the existence of non- or hardly erodible banks, islands and floodplains. At the inflow, bars are passing from different directions with a speed up to approximately 600 metres per year, making the channels shift in different directions. The passing bars and shifting channels create different conditions at the trifurcation, which leads to a different distribution of the flow and sediment over the channels between and around the islands. The island heads are eroded during high water, making the islands move in downstream direction. Islands grow in upstream direction again, when passing bars collide with them. The changing conditions at the trifurcation also cause variation in the downstream channels. Where the smallest channels are relatively stable, many side and mid-channel bars develop and move trough the largest of these channels (Mandalay channel). The bars make the channel widen and narrow. The different channels finally confluence in the downstream end of the research area. The position, shift and rotation of the confluence is determined by the distribution of the discharge at the trifurcation as well. This means that the morphodynamics of the complete system are influenced by the changes at the upstream end of the research area, so by the passing of bars and shift of the channel.

Model simulations are in agreement with these observations of downstream propagating distur-

bances and show that the influence of the passing and shifting bars at the upstream boundary are the essential driving factor of the complete system. The bars are created by pulses in the sediment transport and collide with the islands to make these grow in upstream direction or pass by to the Mandalay channel (largest channel). In the Mandalay channel the bars cause narrowing, widening and shift of the channel. The bars also influence the shape of the trifurcation with redistribution of the discharge over the downstream channels as response. Due to this redistribution of discharge over the channels disturbances propagate even faster downstream.

Whether the system is dynamic is determined by the input of sediment, but how the system will develop is also influenced by other processes. A dominant role in the shape of the islands, bars and channels is there as well for the hydrological variations, sediment transport by primary flow and the deflection of sediment transport by spiral flow and bed-slope effects. During the different stages of the hydrograph, different flow distributions can be found. These all have different morphodynamics as consequence. During high water, the whole area is morphological active. All the islands and bars move, which can cause closure of the channels perpendicular to the main flow direction during this stage. The falling and rising stage can have a large influence on deepening of these same channels, but also incision of new channels. During low water, some erosion and deposition can be found in the main channel, but no significant changes can be found here. Due the combination of the morphodynamics during these periods, different shapes of bars and channels can be created compared to with a constant high discharge.

Sediment transport by primary flow and the deflection of sediment transport by spiral flow and bed-slope effects all have large influence on the width of the channels and the depth in these channels. These processes also had other effects on the morphology. The bed-slope effect does not only flatten the channel, but also has this effect on the bars and islands. The spiral flow enhances curvatures of the channels with incision of new channels (meander cutoffs) as consequence. Sediment transport by primary flow is tested with different powers above the velocity in the sediment transport estimators. A lower power results in lower bars which propagate with a higher velocity.

Minor influence on the shape of the islands, bars and channels were found by variations of the peak discharges and period of the falling stage. A larger peak discharge lead to a more rapid development of the river (especially where the system is most narrow), but does not have significant influence on bar and channel shape. Variations in the period of the falling stage did results in almost no differences in the morphology.

The second part of the goal was to asses what the predictive value is of a 2D morphodynamic model. The results of the model were tested on the historical series of satellite images. Especially due to the large uncertainty in the sediment input, which is the main driving force of the dynamics of the system, it is not possible to forecast the exact morphodynamics of the river. Also the absence in the model of the processes vegetation and bank erosion by failure are a limitation in the predictive value of the model. The absence of vegetation has too large dynamics of the islands as result and the absence of the bank erosion by failure has as consequence that mid-channel bars do not develop in the model. The model still showed to be able to simulate local morphodynamics as were seen on satellite imagery. The model should therefore not be used to make predictions of the exact time and amount of erosion and deposition at a certain location, but it can be used to get a better understanding of what kind of morphodynamics could occur and what risk areas are for erosion (except for erosion of dry banks) and deposition.

7.2 Recommendations

For further study on the Ayeyarwady River the following recommendations are given:

- More quantitative analysis can be performed with the satellite data. Determination of bank line shifts, determination of (incoming) bar sizes and velocities and the quality of vegetation (for erosion resistance) could be valuable information for a better understanding of the system and for validation of the model.
- For more accurate results, data are needed of the sediment transport and bathymetrical change. This is necessary for the calibration of the model parameters for sediment transport, spiral flow and bed-slope effects.
- For simulating realistic as possible morphodynamics, a complete hydrograph must be used instead of a constant high discharge.
- A more realistic input of sediment is needed at the upstream boundary. The pulses in sediment input have to be large enough to create bars, but must also be varied over the width of the boundary to induce a shift of the channel. This is necessary for later mobility of the system.
- It is important to use the model for the correct purposes. The model cannot be used to make predictions of exact locations, moments in time and amounts of erosion and sedimentation. Meanwhile, it can be used to assess risk areas for erosion and deposition, to evaluate possible effects of river training measures and to determine locations of where to dredge and the amounts to dredge.

Bibliography

Ashmore, P. Bed load transfer and channel morphology in braided streams. *Erosion and Sedimentation in the Pacific Rim, International Association of Hydrologic Sciences Publication*, 165:333–42, 1987.

Ashmore, P. E. Laboratory modelling of gravel braided stream morphology. *Earth Surface Processes and Landforms*, 7(3):201–225, 1982.

Ashworth, P. and Ferguson, R. Interrelationships of channel processes, changes and sediments in a proglacial braided river. *Geografiska Annaler. Series A. Physical Geography*, pages 361–371, 1986.

Baedeker, K. *Indien: Handbuch für Reisende*. Leipzig, 1914.

Baki, A. B. M. and Gan, T. Y. Riverbank migration and island dynamics of the braided Jamuna River of the Ganges–Brahmaputra basin using multi-temporal Landsat images. *Quaternary International*, 263:148–161, 2012.

Bhunia, G. S., Shit, P. K., and Pal, D. K. Channel dynamics associated with land use/cover change in Ganges river, India, 1989–2010. *Spatial Information Research*, 24(4):437–449, 2016.

Chein, N., Zhou, W.-h., and Hong, R.-J. The characteristics and genesis analysis of the braided stream of the lower Yellow River. *Acta Geographica Sinica*, 10(6):734–754, 1961.

Coleman, J. M. Brahmaputra River: channel processes and sedimentation. *Sedimentary Geology*, 3(2-3):129–239, 1969.

Commandeur, A. The Ayeyarwady River: A graphical introduction to myanmar's main river. Unpublished presentation, 2014.

Deltares. Delft3d-flow user manual: Simulation of multi-dimensional hydrodynamic flows and transport phenomena, including sediments. *Delft, The Netherlands*, 2016.

Donchyts, G. Deltares aqua-monitor: Surface water changes (1985-2016). urlhttp://aqua-monitor.appspot.com/, November 2016.

Donchyts, G., Baart, F., Winsemius, H., Gorelick, N., Kwadijk, J., and van de Giesen, N. Earth's surface water change over the past 30 years. *Nature Climate Change*, 6(9):810–813, 2016a.

Donchyts, G., Schellekens, J., Winsemius, H., Eisemann, E., and van de Giesen, N. A 30 m resolution surface water mask including estimation of positional and thematic differences using Landsat 8, SRTM and OpenStreetMap: A case study in the Murray-Darling Basin, Australia. *Remote Sensing*, 8(5):386, 2016b.

Egozi, R. and Ashmore, P. Defining and measuring braiding intensity. *Earth Surface Processes and Landforms*, 33(14):2121–2138, 2008.

Engelund, F. and Hansen, E. A monograph on sediment transport in alluvial streams. Technical report, Teknis Forlag, Copenhagen, 1967.

Ferguson, R. Understanding braiding processes in gravel-bed rivers: progress and unsolved problems. *Geological Society, London, Special Publications*, 75(1):73–87, 1993.

Ferguson, R., Ashmore, P., Ashworth, P., Paola, C., and Prestegaard, K. Measurements in a braided river chute and lobe: 1. flow pattern, sediment transport, and channel change. *Water Resources Research*, 28(7):1877–1886, 1992.

Floodlist. Myanmar – 200 million dollars for flood recovery and resilience projects. urlhttp://floodlist.com/asia/myanmar-200-million-flood-recovery-resilience-projects, 2016a.

Floodlist. Myanmar – floods affect almost half a million people. urlhttp://floodlist.com/asia/myanmar-floods-affect-half-million-august-2016, 2016b.

Gao, B.-C. NDWI—a normalized difference water index for remote sensing of vegetation liquid water from space. *Remote sensing of environment*, 58(3):257–266, 1996.

Gran, K. and Paola, C. Riparian vegetation controls on braided stream dynamics. *Water Resources Research*, 37(12):3275–3283, 2001.

Gurnell, A. M., Petts, G. E., Hannah, D. M., Smith, B. P., Edwards, P. J., Kollmann, J., Ward, J. V., and Tockner, K. Riparian vegetation and island formation along the gravel-bed Fiume Tagliamento, Italy. *Earth Surface Processes and Landforms*, 26(1):31–62, 2001.

Hadden, R. The geology of burma (myanmar): An annotated bibliography of burma's geology, geography and earth science. Technical report, DTIC Document, 2008.

Jagers, H. *Modelling planform changes of braided rivers*. University of Twente, 2003.

Jang, C.-L. and Shimizu, Y. Numerical simulations of the behavior of alternate bars with different bank strengths. *Journal of Hydraulic Research*, 43(6):596–612, 2005.

Ko, K. K. Mandalay increases spending to counter riverbank erosion. urlhttp://www.mmtimes.com/index.php/national-news/mandalay-upper-myanmar/22787-mandalay-increases-spending-to-counter-riverbank-erosion.html, September 2016.

Marti, C. Morphodynamics of widenings in steep rivers. *River flow 2002: Proceedings of the international conference on fluvial hydraulics*, 2:865–873, 2002.

Marti, C. and Bezzola, G. R. *Bed load transport in braided gravel-bed rivers*. Wiley-Blackwell, Oxford, 2009.

Meyer-Peter, E. and Müller, R. Formulas for bed-load transport. IAHR, 1948.

Molinas, A. and Wu, B. Transport of sediment in large sand-bed rivers. *Journal of hydraulic research*, 39(2):135–146, 2001.

Mosselman, E. Bank protection and river training along the braided Brahmaputra-Jamuna River, Bangladesh. *Braided Rivers: Process, Deposition, Ecology and Management, edited by: Smith, GHS, Best, JL, Bristow, CS, and Petts, GE, Blackwell, Oxford, UK*, pages 277–287, 2009.

Nam, K. and Win, E. Competitiveness between road and inland water transport: the case of Myanmar. *Transport Problems*, 9(4):49–61, 2014.

Netherlands Enterprise Agency (Rijksdienst voor ondernemend Nederland, RVO). Fact sheet: Water in Myanmar, 2015.

Nicholas, A. Morphodynamic diversity of the world's largest rivers. *Geology*, 41(4):475–478, 2013.

Otsu, N. A threshold selection method from gray-level histograms. *Automatica*, 11(285-296): 23–27, 1975.

Pahlowan, E. and Hossain, A. S. Jamuna River erosional hazards, accretion & annual water discharge-a remote sensing & gis approach. *The International Archives of Photogrammetry, Remote Sensing and Spatial Information Sciences*, 40(7):831, 2015.

Partheniades, E. Erosion and deposition of cohesive soils. *Journal of the Hydraulics Division*, 91(1):105–139, 1965.

Peakall, J., Ashworth, P., and Best, J. Physical modelling in fluvial geomorphology: principles, applications and unresolved issues. *The scientific nature of geomorphology*, pages 221–253, 1996.

Richard, G. and Julien, P. Dam impacts on and restoration of an alluvial river-Rio Grande, New Mexico. 2003.

Rinaldi, M. and Darby, S. E. Modelling river-bank-erosion processes and mass failure mechanisms: progress towards fully coupled simulations. *Developments in Earth Surface Processes*, 11:213–239, 2007.

Sarker, M. H., Huque, I., Alam, M., and Koudstaal, R. Rivers, chars and char dwellers of Bangladesh. *International Journal of River Basin Management*, 1(1):61–80, 2003.

Schuurman, F. and Kleinhans, M. Major bed slope effects affecting all river morphodynamic models. 2013.

Schuurman, F., Marra, W., and Kleinhans, M. Physics-based modeling of large braided sand-bed rivers: Bar pattern formation, dynamics, and sensitivity. *Journal of geophysical research: Earth Surface*, 118(4):2509–2527, 2013.

Schuurman, F., Kleinhans, M., and Middelkoop, H. Network response to disturbances in large sand-bed braided rivers. *Earth Surface Dynamics*, 4(1):25, 2016a.

Schuurman, F., Shimizu, Y., Iwasaki, T., and Kleinhans, M. Dynamic meandering in response to upstream perturbations and floodplain formation. *Geomorphology*, 253:94–109, 2016b.

Schuurman, F. *Bar and channel evolution in meandering and braiding rivers using physics-based modeling*. Number 79. Utrecht University, 2015.

Schuurman, F. and Kleinhans, M. G. Bar dynamics and bifurcation evolution in a modelled braided sand-bed river. *Earth Surface Processes and Landforms*, 40(10):1318–1333, 2015.

Shields, A. Anwendung der aehnlichkeitsmechanik und der turbulenzforschung auf die geschiebebewegung. Technical report, Preussischen Versuchsanstalt für Wasserbau, 1936.

Society, M. G. *Geological map of the Socialist Republic of the Union of Burma*. Burma: The Division, 1977.

Surian, N. Fluvial processes in braided rivers. In *Rivers–Physical, Fluvial and Environmental Processes*, pages 403–425. Springer, 2015.

Talmon, A., Struiksma, N., and Van Mierlo, M. Laboratory measurements of the direction of sediment transport on transverse alluvial-bed slopes. *Journal of Hydraulic Research*, 33(4): 495–517, 1995.

Thorne, S. D. and Furbish, D. J. Influences of coarse bank roughness on flow within a sharply curved river bend. *Geomorphology*, 12(3):241–257, 1995.

van der Velden, J. Understanding river dynamics of the ayeyarwady river (master thesis). Master's thesis, Utrecht University, 2015.

van Ledden, M. *Sand-mud segregation in estuaries and tidal basins*. University of Technology, 2003.

Van Rijn, L. *Principles of sediment transport in rivers, estuaries and coastal seas*, volume 1006. Aqua publications Amsterdam, 1993.

Wang, G., Xia, J., and Wu, B. Numerical simulation of longitudinal and lateral channel deformations in the braided reach of the lower Yellow River. *Journal of Hydraulic Engineering*, 134(8):1064–1078, 2008.

Wang, S., Li, L., Cheng, W., et al. Variations of bank shift rates along the Yinchuan Plain reach of the Yellow River and their influencing factors. *Journal of Geographical Sciences*, 24 (4):703–716, 2014.

Williams, R. D., Brasington, J., and Hicks, D. M. Numerical modelling of braided river morphodynamics: Review and future challenges. *Geography Compass*, 10(3):102–127, 2016.

World Bank. Myanmar: Protecting millions in the Ayeyarwady River basin. urlhttp://www.worldbank.org/en/news/video/2015/04/10/myanmar-protecting-millions-in-the-ayeyarwady-river-basin-slideshow, April 2015.

World Bank. Ayeyarwady integrated river basin management project: Environmental and social management plan - final, April 2016.

Xu, H. Modification of normalised difference water index (NDWI) to enhance open water features in remotely sensed imagery. *International Journal of Remote Sensing*, 27(14):3025–3033, 2006.

Yang, H., Lin, B., and Zhou, J. Physics-based numerical modelling of large braided rivers dominated by suspended sediment. *Hydrological processes*, 29(8):1925–1941, 2014.

Ziliani, L. and Surian, N. Evolutionary trajectory of channel morphology and controlling factors in a large gravel-bed river. *Geomorphology*, 173:104–117, 2012.

Appendices

Appendix A

Processing of satellite data

Where in previous studies on braided rivers instantaneous satellite images were processed semi-automatic (distance and surface calculation with software after determining edges by visual inspection) (Baki and Gan, 2012; Wang et al., 2014; Bhunia et al., 2016; van der Velden, 2015), new processing software as the Google Earth Engine provide chances far faster and more accurate analysis of satellite data. One of the newest developments of automatic detection of water is the Deltares Aqua Monitor (www.auqa-monitor.appspot.com), of which the application is described in Donchyts et al. (2016a). With this application it is possible to determine the earth surface water changes of the past 30 years with a resolution of 30 metres (Donchyts et al., 2016b). This application is also very useful to analyse horizontally dynamic rivers as the Ayeyarwady. In this appendix is described which satellite data is used and how this data is processed in this study. The processing is consist of the creation of average reflectance composite images, the visualization of data and the automatic detection of water to visualize water masks.

A.1 The data and data processor

The application used in this study to process satellite data, is the free of use Google Earth Engine (GEE). This is a platform where all types of open source satellite data (Landsat, Sentinel, SRTM, etc.) can be processed and mapped. This can also be combined with all types of location specific data, which can be uploaded via Google Fusion Tables. A large advantage of this platform, is that it gives access to all data measured with satellite (so more than only images visible with with human eye). This gives the possibility to make extensive analysis. The processing is done with scripting, which can also easily be shared and re-used. The links to the scripts used for this study can be found at the end of the this appendix.

In this study the data given below is used. This can all be found in the the library of the GEE. For the research area, Landsat 4, 5, 7 and 8 were used to create average reflectance composites (explained in the next section) of the dry season during the period of 1988 up to 2016. Landsat 3 was used to provide two instantaneous images of the dry season in 1975 and 1977. The used bands are short wave infrared, near infrared, green, red and blue.

- USGS Landsat 3 MSS Raw Scenes (Orthorectified) (Mar 5, 1978 - Mar 31, 1983)
- USGS Landsat 4 TM TOA Reflectance (Orthorectified) (Aug 22, 1982 - Dec 14, 1993)
- USGS Landsat 5 TM TOA Reflectance (Orthorectified) (Jan 1, 1984 - May 5, 2012)
- USGS Landsat 7 TM TOA Reflectance (Orthorectified) (Jan 1, 1999 - May 1, 2017)
- USGS Landsat 8 TM TOA Reflectance (Orthorectified) (Apr 11, 2013 - present)

A.2 Computing average reflectance composites

Average reflectance composites are computed from a series of satellite data measured at one location. Using averaging over the series of satellite data, for example clouds and shadows can be removed from images. How this can be done is explained in this section and is based on G. Donchyts (personal communication, 2016).

Satellites receives signals in different bands. The Landsat 8 satellite for example, receives eleven different bands. Only three of these bands give colours visible for the human eye, namely green, red and blue. Other bands receive for example different types of infrared (Near Infrared (NIR), Shortwave Infrared (SWIR), Thermal Infrared (TIR)). The idea of an average reflectance composite, is that it computes a representative intensity for each band for every pixel from a series of data. In the left graph of Figure A.1 is shown how the received intensity for a certain band can vary over time. This variation can be caused by for example clouds, changes in temperature or more interesting for this study, the change of water into land or visa versa. Of this intensity over time a cumulative distribution has to be made, as done in the right graph of Figure A.1. In this graph is visible that three different intensities occur most in this graph (given with orange lines), which could for example represent shadow on water, water and clouds. Three different thresholds of occurrence are given in the figure (given with red lines), which will all represent something else. Choosing this threshold is therefore of main importance. For the detection of water, which is poorly reflecting, a rather low threshold should be chosen. In this study a range between 10% and 25% is used.

Varying the threshold could also be useful. Looking at the difference between the wet and the dry season for example, can be done by compositing an image with a very low threshold and with a higher threshold. This is done for Figure 3.10, where a threshold of 4% and 20% are used to show the water masks of the wet and dry season. This is done for of a collection of data of the whole year 2000.

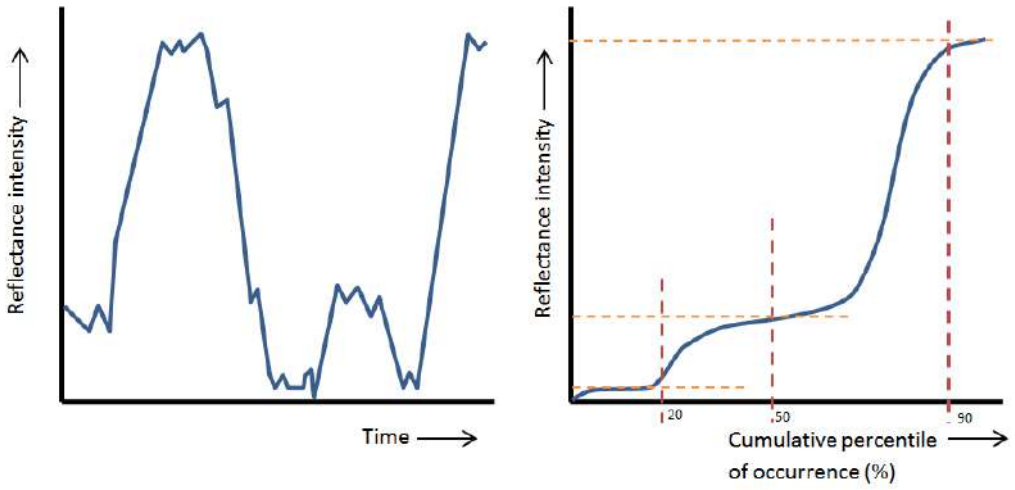

Figure A.1: Intensity-time and cumulative intensity-percentile diagram

A.3 Displaying data

Mapping of satellite data is very useful, because the data is location specific. For mapping the data, there are different possibilities. From the colours red, blue and green, all colours visible for the human eye can be created. Using these three bands received by the satellite, a normal colour or RGB (red, green, blue) image can be created. However, for Landsat 8 there are 8 other bands that also contain information. With a limitation of the human eye to see just the

bands red, green and blue, one fo these bands must be replaced by another band to display other information. This means that for example the intensity of short-wave infrared can be displayed with the colour red, which excludes the information there is of the intensity received from the band 'red'. In this way, a so-called false colour image is created. This means that the colour observed from the image is not the colour that it represents. When looking at land water differences, RGB images do not always give a clear view. It could be better to use a SNG image (short-wave infrared, near infrared and green are displayed in respectively red, green and blue). With SNG images, water is displayed in a very dark blue and vegetation in bright green. This clear difference is very useful for this study. An example between the difference of an RGB and SNG image is given in Figure A.2.

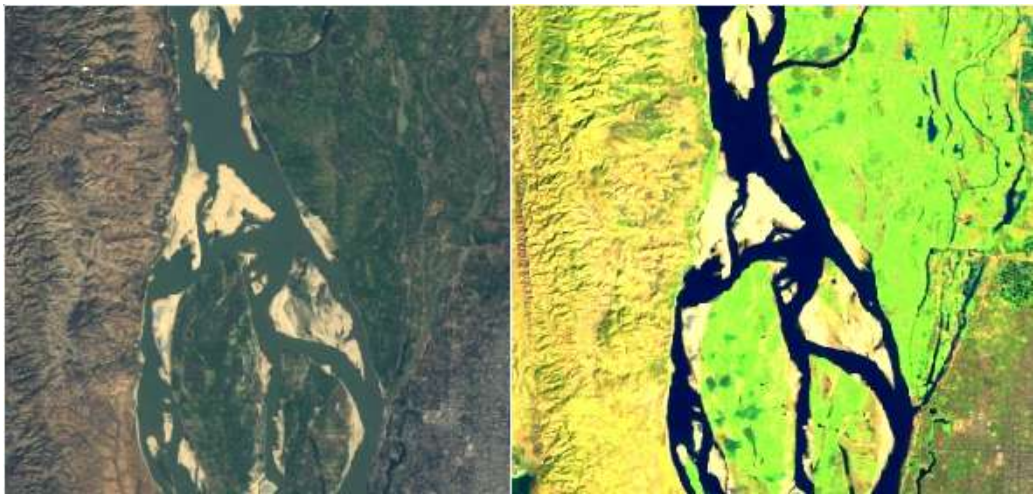

Figure A.2: Comparison of an RGB (left) and SNG (right) image of a part of the river in the research area.

With the focus on the development of the river, it is very useful to create a video of subsequent images. The differences within the dry season turned out to be me minimal, where in the wet season only one large water mask could be observed. For this reason is chosen to create a video showing an image of every dry season. These images were composites from data measured in the months January to March.

A.4 Automatic detection of water

For the detection of water, different indices were introduced. The first is the Normilized Difference Water Index (NDWI) (Gao, 1996). This index can be calculated by:

$$NDWI = \frac{\rho_{green} - \rho_{nir}}{\rho_{green} + \rho_{nir}} \tag{A.1}$$

However, this measure gave noise with different types of landscape, and so overestimates the water surface. This is why the Modified Normalized Difference Water Index (MNDWI) was introduced Xu (2006). This measure proved to be more useful at locations where backgrounds where land dominated.

$$MNDWI = \frac{\rho_{green} - \rho_{swir1}}{\rho_{green} + \rho_{swir1}} \tag{A.2}$$

Normally, the threshold for water or no water using the MNDWI is 0. However, also this threshold can be time and location specific, due to for example shadows. To find the correct thresholds to compute the right projection of an area can be very time consuming. Donchyts et al. (2016b) introduced automatic Otsu thresholding in combination with a canny edge filter

to compute the threshold automatically. With Otsu thresholding (Otsu, 1975), the MNDWI will be calculated for all the pixels in the research area and summarized in a histogram. In an ideal case, the histogram has two peaks for the MNDWI values, indicating water or no water, with less records in between. In this case, it would be easy to state that the threshold will be in between the peaks. In reality more complex histogram will be found. Here the Otsu thresholding method is needed to determine this threshold. This method optimizes the separability between two classes and determines the threshold between water pixels and non-water pixels. However, this separability could be vague when the number of water pixels is very low compared to the number of non-water pixels. This is were the canny edge detector is used for. This edge detector is able to find the edges of the water lines. Around these edges a buffer area is taken and the Otsu thresholding is applied for this buffer op pixels. In this way the rate of water pixels used for the Otsu thresholding is higher, giving a higher reliability of the method. This process is given in Figure A.3. Finally, the determined water masks can be displayed, also in combination with other mapped data.

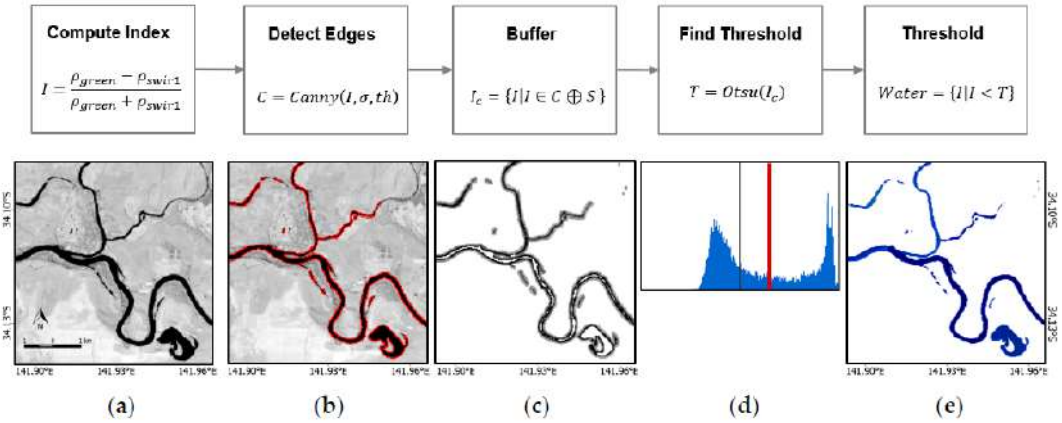

Figure A.3: Various steps of water detection from Landsat imagery (Donchyts et al., 2016b)

A.5 Google Earth Engine scripts

Links of the two mainly used scripts are given below. The first script is to compute average reflectance composites and with the second water reflectance composites can be created for which water will be detected automatically.

Creating average reflectance composites:

https://code.earthengine.google.com/3f529534e8edd365d3544b38cd24e8c7

Automatic detection of water mask for average reflectance composites:

https://code.earthengine.google.com/92f00c4bef6e2b5be86e490285c9ea83

Appendix B

Mega scale morphological processes in the Mandalay river region

On mega scale Jagers (2003) describes six different morphodynamic processes. These processes are:

- Channel migration
- Channel widening and narrowing
- Mid-channel bar growth
- Channel formation
- Channel abandonment
- Node deformation

In the following sections different morphodynamic processes are described. All these changes contain one or more of the previous mentioned processes and mostly occur under high water conditions. The analysis of these changes is important to learn about the development of the river. In Figure B.1, an overview is given of the described locations. Since the upstream part affects the downstream area, the order of described locations is from upstream to downstream.

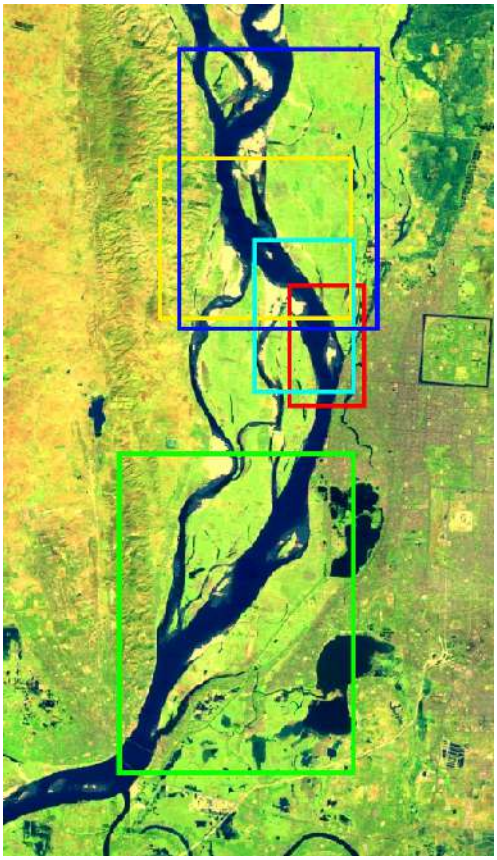

Figure B.1: Overview of the different analysed area's on a SNG image of the year 2016. Delineated in blue an area conducting bank erosion, with yellow bank erosion and the rotation of the bifurcation, in light blue a channel cut off, in red the movement of a bar and in green the movement of the confluence.

B.1 Rotation of the bi- or trifurcation

In Figure B.2, the rotation of the main bifurcation in the research area is visualized. The geometry of bifurcations plays a major role in the development of a braided river (Schuurman and Kleinhans, 2015), meaning that the geometry of this bifurcation probably influences the morphology in the whole research area. This will become evident in the following sections.

In Figure B.2a, a more or less symmetrical bifurcation can be seen and in the upstream part already a small bar can be found. In Figure B.2b, this bar is already growing, forcing the main channel to the left. The reshape and movement of this bar in the Figures B.2c to B.2d causes a very unnatural looking shape of the river in Figure B.2e. Finally, the branch to the right is closed by a part of this same bar, displayed in Figure B.2f. This rotation of the bifurcation has an obvious effect on the division of the flow to the downstream channels. In these Figures not only the change of this node is visible. Important events are also the incisions in the side bars between 1995 and 1998 and between 1999 and 2000. Important as well, is the attachment of the incoming bar to the islands. This also emphasizes that the movement of the islands in downstream direction, mentioned in section 3.2.2, does not go gradually.

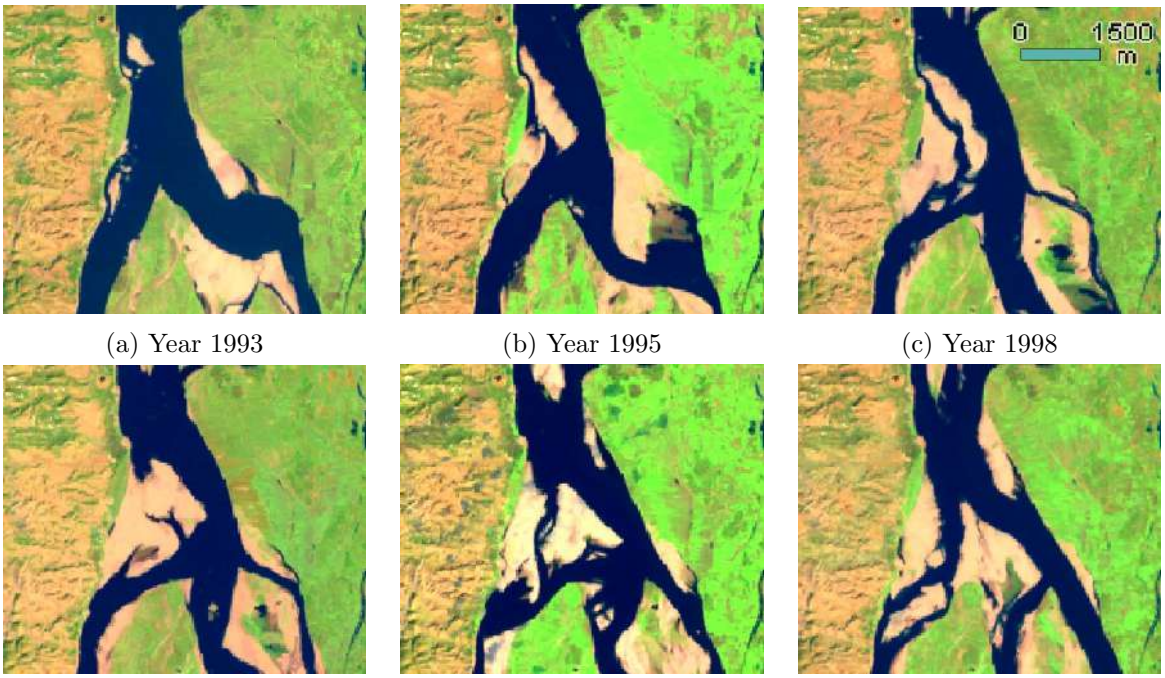

(a) Year 1993 (b) Year 1995 (c) Year 1998

(d) Year 1999 (e) Year 2000 (f) Year 2001

Figure B.2: The rotation of the bifurcation due to incoming bars with redistribution of flow over the downstream channels as consequence

B.2 Channel cutoff

Due to the change of the bifurcation discussed in the previous section, a channel cutoff takes place, displayed in Figure B.3. This Figure partly overlaps with the right bottom of Figure B.2d. Between Figure B.3a and B.3b, the direction of the right channel changes, making it more difficult for the flow to turn left, through the connecting channel, to the left channel. This induces a reduction in flow, visible in Figure B.3c, causing sedimentation in the channel. In Figure B.3d the connecting channel has an angle of approximately 90 degrees with the right channel, making it too difficult to attract water. This leads to the cutoff, visible in Figure B.3e. Cutoffs of channels generally also lead to redistribution of discharge in the downstream channels.

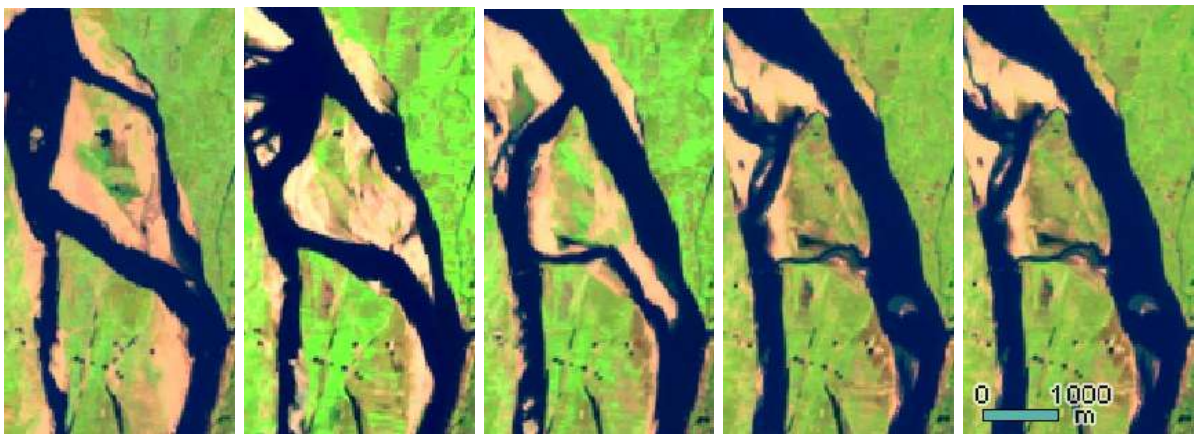

(a) Year 1999 (b) Year 2000 (c) Year 2001 (d) Year 2002 (e) Year 2003

Figure B.3: A cut off a channel due to a change in flow direction by the change at the bifurcation

B.3 Bar creation and movement

In Figure B.4, the development of a mid-channel bar is visible. A decrease in discharge took place in this branch, due to the closure of the channel discussed in the previous section. This has as results that the width of the channel is too large for the present discharge, causing the development of a mid-channel bar (figure B.4b). This bar is moved by the flow to the middle of the channel, while it also grows (figure B.4c and B.4d). In Figure B.4d is already visible that the flow right around the bar has a higher resistance (due to the bend), than the way left around the bar. This results in the gradual closure of the right channel, visible in the Figures B.4e and B.4f. Due to its connection with the channel cut off, the creation this bar can also be connected to the change of the bifurcation. So a formation of a bar can be caused by a redistribution of the discharge, but other reasons also a exist.

(a) Year 2002 (b) Year 2003 (c) Year 2004 (d) Year 2005 (e) Year 2006 (f) Year 2007

Figure B.4: The development and movement of a bar in the left (Mandalay) channel. Between Figure (a) and (b) the cut off of a channel is visible, resulting in the development of the bar, which visible in Figures (c) tot (f)

B.4 Confluence movement

South in de research area, a large confluence can be found. Jagers (2003) tells that the rotation and movement of the confluence are influenced by the direction, the magnitude and the velocity

of the flow of the merging channels. Since the geometry of the bifurcation determines distribution of discharge over the different channels, it also influences the geometry of this confluence. When the discharge in the left channel is smaller compared to the right channel, the confluence is pushed to the right and visa versa. This lateral displacement of the confluence is always accompanied with a downstream movement, visible in Figure B.5. The confluence is shown for the years 1975, 1990 and 2016. In 1975 the confluence is located relatively far upstream. This confluence moved in downstream direction till the year 1990, where a new confluence further upstream is created. Till the year 2016, the confluence moved in downstream direction again. This process of downstream movement of the confluence seems like a repeating process.

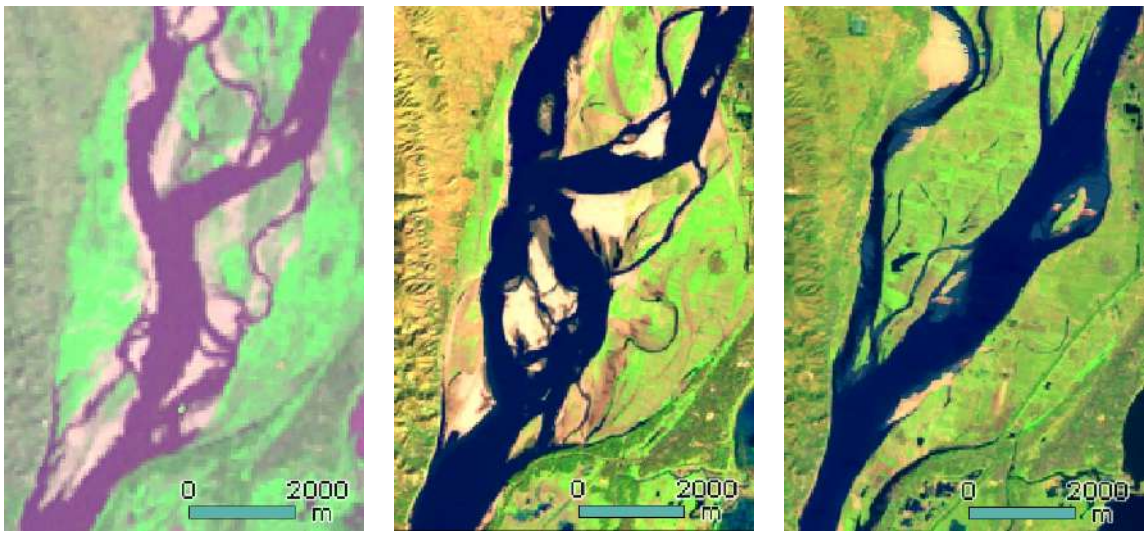

(a) Year 1975 (b) Year 1990 (c) Year 2016

Figure B.5: The repeating process of the downstream movement of the confluence

Appendix C

Set-up of physics-based numerical model Delft3D

This appendix describes the model used as basis model for the sensitivity analysis. Discussed are the model software Delft3D (version 4.02.02) and all the essential input. Part of the input is derived from data as discussed in the system analysis (chapter 3) and part from literature.

C.1 The Delft3D model software

Delft3D is a physics-based numerical model, used to simulate hydro- and morphodynamics. The model is especially suitable when the horizontal lengths and time scales are significantly larger than the vertical scales, as can be found in rivers, estuaries and coastal zones. It is able to solve the flow equations in 3D as well as in depth-averaged 2D. In this study is chosen to use the 2D depth-averaged equations to limit the computational time.

The basis flow equations are two equations for conservation of momentum (equation C.1 and C.2), and one for the conservation of mass (equation C.3).

$$\frac{\partial u}{\partial t} + u\frac{\partial u}{\partial x} + v\frac{\partial u}{\partial y} + g\frac{\partial z_w}{\partial x} + \frac{gu\sqrt{u^2+v^2}}{C^2 h} - V\left(\frac{\partial^2 u}{\partial x^2} + \frac{\partial^2 u}{\partial y^2}\right) + F_x = 0 \tag{C.1}$$

$$\frac{\partial v}{\partial t} + u\frac{\partial v}{\partial x} + v\frac{\partial v}{\partial y} + g\frac{\partial z_w}{\partial x} + \frac{gu\sqrt{u^2+v^2}}{C^2 h} - V\left(\frac{\partial^2 u}{\partial x^2} + \frac{\partial^2 u}{\partial y^2}\right) + F_y = 0 \tag{C.2}$$

$$\frac{\partial h}{\partial t} + \frac{\partial hu}{\partial x} + \frac{\partial hv}{\partial y} = 0 \tag{C.3}$$

where x is the coordinate in downstream direction (m), u is the velocity in x-direction (m/s), y is the lateral coordinate (m), v is the velocity in y-direction (m/s), z_w the free water surface level (m), h the water depth (m), g the gravitational acceleration (m/s^2), C the Chézy roughness $(m^{1/2}/s)$, V is horizontal eddy viscosity (m^2/s) and Fy, x external forcing due to streamline curvature.

For the transport of sediment many formulations can be chosen. Most typical for rivers are the the Engelund and Hansen formula (Engelund and Hansen, 1967), the Meyer-Peter & Müller formula Meyer-Peter and Müller (1948) and van Rijn formula (Van Rijn, 1993). In this study the general formula is used, which can be modified by the user and reads:

$$s = \alpha D_{50}\sqrt{\triangle g D_{50}}\theta^b(\mu\theta - \xi\theta_{cr})^c \tag{C.4}$$

in which:

$$\theta = \left(\frac{q}{C}\right)^2 \frac{1}{\triangle D_{50}} \tag{C.5}$$

where α, b, c, μ and ξ are user defined variables, D_{50} the median particle diameter (m), $\triangle$ the relative density $(-)$, θ the shields mobility parameter $(-)$ and q the discharge (m^2/s).

The general formula calculates total transport for each cell centre, including the direction and magnitude. Different factors can still influence this magnitude and direction. Examples that can reduce sediment transport are a too low availability of sediment at the bed or hiding and exposure phenomena. The two factors used in this study that change the direction are the bed-slope effect and the spiral flow. These both result in a deflection of the sediment transport. The equations used for spiral flow read:

$$tan(\phi_\tau) = \frac{v - \alpha_I \frac{u}{U} I_s}{u - \alpha_I \frac{v}{U} I_s} \tag{C.6}$$

in which:

$$\alpha_I = \frac{2}{\kappa^2} E_{spir} \left(1 - \frac{1}{2} \frac{\sqrt{g}}{\kappa C}\right) \tag{C.7}$$

where κ is the Von Kármán constant $(-)$, U the depth-averaged flow velocity (m/s) and E_{spir} the user defined coefficient for the magnitude of the spiral flow $(-)$.

The equations used to determine the bed-slope effect are:

$$tan(\phi_s) = \frac{sin(\phi_\tau) + \frac{1}{f(\theta)} \frac{\mathrm{d}z_b}{\mathrm{d}y}}{cos(\phi_\tau) + \frac{1}{f(\theta)} \frac{\mathrm{d}z_b}{\mathrm{d}x}} \tag{C.8}$$

in which:

$$f(\theta) = A_{shield} \theta_i^{B_{shield}} \left(\frac{D_i}{H}\right)^{C_{shield}} \left(\frac{D_i}{D_m}\right)^{D_{shield}} \tag{C.9}$$

where A_{sh}, B_{sh}, C_{sh} and D_{sh} are user defined variables $(-)$, D_i the median grain size of the fraction (m), D_m the median grain size of the bed $(-)$, θ_i the fraction mobility $(-)$, ϕ_s the direction of sediment transport $(^\circ)$, z_b the bed level (m) and ϕ_τ the direction of the shear stress $(^\circ)$.

C.2 The digital elevation map and grid

The grid and digital elevation map (DEM) are created in the coordinate system UTM 47N. The DEM is acquired by combining four different data sets, which are obtained (except SRTM, which is from 2000) by MBCCDL (Mandalay business capital city development ltd., 2016). These data sets are:

- Multibeam echo-soundings
- Stereophotogrammetry
- Levelling measurements
- SRTM (Shuttle radar topography mission, 2010)

The levelling measurements are used for the islands, the multibeam echo-soundings for the channel, the stereophotogrammetry for the banks and the SRTM for the floodplain north of Mandalay. Since the SRTM mission was in 2000, the data is not up to date and not fitting the other data sets. However, the flow and sediment transport on top of the floodplain are assumed

to have a minimal effect on the shift the channels and movement of the islands, which is where this research is focussed on. Although effects are assumed to be small, attention still has to be paid on this.

The used grid is a curvilinear grid. According to Schuurman et al. (2013), the formation of larger bars and channels is grid independent (where he uses a grid size up to 80*200 m^2). Only smaller morphological features are influenced by the grid. Grid cell lengths in the used grid vary between 30 and 200 metres, where the width is between 50 and 250 metres. Only on the floodplain north of Mandalay, where morphological changes are assumed to be relatively unimportant, much larger grid sizes can be found.

C.2.1 Boundary conditions

The boundary conditions are derived from data of the DMH (Department of meteorology and hydrology, 2014) and a feasibility study of RVO, performed by Royal HaskoningDHV, Rebel, Arcadis and Deltares (2015). Some statistics of the discharge are displayed in Figures 3.2 to 3.4. The hydrograph is essential for a good result in the simulation. Different stages that can be distinguished in the hydrograph are low water, rising stage, high water and falling stage. To investigate the effects of the different stages, which is done in this study, it is necessary that these are strictly separated in the hydrograph.

The used hydrograph is given in Figure C.1. The discharge during high water, Q_{high}, is chosen at 18,000 m^3/s and the discharge during low water at 2,000 m^3/s. The threshold for submerging of the islands is approximately 11,000 m^3/s, so with the choice of these discharges a clear distinction is there between periods where the islands are submerged, and where not. In between high and low water, there are the rising and falling stage. A fluent decrease/increase of the discharge is implemented in the hydrograph to avoid abrupt changes in flow velocity and sediment transport. The of the rising and falling stage are respectively 120 days and 80 days in morphodynamic time. High water takes 50 days and low water 115 days. With this input, the hydrograph gives an good representation of the yearly hydrographs. An example of the year 1988 is given in Figure C.1.

As downstream boundary a QH-relation is used. This is derived from a Sobek model from a RVO study and given in Figure C.2

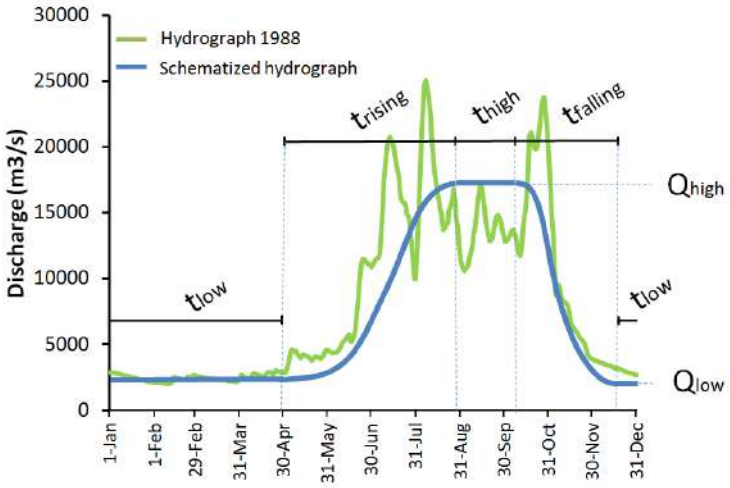

Figure C.1: Hydrograph 1988 and the schematized hydrograph used in this study with the different parameters to vary

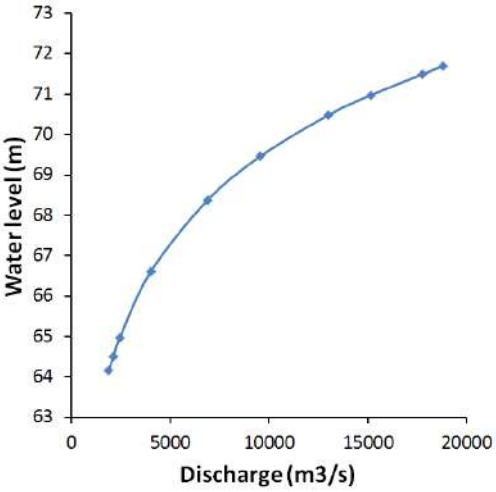

Figure C.2: QH-relation as downstream boundary derived from the Sobek model from the study RVO

C.2.2 Bed roughness model

To solve the flow equations (equation C.1 and C.2) and to determine the sediment transport, the bed roughness has to be expressed in a Chézy value. In the Delft3D software three different bed roughness models can be chosen to determine this value. The default is an uniform Chézy value for the complete model. In this option it is also possible to vary the Chézy value over space. Variation in time is not possible. The other two models are Manning en White-Colebrook, which are both depth-dependent. Even though the roughness with Manning is dependent on the water depth to a power one-sixth, and with White-Colebrook a logarithmic profile is used, the methods show a similar behaviour. The most important choice for the roughness is to use a dependency on depth or not.

With a depth dependent roughness, the roughness will be higher on top of the bars, compared to in the channels. A higher roughness leads to a decrease in flow velocity, which causes a decrease of the sediment transport. However, the roughness is also included in the sediment transport formulations, where a higher roughness would mean a higher transport. With these counteraction effects it is always hard to predict what the cumulative effect on the sediment transport would be. (Schuurman et al., 2013) found a higher movability of the bars using manning, which means that he found higher transport on top of the bars compared to in the channels. Where braided rivers are characterized by their movability, it might be favourable to choose a depth-dependent roughness model.

Still is chosen to use a uniform Chézy in this study. This has two reasons. The first reason has to do with the calibration of the model. Calibration was done on water levels and flow distribution over the channels. Chézy performed best here. The other reason is that the roughness-depth dependency is also used in the derivation of the transport formula (shown in section C.2.4). This would mean that this dependency is used twice.

C.2.3 Sediment fractions

In the sediment samples in the different channels, as discussed in chapter 3, mostly sand can be found. In the different channels and on different locations in these channels, a variation of sediment sizes can clearly be found. This is the reason why multiple fractions are used in the model. The different chosen D_{50}'s are 0.16 millimetre, 0.32 millimetre and 0.6 millimetre.

Chosen is also to use a multiple layer arrangement to be able to model the sorting in the bed. According to (Yang et al., 2014), this is something which enhances the braided pattern in the model. The fines can be found on top and just behind the bar, where the coarse sediments are predominantly found inside the channels. This enhances the moveability of the bars, relative to the channels.

C.2.4 Sediment transport formula

Widely used sediment transport formulas for sand bed rivers are the Engelund and Hansen formula (Engelund and Hansen, 1967), the Meyer-Peter & Müller formula Meyer-Peter and Müller (1948) and the van Rijn formula (Van Rijn, 1993). First results with these formulas are shown in Figure C.3a to C.3c. The van Rijn formula gave relative elongated narrow islands as result, which differs from observations of satelitte imagery. With Engelund and Hansen deep channels and high islands were created, which is much different then found from the initial bed. Meyer-Peter & Müller performed better there, but showed lower mobility of the islands.

Where Molinas and Wu (2001) also state that the widely used sediment transport formulas are most of the time not a good estimator for sediment transport in large sand-bed rivers, E.

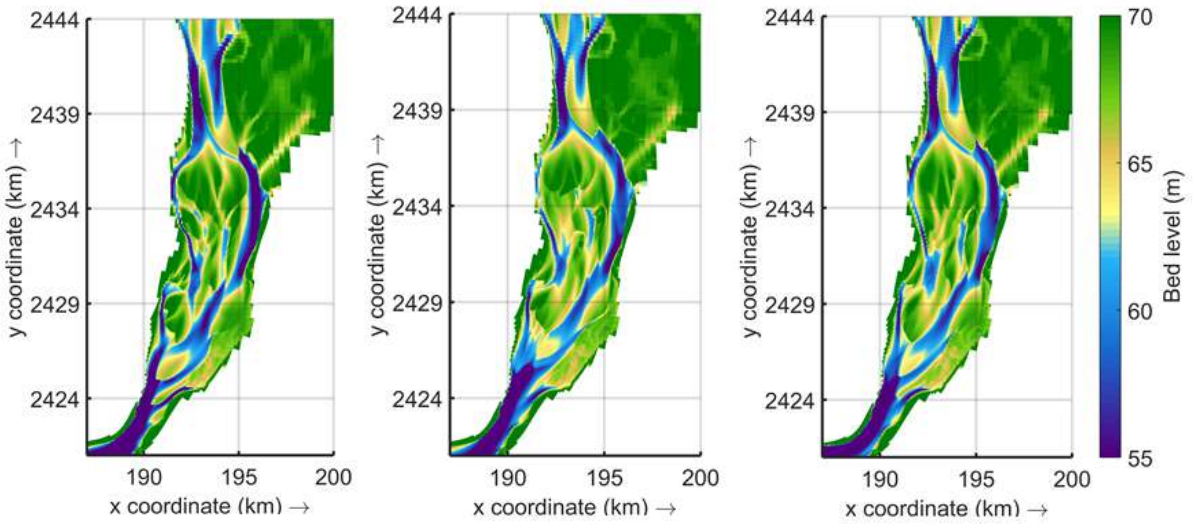

(a) Engelund and Hansen (b) Meyer-Peter & Müller (c) van Rijn

Figure C.3: Simulation results with different sediment transport formulas after a period of 2 years with a constant discharge of $18,000 m^3/s$

Mosselman (personal communication, December, 2016) advised to use an adjusted version of the Engelund and Hansen formula. In this adjusted version a lower power for the flow velocity must be used. To keep the unit of the constant equal, this is translated to a change in the dimensionless shield mobility parameter. The derivation of this formula will be shown in this section. The expectation for better results lays in the relation between the bed roughness and the water depth. This relation evolves from combining the formulations for flow velocity of Chézy and Manning, and reads:

$$C = C_0 h^{1/6} \tag{C.10}$$

In this formula C is the Chézy roughness ($M^{1/2}/s$), C_0 a constant ($M^{1/3}/s$) and h the water depth (m). Important in this relation is the power of 1/6. It is expected that a relation with a power of a half would be a better fit. Then the relation reads:

$$C = C_0 h^{1/2} \tag{C.11}$$

If we rewrite the Chézy formula to $C^2 = \frac{u^2}{hi}$ and equation C.11 to $h = C^2/C_0^2$, you can find that:

$$C^2 = \frac{u^2 C_0^2}{iC^2} \tag{C.12}$$

This means that $C^4 \propto u^2$, and so:

$$C^3 \propto u^{3/2} \tag{C.13}$$

If we take the Engelund Hansen equation, which reads:

$$q_s = \frac{m}{C^3} u^5 \tag{C.14}$$

and fill in equation C.13, we can conclude:

$$q_s \propto \frac{u^5}{u^{3/2}} \propto u^{3.5} \tag{C.15}$$

Since the power of 1/2 in equation C.11 is not a precise fit, the power of 3.5 in equation C.15 is not strict. However, following this formulation, a lower power above the velocity could be

more appropriate. For this research a power of 4 is chosen. This is implemented in the model by using the general formula (equation C.4). With the user defined variables $\alpha = 20$, $b = 2$ and $c = 0$, the formula reads:

$$S = 20 D_{50} \sqrt{\triangle g D_{50}} \theta^2 \tag{C.16}$$

in which:

$$\theta = \left(\frac{q}{C}\right)^2 \frac{1}{\triangle D_{50}} = \left(\frac{uh}{C}\right)^2 \frac{1}{\triangle D_{50}} \tag{C.17}$$

Here is visible that the sediment transport is formula is dependent on u^4. Using this formula increased the mobility of the bars and islands significantly. With flow velocities on top of the bars below 1 m/s (which is as observed in the model always the case), this lower power above the velocity increased the sediment transport on top of the bars. In the channels, where velocities with high water are above 1 m/s, this lead to a decrease of of the sediment transport. This results in higher differences of the sediment transport around bars and so faster movement of the bars.

In the sensitivity analysis, transport formulas with three different powers above the velocity are tested, namely 3, 4 and 5 (where 5 is the actual Engelund and Hansen formula). To make these formulations comparable, total sediment transport was calibrated for all the formulations with calibration parameter α. C.J. Sloff (personal communication, December, 2016) made a first estimation of 20 for α using u^4, based on measured total sediment transport (including wash load). This has just been an estimation, since it was unknown which part of the total load was the bed and suspended load. To keep the different formulations comparable, a similar amount of sediment transport has to be computed for them. Calibration of the amount of sediment transport for a certain moment in time is not straight forward. Changing the amount of sediment transport influences the bed development, which is also of influence on the sediment transport again. After two iterations the fit in Figure C.4 is obtained. Found magnitudes for α are 14.6 and 26.8 with u^3 and u^5 respectively. The calibration was done at the bridge near Sagaing (see Figure 3.5).

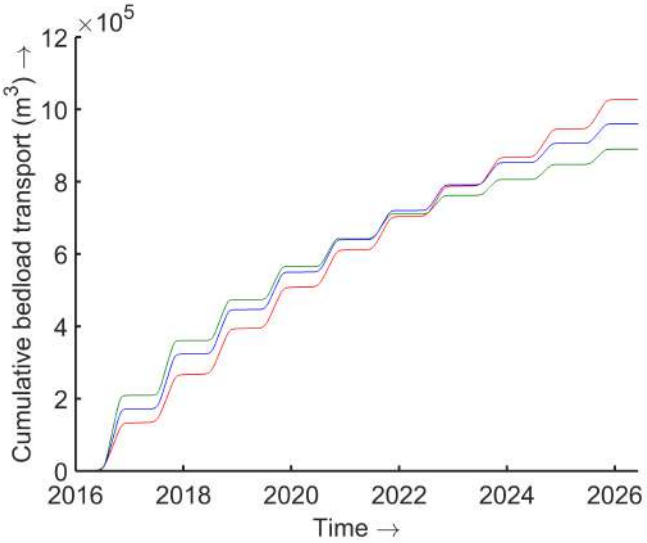

Figure C.4: Cumulative bedload transport of the sediment transport formulas proportional to u^3 (red), u^4 (blue) and u^5 (green)

In the model all sediment transport is defined as bedload. This has as consequence that the advection and diffusion of the suspended sediment concentrations do not have to be solved, which reduces the computational time significantly. This change can only be made when the grid size is larger than the adaptation length of the suspended sediment. The results of the two

methods (using only bedload and using both bedload and suspended load) are compared and show equal results (bed levels and sediment transport). For sensitivity analysis it was necessary to be able to control the amount of sediment input. Using only bedload, the input of sediment had to be determined as sediment discharge per metre width. With the complex bed and the continuously changing water level it was impossible to determine a specified amount of sediment input. In order to predefine the amount of sediment input, it was necessary to switch to the use of both bedload and suspended load. This gave the possibility to determine a predefined sediment input as concentration. The sediment in the concentration was directly dropped on the bed, since the flow was not able to carry it.

C.2.5 Morphological parameters

In many research the bed-slope effect is mentioned as a very important parameter to influence the braided behaviour of the river (Schuurman et al., 2013; Jang and Shimizu, 2005). It is the only negative feedback on bar growth, which enhances a dynamic system needed to model a braided river. In addition, the spiral flow is also an important factor (Schuurman et al., 2013). For the bed-slope effect the parameters A_{shield} and B_{shield} (see equation C.9) are set to 0.7 and 0.5 respectively. These are default values. For the spiral flow a magnitude of 1.0 is chosen (see equation C.7). Variations in the magnitude of the bed-slope effect and the spiral flow are both tested in the sensitivity analysis.

In this study the morphological factor is used to reduce the computational time. This did have an influence on the sediment transport in the model with the used hydrograph. In Figure C.5, the differences between a simulation with a morphological factor of 10 and 30 are displayed for three different locations. Differences at the inflow boundary are largest and decrease further downstream. When a morphological factor is used, this squeezes the hydrograph (in hydrodynamic time). This leads to more rapid increase and decrease of the discharge during the rising and falling stage. When the change in discharge is more rapid than the water level is able to adopt, this leads to unrealistic velocities. The large flow velocities cause large sediment transports. In Figure C.5 can be seen that with a morphological factor of 30 the sediment transport is much higher just after the rising stage. With a rising period of 80 days morphodynamic time and a morphological factor of 30, the hydrodynamic time of the rising stage is 2.7 days. This is unrealistic short, so unrealistic sediment transport occurs. This is especially at the inflow boundary, and decreases further in the system as the flood wave dampens out. With a morphological factor of 10, the peak in sediment transport is already more than 40% lower. Still is chosen to use a morphological factor of 30, because this decreases the computational time significantly. Differences in bed level are predominantly found in the first 10 kilometres of the system, which is similar to changes in the sediment input in the system (see section 4). Because the 'real' magnitude of sediment transport is unknown and degradation of the bed in the first 10 kilometres is still found (with a morphological factor of 30), input of extra sediment in the system is assumed to form no problems for the results.

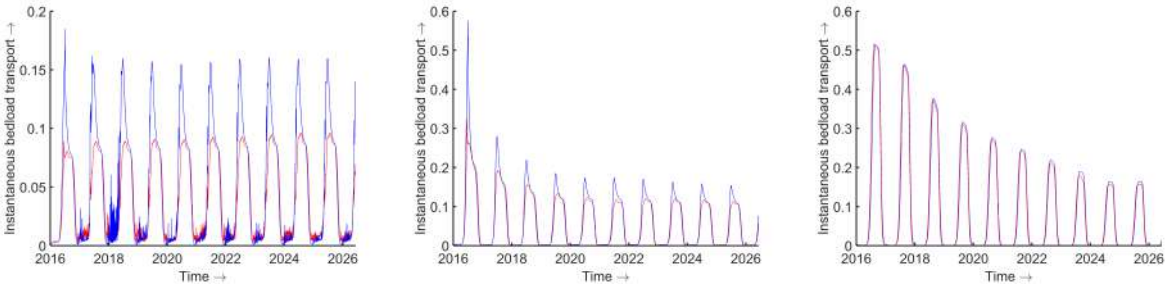

(a) Inflow (b) Min Kun (c) Sagaing

Figure C.5: Instantaneous bedload transport at the inflow of the research area, Min Kun (just before the first large bifurcation) and at Sagaing for in red the simulation with a morphological factor 10 and in blue the morphological factor of 30.

C.3 Modelling changing inflow direction and bars moving into the system

This section only holds for the parts where a changing inflow direction is used. In the sensitivity analysis (chapter 4) this is used for one run and in the evaluation of the model (chapter 5) to create a more dynamic situation. Both are used in slightly different ways, so they are discussed separately in this section.

First attempts were done by putting five boundaries at the upstream end of the system. The inflow was varied yearly by changing the magnitude of discharge of the different boundaries. Changing the flow on such an irregular bed resulted in instabilities of the model. This gave reason to extend the with sixteen rows of grid cells. The bed level on the floodplain were determined using the SRTM data, just like with the rest of the floodplain. At the new inflow boundary a bed level of 64 metres was chosen. The remaining part of the bed was created using the 'internal diffusion' option in Delft3D, which created an almost flat bed. This part of the grid and bed are shown in Figure C.6.

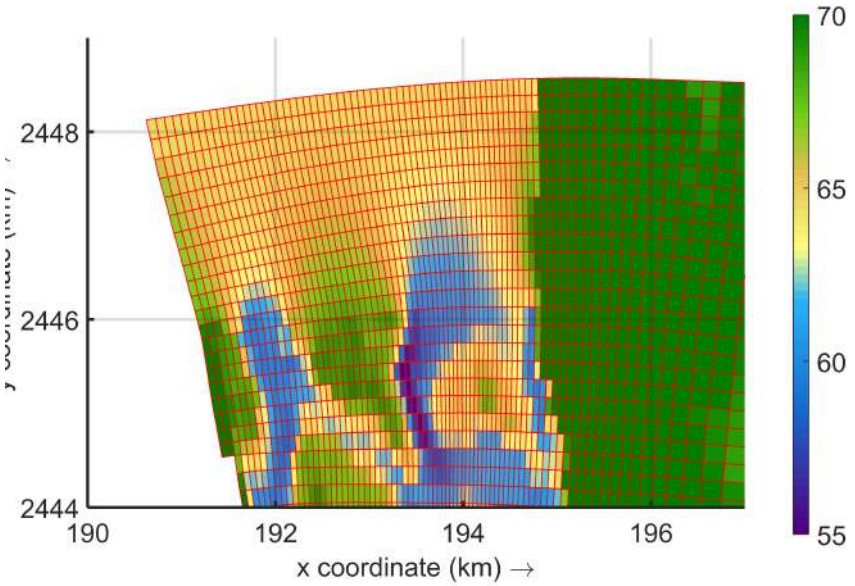

Figure C.6: The extended grid and new bed levels

Creating bars moving into the system with changing boundaries

Bars moving into the system were simulated using five boundaries of equal length in the channel area. The distribution of the discharge changed every five year as displayed in table C.1. A sixth boundary was used for the floodplain. As soon as the discharge was high enough to fill the floodplain, twenty percent of the discharge was assigned to the floodplain. This turned out to be an overestimation of the discharge there, with erosion channels in the floodplain as consequence. This problem was solved for the run with changing boundaries for the sensitivity analysis, as described in the next section.

Table C.1: Flow distribution over time used to create bars

Year	Q1	Q2	Q3	Q4	Q5
1	0.4	0.3	0.1	0.1	0.1
5	0.1	0.1	0.1	0.3	0.4

For the sediment input the option in Delft3D to calculate an equilibrium amount of sediment with the corresponding flow was used. This gave as result, with a large discharge on one side of the system and a low discharge on the other side of the system, that sediment input was also non-uniform over the width. With the water level approximately uniform over the width, but with large variation in discharge over the width, differences in flow velocity were also significant. This caused a large sediment input at the location of high flow velocity and low sediment input on the location of low flow velocity. Because the flow merged directly after inflow, the relatively high flow velocity decreased directly and the overload of sediment was deposited. In this way bars were created, which slowly moved into the system. This is shown in Figure C.7. With this method it was possible to increase the dynamics of the system, but it cannot be used for a correct simulation of the input of sediment. The amounts of incoming sediment are hard to control and also the location op deposition is uncertain.

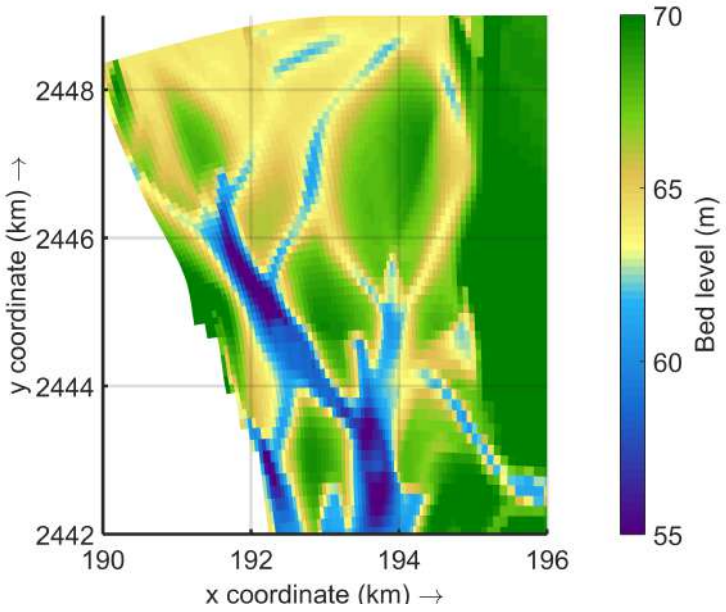

Figure C.7: The creation of new bars at the boundary of the system

Changing inflow direction for the sensitivity analysis

With the sensitivity analysis the open boundary at the upstream side is divided into four different boundaries. One boundary for the floodplain and three boundaries with equal length for the channel area. The number of boundaries differed from the method in the previous section for an easier implementation. The inflow direction was changed every year by changing the magnitude of the discharge of the three boundaries in the channel area. This in periods of eight years, as shown in table C.2. To solve the problem with the erosion channels in the floodplain discussed in the previous section, the discharge assigned to the floodplain was changed. Most important here, is that the floodplain is filled from the downstream side. For this reason it was necessary to assign a discharge to the floodplain in a later stage. This was done when the total discharge reached $16,000 m^3/s$.

Because the sediment input had to be controlled in the sensitivity analysis to make the simulation comparable with the other runs, sediment input had to be controlled. Switched is therefore to the use of both bedload and suspended load instead of only bedload, because sediment input could than be controlled as concentration.

Table C.2: Flow distribution over time used for the sensitivity analysis

year	Q1	Q2	Q3
1	0.7	0.2	0.1
2	0.5	0.3	0.2
3	0.3	0.2	0.3
4	0.2	0.3	0.5
5	0.1	0.2	0.7
6	0.2	0.3	0.5
7	0.3	0.2	0.3
8	0.5	0.3	0.2

C.4 Input of all runs sensitivity analysis

Table C.3: Input parameters runs sensitivity analysis

run	Bed-slope effect $A_{shields}$	Spiral flow E_{spir}	Sed. Trans. formula u^x	Period high discharge	Period low discharge	Period falling stage	Period rising stage	High discharge	Low discharge	Sediment input	Inflow direction
Reference	0.7	1	4	50	115	80	120	18000	2000	eq.	constant
Constant high Q	0.7	1	4	50	115	80	120	18000	-	eq.	constant
Large Q_{high}	0.7	1	4	50	115	80	120	20000	2000	eq.	constant
Low Q_{high}	0.7	1	4	50	115	80	120	16000	2000	eq.	constant
Short falling period	0.7	1	4	75	140	30	120	18000	2000	eq.	constant
Long falling period	0.7	1	4	25	90	130	120	18000	2000	eq.	constant
Extra sed. input	0.7	1	4	50	115	80	120	18000	2000	2x eq.	constant
Changing infl. direct.	0.7	1	4	50	115	80	120	18000	2000	2x eq.	changing
Low power sed. transp. form.	0.7	1	3	50	115	80	120	18000	2000	eq.	constant
High power sed.transp. form.	0.7	1	5	50	115	80	120	18000	2000	eq.	constant
No spiral flow	0.7	0	4	50	115	80	120	18000	2000	eq.	constant
High spiral flow	0.7	2	4	50	115	80	120	18000	2000	eq.	constant
Low bed-slope effect	0.4	1	4	50	115	80	120	18000	2000	eq.	constant
High bed-slope effect	1	1	4	50	115	80	120	18000	2000	eq.	constant

C.5 Input of runs chapter 5

Table C.4: Input parameters used models chapter 5

Model	Bed-slope effect $A_{shields}$	Spiral flow E_{spir}	Sed. Trans. formula u^x	Period high discharge	Period low discharge	Period falling stage	Period rising stage	High discharge	Low discharge	Sediment input	Inflow direction
1	0.7	1	4	50	115	80	120	18000	2000	eq.	constant
2	0.3	1	4	0	0	182.5	182.5	18000	2000	eq.	Large inflow from left side
3	0.7	1	4	50	115	80	120	18000	2000	2x eq.	constant
4	0.7	1	4	0	0	182.5	182.5	18000	2000	eq.	constant
5	0.3	2	4	0	0	182.5	182.5	18000	2000	eq.	changing incl. bar creation
6	0.7	1	4	50	115	80	120	18000	2000	4x eq.	constant

Appendix D

Bed levels after different runs sensitivity analysis

In this appendix the bed levels after 10 years simulation time are given for all the different runs performed for the sensitivity analysis. The input for the different runs can be found in appendix C.4.

D.1 The use of a hydrograph

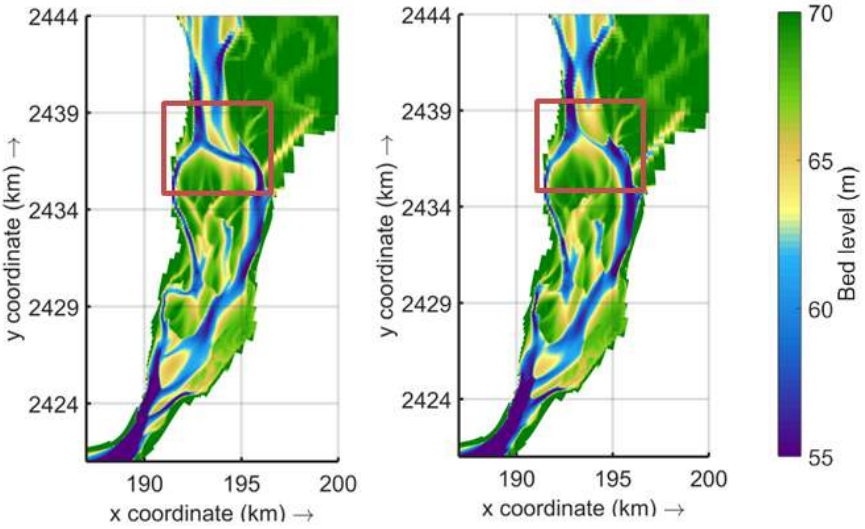

(a) Hydrograph (reference) (b) Only high water

D.2 Variation in peak discharge

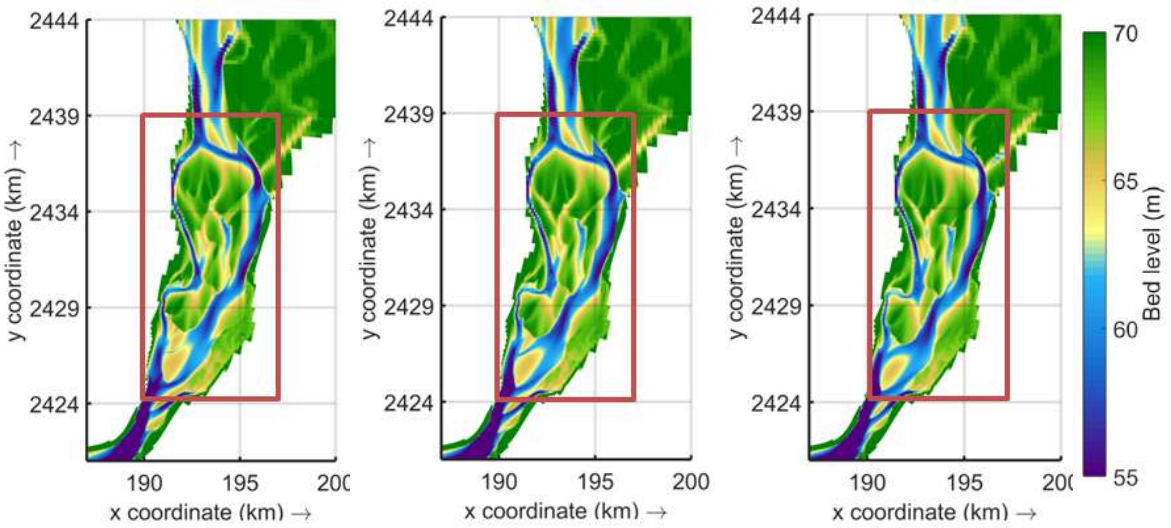

(a) Peak discharge $Q = 16,000\ m^3/s$

(b) Peak discharge $Q = 18,000\ m^3/s$ (reference)

(c) Peak discharge $Q = 20,000\ m^3/s$

D.3 Variation in falling period

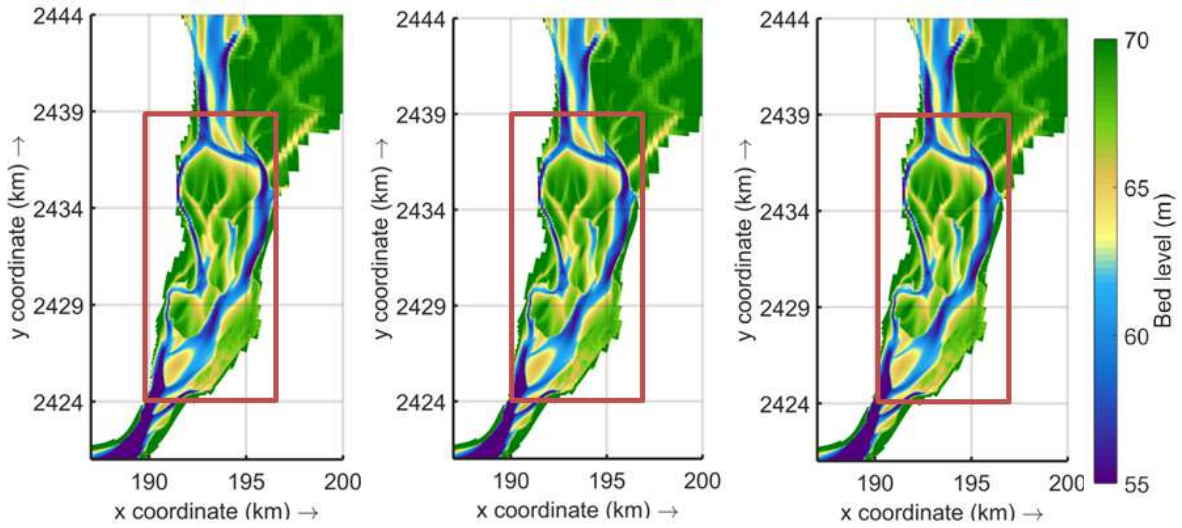

(a) Falling period 30 days

(b) Falling period 80 days (reference)

(c) Falling period 130 days

D.4 Variation in sediment input

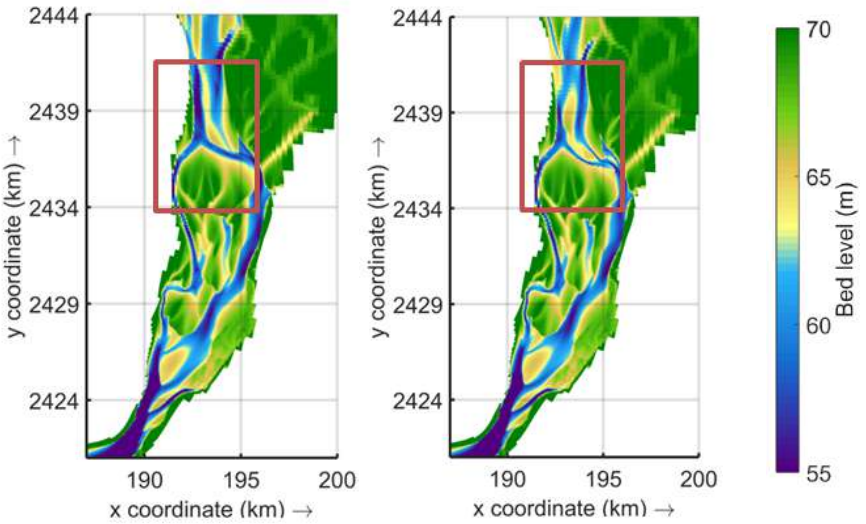

(a) Equilibrium sediment input (reference)

(b) Two times equilibrium sediment input

D.5 Variation in sediment transport formula

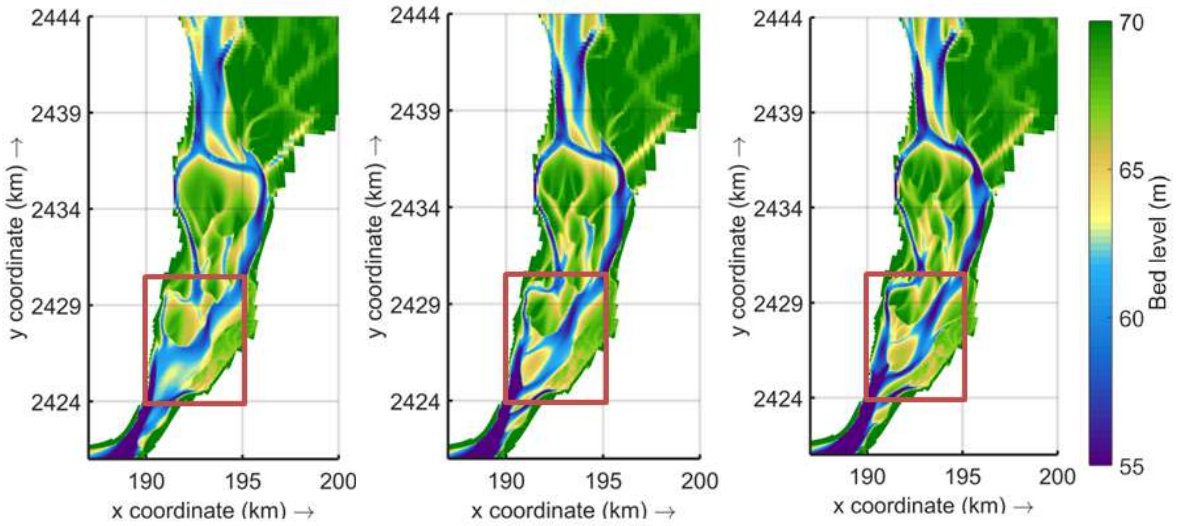

(a) $S \propto u^3$

(b) $S \propto u^4$ (reference)

(c) $S \propto u^5$

D.6 Variation in magnitude spiral flow

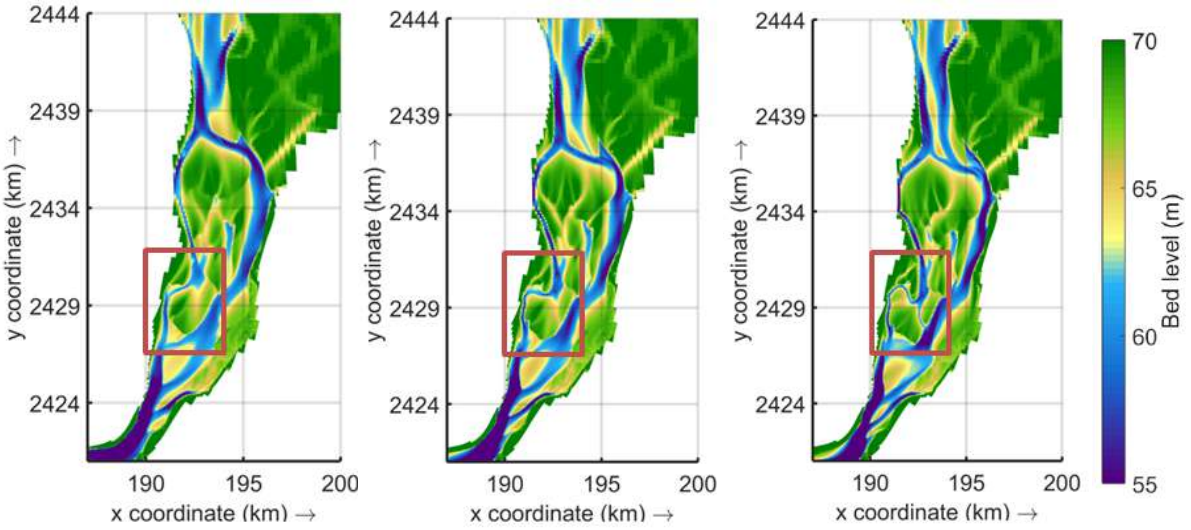

(a) No spiral flow ($E_{spir} = 0$) (b) Default spiral flow ($E_{spir} = 1$, reference) (c) Two times larger spiral flow ($E_{spir} = 2$)

D.7 Variation in magnitude bed-slope effects

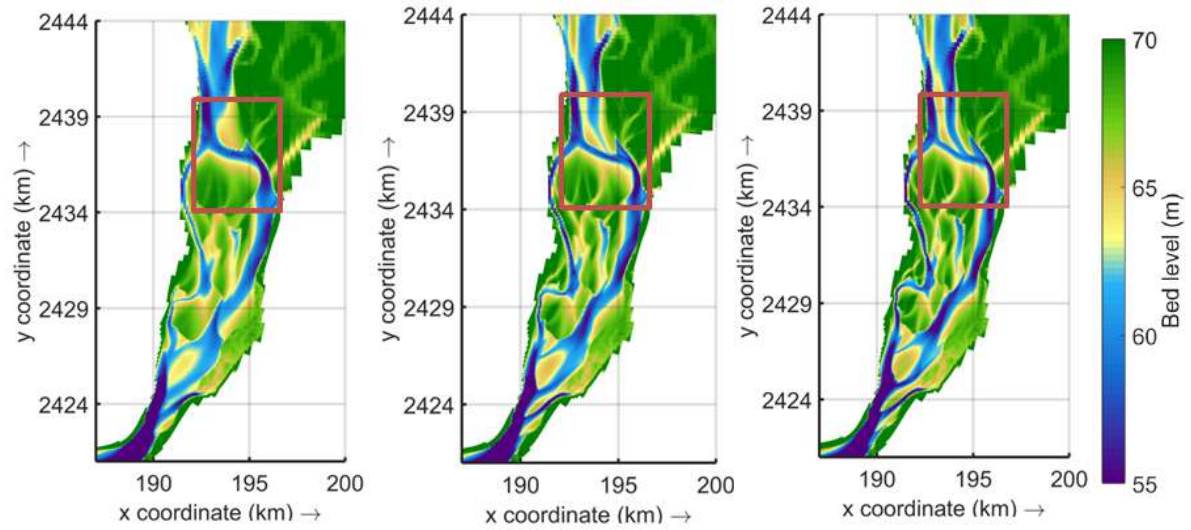

(a) High bed-slope effect ($A_{shield} = 0.3$) (b) Default spiral flow ($A_{shield} = 0.7$, reference) (c) Low bed-slope effect ($A_{shield} = 1.0$)

Appendix E

Channel width correction for varying discharge on satellite imagery

On the satellite images the width of the channels can vary due to variations in discharge. For the investigation of change in channel width, it is necessary to subtract the perturbations in width due to variations in discharge. How this is done, is explained in this appendix.

The first step is to derive a relation between the width of the channels and the discharge. This is done separately for both the left channel and right channel in the same cross-sections as used in the sensitivity analysis (see Figure 4.5). The relation is obtained using the initial bed with varying discharge. The necessary assumption her is that the slopes of banks over the twenty five cross-sections are on average equal over time. Measurements were performed within the range of 500 m^3/s to 5,000 m^3/s. The found relations are displayed in Figure **??**. Visible for both channels, is that the width does not decrease any further after a certain discharge. This means that the decrease in width from those points is lower than the grid size.

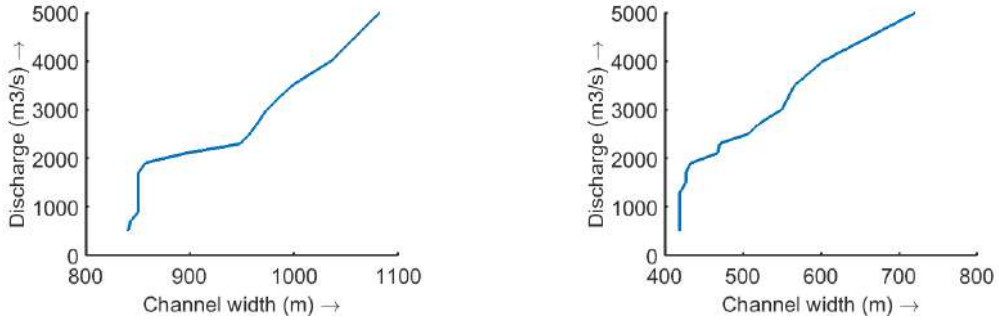

(a) Left channel (b) Right channel

Figure E.1: Discharge-width relation

The next step is to determine the discharge representative for the used images. The composite images are an average over approximately eight measurements (eight fly-overs of Landsat in periods of four months). With a relatively constant discharge over the dry season, it is assumed that the discharge representing the image is the average of the discharges over the whole period. With this assumption, fly-over times do not have to be looked up to find the average discharge of the moments at which the satellite data was obtained. This is assumed to be allowed, because just some peaks in discharge can be found during the dry season. With the appearance of such a peak discharge at a fly-over time of the Landsat satellite, the channel width during this high

discharge will be fade out in the composite image.

Knowing the average discharges for the images, all widths measured on the satellite imagery can be corrected for the varying discharge. Correction will be done to a width for a discharge of 2,000 m^3/s. In table E.1, the representative discharges and width corrections are given. Negative values mean a decrease of the measured with (a discharge higher than 2,000 m^3/s) and positive values an increase of the measured width (a discharge lower than 2,000 m^3/s). In this table is visible that the correction for most years is equal, which means that this analysis does not have a significant effect on the results in the change of width.

Table E.1: Representative discharge for the different years with corresponding correction of the width of the two different channels

Year	**Discharge (m3/s)**	**Correction right channel (m)**	**Correction left channel (m)**
1994	2475	-30	-45
1995	2287	-22	-40
1996	2540	-43	-55
1997	1478	22	35
1998	1953	9	5
1999	1311	22	35
2000	1122	22	35
2001	820	22	35
2002	834	22	35
2003	658	22	35
2004	691	22	35
2005	1746	14	30
2006	754	22	35
2007	704	22	35
2008	1342	22	35
2009	916	22	35
2010	530	22	35
2011	1229	22	35
2012	964	22	35
2013	652	22	35
2014	731	22	35